National Library of Canada | Bibliothèque nationale du Canada

CANADIAN THESES ON MICROFICHE

THÈSES CANADIENNES SUR MICROFICHE

NAME OF AUTHOR/*NOM DE L'AUTEUR* Gerard BISCHOFF

TITLE OF THESIS/*TITRE DE LA THÈSE* "Total Beta Decay Energies of Neutron-Rich Nuclides in the A = 100 Mass Region"

UNIVERSITY/*UNIVERSITÉ* Simon Fraser University

DEGREE FOR WHICH THESIS WAS PRESENTED/ *GRADE POUR LEQUEL CETTE THÈSE FUT PRÉSENTÉE* Ph.D.

YEAR THIS DEGREE CONFERRED/*ANNÉE D'OBTENTION DE CE GRADE* 1980

NAME OF SUPERVISOR/*NOM DU DIRECTEUR DE THÈSE* Dr. J.M. D'Auria, Associate Professor

DATED/*DATÉ* Dec 3rd 1979 SIGNED/*SIGNÉ*

PERMANENT ADDRESS/*RÉSIDENCE FIXÉ* [redacted]

TOTAL BETA DECAY ENERGIES OF NEUTRON-RICH NUCLIDES IN THE A = 100 MASS REGION

by

Gerard Lucien Victor Bischoff

D.E.A., Universite de Paris, France, 1972

A THESIS SUBMITTED IN PARTIAL FULFILLMENT OF

THE REQUIREMENTS FOR THE DEGREE OF

DOCTOR OF PHILOSOPHY

in the Department

of

Chemistry

SIMON FRASER UNIVERSITY

November 1979

PARTIAL COPYRIGHT LICENSE

Title of Thesis/~~Project/Extended Essay~~

"Total Beta Dacay Energies of Neutron-Rich Nuclides in the A = 100 Mass Region"

Author:

(signature)

Gerard BISCHOFF

(name)

Dec 3rd 1979

(date)

APPROVAL

Name: Gerard L.V. Bischoff

Degree: Doctor of Philosophy

Title of Thesis: Total Beta Decay Energies of Neutron-Rich Nuclides in the A = 100 Mass Region.

Examining Committee:

Chairman: C.H.W. Jones

J.M. D'Auria
Senior Supervisor

~~Walkley~~

B.D. Pate

K.P. Jackson

P.L. Reeder
External Examiner
Battelle Pacific Northwest Laboratories

Date Approved: November 19, 1979

ABSTRACT

An experimental study of decay properties of 40 short-lived neutron-rich nuclides including $^{91,94}Rb$, $^{94-96}Sr$, $^{96-97}Y$, $^{99-100}Zr$, $^{99-104}Nb$, $^{103-106}Mo$, $^{107-108}Tc$, $^{109-110}Rh$, $^{115-116}Pd$, $^{114-118}Ag$ and $^{120-123}In$ is presented.

The radioactive sources were produced at TRIUMF using intermediate energy protons to induce fission of natural uranium.

A gas-jet recoil transport system with methanol aerosol particles was developed to transfer the radioactive nuclides rapidly from the point of production to an area of low radiation where various combinations of detectors were used.

The total transport efficiency of the system is shown to be largely independent of the elemental composition of the collected fission products.

Gamma-ray energies, half-lives and coincidence relationships between different emitted gamma-ray lines were determined. The half-lives (in the range of 10 to 150ns) of 20 nuclear excited states were measured.

The relative positions in energy of isomeric states were determined in a few favorable cases. End-point energies of beta transitions were determined by applying beta-gamma coincidence methods. A telescope system of two plastic scintillators was used to measure beta energies.

Of particular interest were determinations, in several cases for the first time, of the total decay energies for neutron-rich nuclides of high neutron-to-proton ratios. These experimental Q_β-values were then compared with the predictions from current mass formulas to assess the degree of confidence that one can expect from their extrapolations to nuclides away from beta-stability.

Two-neutron separation energies were calculated for Rb, Sr, Y, Zr, Nb and Mo isotopes in the mass region near A=100. The occurence of a change of slope at N=60 in the plots of these energies versus neutron number supports the hypothesis that an onset of deformation of the nuclear shape takes place in the neutron-rich nuclides of masses near A=100 with $N \geqslant 60$.

DEDICATION

A mes parents

A Dominique

A notre futur

Men and women are not content to comfort themselves with tales of gods and giants, or to confine their thoughts to the daily affairs of life; they also build telescopes and satellites and accelerators, and sit at their desks for endless hours working out the meaning of the data they gather. The effort to understand the universe is one of the very few things that lifts human life a little above the level of farce, and gives it some of the grace of tragedy.

S. Weinberg

I like to think, now more than ever that it does not matter how little "a little above" may be.

ACKNOWLEDGMENTS

I want to express my gratitude to Dr. J. D'Auria for his supervision. The good atmosphere that he has created in his group has been very appreciated.

I am very grateful to Dr. B.D. Pate for his continuous support.

I own special thanks to Dr. K.P. Jackson for his pertinent remarks and always constructive advice.

I am indebted to the department of Chemistry of Simon Fraser university for its financial support and for providing the facilities which have made the accomplishment of this project possible.

My sincere appreciation goes to W. Bishop, M. Kiely, A. Kurn and R. Toren for their consultation and programming.

Dr. W. Weisehahn ben ih veel dank verschuldigd voor de computerprogrammas en discussies. Zijn bereidwillige hulp op mijn "It would be nice if..." was zeer waardevol.

Je remercie très vivement Dr. H. Dautet pour les longues nuits passées auprès de l' accélérateur, son esprit d'équipe et sa bonne camaraderie.

Je remercie aussi vivement toute la petite colonie française de l'université Simon Fraser pour son amitié.

TABLE OF CONTENTS

LIST OF TABLES

LIST OF FIGURES

FIGURE CAPTION

Fig.

1- Tradional Z versus N representation of the nuclides. The black squares are the stable nuclides. The circles represent the known and postulated regions of nuclear deformation.
The inside lines define the limits for known nuclides.
The ouside lines define the proton and neutron drip lines. (data taken from Sor-70 and She-76)

2- Representation of the postulated paths for the creation of heavy elements. The region around Fe corresponding to neutron-rich nuclides of A=60-70 represents the r-process (rapid-capture-process) seed.

3- Energies of the first 2+ excited states and ratios E4+/E2+ versus neutron number for Sr,Zr,Mo,Ru and Pd neutron-rich isotopes. (data taken from Wol-77)

4- Schematic representation of the TRIUMF 6-sector isochronous cyclotron

5- Schematic representation of the gas-jet transport system. The pressure in the target chamber was typically about 1atmosphere whereas it was in the order of 1mm of Hg in the collecting chamber.

6- Schematic representation of the target chamber at TRIUMF. Targets are mounted on a ladder electronically controlled. Different lengths of the production chamber are available.

7- Schematic representation of the aerosol generator.

8- Schematic representation of the gas-supply system for the determination of collection yields using different liquids as transporting media..

9- Collection yield curves for water, methanol, pump oil and ethylene used as different transporting media.

10- Comparison of two gamma spectra of recoils from an argon gas target. One spectrum was collected using ethylene as gas carrier whereas for the other methanol droplets in nitrogen were used. Photopeaks from halogen products are only seen in the second spectrum.

11- The top part of the figure is a representation of the number of events registered in the DE counter as a function of the deposited energy. The ordinate axis is in arbitrary linear units. Signals with an amplitude corresponding to a deposited energy between 100 and 300keV are allowed to enter the coincidence circuit.

12- Calibration line, energy versus channel number, for the beta analysis performed with the KURIE code.

13- Schematic representation of the two electronic set-ups used in coincidence experiments. Both used the fast-slow coincidence technique.

14- Total gamma spectrum in coincidence with all beta-rays. The total energy range (100-2200keV) has been divided in 4 energy sections. The number above individual peak is the associated energy.

15- Total low-energy (5-300keV) gamma spectrum in coincidence with all high energy gamma-rays (100-2000keV). The most intense Xrays are assigned by their atomic symbols.

16- Low energy gamma spectra in coincidence with Mo, Cd, Sn and Tc Xrays corresponcing to Nb, Ag, In and Mo isotopes, respectively. The lines in coincidence are identified by the mas number of the nuclides they come from.

17- Decay curves of the long-lived 85.4 and 1264keV states in ^{105}Mo and ^{97}Zr, respectively. The promt peak has been subtracted. For the decay of the 85.4keV state each data point is the sum of the counts over 4 channels whereas for the decay of the 1264keV state it is the sum over 8 channels.

18- Shape of the response function used in KURIE. It represents the response of the beta detector for monoenergetic electrons of 5MeV.

19- Representation of a part of the chart of the nuclides where the 40 isotopes stidied in this work are pointe out.

20- Beta spectrum and associated Kurie-plot in coincidence with the 93.5keV gamma line in the decay of ^{91}Rb. The black solid line is the fit generated by KURIE. A simplified decay scheme of ^{91}Rb is also shown.

21- Decay curve of the 93.5keV gamma-line. The black solid line is the fit generated by the FITTIM program. This fit corresponds to the sum of two individual components:
- - - - represents the accumulation due to the parent.
- * - * represents the decay of the 93.5keV gamma line after subtraction of the parent contribution.

22- Tentative decay scheme for ^{94}Rb

23- Decay curves of the 837 and 1428keV gamma lines. The solid lines represent the fits whereas the broken lines are individual components.

I- INTRODUCTION

I-1 General

The aim of this work was to carry out an experimental study of the radioactive decay and nuclear spectroscopic properties of nuclides far from beta-stability. Of particular interest in this regard were the neutron-rich fission products with mass numbers, A, of around 100. A total of 40 nuclei have been investigated. From the resulting data 12 new ground-state Q_β-values have been determined and for a few of the other previously reported Q_β-values more precise values have now been obtained. These data may be expected to lead to further refinements of the semi-empirical mass equation as well as to a better understanding of the collective properties of the neutron-rich nuclides in the A=100 mass region.

I-2 Nuclei far from stability

Fig.1 displays the traditional Z versus N representation of the nuclides. The black squares represent the stable nuclei and constitute the "valley of beta stability". As one moves away from the bottom of this valley, the instability towards beta decay increases,i.e, the nuclear half-life decreases. In general, the energy available for the decay also increases and this implies that the levels available as final states of such nuclear decay transitions are more numerous.

The study of nuclei which lie far from beta-stability is of considerable interest since the ability to predict the properties, and in particular the mass, of such "exotic" nuclei provides a good testing ground for some of the theories of nuclear structure. Furthermore, the large amount of energy available in the decay of such nuclei may lead to the discovery of unexpected phenomena, e.g, beta delayed single and double particle emission and coulomb delayed particle emission. Also, away from the valley of stability one may reach new regions of permanent deformations where nuclei display a dominant collective behavior.

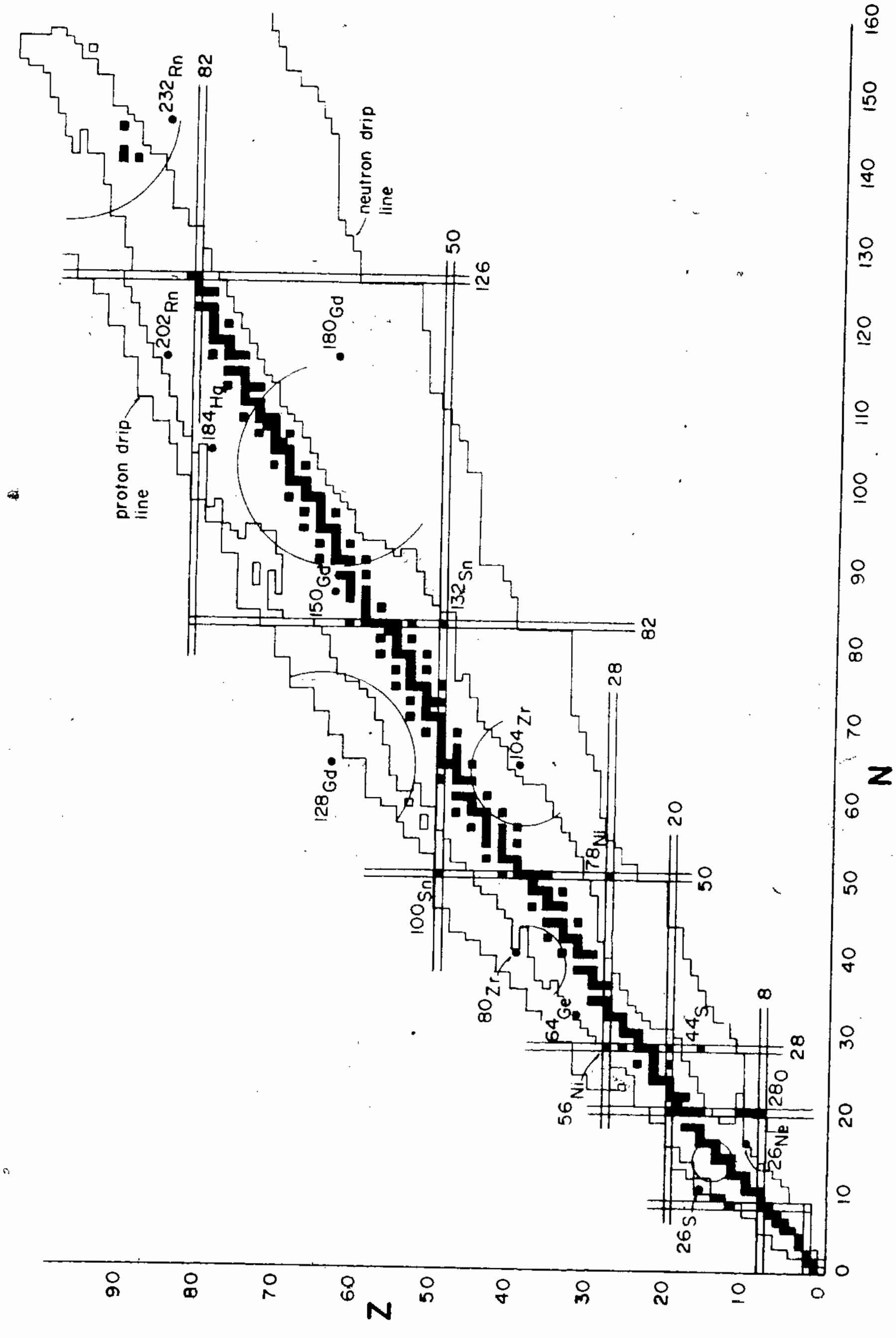

Figure 1. The nuclear chart.

I-3 General methods of production

The production of nuclei far from stability may be achieved using a number of different methods depending in part on which side of the valley has to be reached.

The principal methods of producing neutron deficient nuclides are reactions induced by medium energy charged particles, e.g. [(p,xn),(α ,xn),...], and reactions induced by high energy particles (spallation) or heavy ions [(H.I.,XnYp)]. These reactions generally induce significant particle evaporation due to the high "temperatures" of the intermediate reaction species.

The principal way to reach the neutron rich side of stability in the laboratory is through the fission of heavy nuclei. Alternatively reactions such as (n,p),(n,α),(p,2p)... can also be used. However the yields of these are much lower and generally produce nuclei which lie close to the stability line. An additional process occurs under the extreme conditions found in stellar interiors and in nuclear explosions, namely multiple neutron capture. However, since these conditions are not normally available to the experimenter, this will not be discussed further.

Fission can be induced when the incident projectile supplies sufficient energy for the resulting nuclear system to overcome the barrier to fission. Only a few nuclei can fission under bombardment with thermal energy neutrons (^{233}U, ^{235}U, ^{239}Pu). When the supplied energy becomes high enough, e.g., with fast neutrons or high energy protons, most of the heavier nuclei can undergo the fission process. At high bombarding energy the mass-symmetric process replaces the well-known assymmetric mass division of thermal-neutron-induced fission. The production yield versus the mass number A is then a bell-shaped curve, the centroid of which is expected to move towards the stability line and to become greater in width as the bombarding energy increases. In general the fission of ^{238}U at high energies leads to products lying mainly in the mass region of A=90-140. This method has been the principal one used in the present study to produce very neutron-rich species.

I-4 Importance of studies of neutron-rich species of masses near A=100

I-4-1 General

Owing to the coulombic repulsion between protons and the resulting nuclear instability, the proton drip line, i.e, the limit for bound protons in proton-rich nuclides, lies closer to the stability valley than the corresponding neutron drip line for neutron-rich nuclides (fig.1).

On the neutron rich side there is no corresponding effect and thus nuclei with relatively high neutron-to-proton ratios can be produced exhibiting beta desintegration energies as high as 20 MeV while still remaining stable against neutron emission. Hence, the data available for mass formula extrapolations on the neutron excess side can be, theoretically more numerous, i.e, more nuclei can be studied.

I-4-2- Nuclei around A=100 : a region of strong deformation

Systematics of the energy levels in excited nuclei show that non-spherical equilibrium shapes develop in nuclei with compositions far from closed-shell configurations. Regions of deformation, such as those for the nuclei around ^{25}Mg, the rare earth region or the actinide nuclides, have been well established (Rog-65a). The reason why these regions have been identified, is that they lie along the valley of stability and are therefore relatively accessible to experimental study. As experimental techniques are developed, other possible areas of deformed nuclei may be reached. In fig.1 the open circles mark the limits of the expected regions of deformation (Sor-70,She-76).

In the region near A = 100 spherical nuclei are found close to either the Z = 50 or the N = 50 shell closures. Deformation is expected to set in as the nuclear composition moves away from these boundaries. As has been pointed out in several theoretical studies (Ars-69,She-72,Fae-74), the neutron rich species from Sr to Ru represent good candidates for exhibiting permanent nuclear deformations.

From the experimental point of view, studies of neutron rich nuclei around A≈100 are hampered by the fact that the most interesting nuclei have rather short half-lives (<10s) for the application of standard nuclear methods of investigation. Further, the chemical properties of most elements of this region, i.e, refractory metals, inhibit the possibility of utilizing on-line isotope separators. In addition a large number of nuclides are produced in the fission process and the identification of those of interest becomes difficult and critical.

I-4-3 The r-process

Fusion reactions of the light elements (such as those proceeding in stellar interiors) can not lead to the formation of nuclei heavier than the group near iron (Hoy-75). Despite this fact, heavier elements exist in nature. Fig.2 shows the two postulated possible paths (s and r) for the creation of such elements. Depending on the stellar conditions, i.e, the neutron flux, only a portion of these pathways will usually be followed.

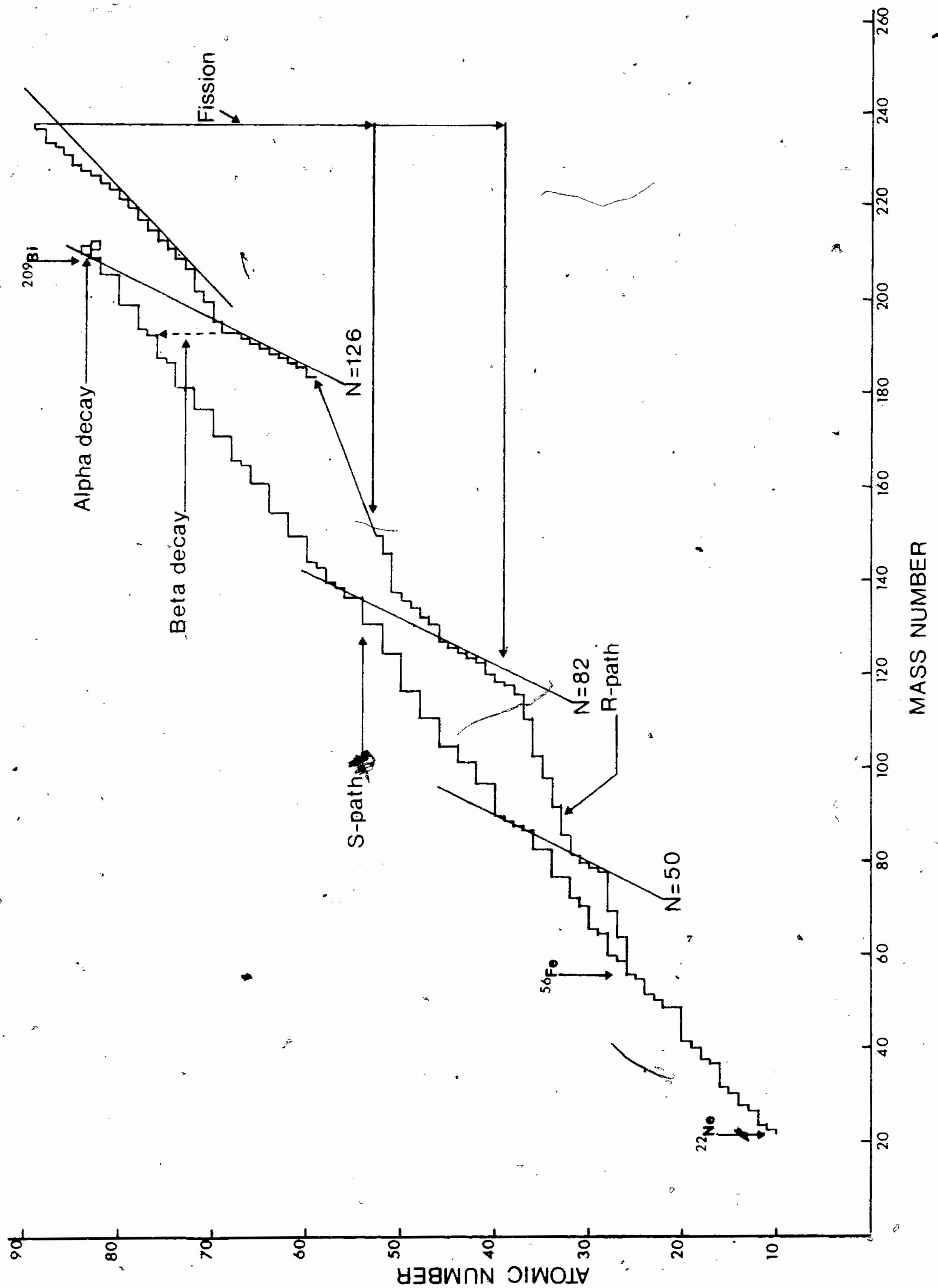

Figure 2. Paths of creation of heavy elements

Since it is still impossible to reach the r-process region experimentally, one has to predict the properties of the exotic nuclei involved in theoretical calculations on models of the processes involved. Mass formulas thus play an important role in the construction of these theoretical models, and tests for mass formula extrapolations are, as a result, of special interest to astrophysicists (Sch-76).

I-4-4 Fission reactor systems

A recent report (Rei-77) gives a detailed review of applications of fission-product data. Of special interest is the importance of the measurement of gross properties (mass, half-life,...) of short-lived fission products in applications such as the determination of the decay-heat source in operating reactors.

Being able to predict with confidence the heat generated by the decay of short-lived fission products is a major task in nuclear engineering. The construction of a safe and efficient emergency core cooling system (ECCS) is directly related to this theoretical problem. The feasibility of the calculations of the decay heat source depends almost exclusively upon an accurate knowledge of the detailed decay scheme of the nuclides produced in the fission process. Decay and spectroscopic studies of specific fission products which are important in determining the amount of heat produced in radioactive decays are thus essential to the development of safe economical nuclear power plants.

I-5 Goals of this dissertation

As the major objective of this study is aimed at the acquisition of new experimental data to test current semi-empirical mass formulas, it is necessary to review first the main features of these theoretical calculations. We shall end this section with a brief presentation of the experimental techniques currently involved in mass measurements. With this preparation we shall then continue with a brief review of nuclear properties of the neutron-rich nuclides in the mass region near A=100.

Following this, we shall present the experimental techniques utilized in this study. This will include a description of some of the studies undertaken to provide a better understanding of the processes which govern the mechanism of transport of fission fragments via the gas-jet recoil system.

The detection and data acquisition systems will be discussed in the following section as well as the off-line analysis and the identification techniques.

The results and the discussion associated with each individual mass number will then be presented. These data will be used for comparison with predictions from current mass formulas and further utilized to provide new insights towards an understanding of the shape of nucleus in the mass region near A=100.

We shall end this dissertation with a brief presentation of possible extensions of this study in the future.

II- MASS AND ENERGY

II-1 General

In nuclear science the "mass" of a nucleus represents the exact mass or its total energy. Mass is thus, a fundamental property from which predictions of a number of the other nuclear properties of a nucleus can be made (decay energies, reaction energies, energies released in fission...).

Since Lagrange, "the theory of the Science of mechanics and the art of solving all problems that arise therein" was reduced "to a general formula whose simple applications give all the equations necessary for the solution of every problem". This general formula is the Hamiltonian function, that is, the total energy of the system written out as a function of the generalized coordinates (or degrees of freedom) specifying the state of motion of the system.

Nuclear forces are not yet well enough understood to derive such a general formula from first principles; the main obstacle being the complexity of nucleon-nucleon interactions within the framework of a many body system.

However, self-consistent calculations of nuclear masses use a simplified nucleon-nucleon interaction to derive the total binding energy of the nucleus. Semi-empirical mass formulas on the other hand constitute a macroscopic description of the nuclear mass where the nucleus is treated as a whole.

Most mass formulas are mathematical expressions of suitable form with parameters adjustable to fit the known masses (experimental data). The different approaches that have been taken to devise such formulas will be examined briefly below.

II-2 Mass Formulas

II-2-1 The liquid drop model equation

The starting point of most semi-empirical mass calculation is the famous Bethe-Weizacker liquid drop model equation (Wei-35, Bet-36)

$$B(A,Z)=a_v A-a_s A^{2/3}-a_{sym}(A-2Z)^2 A^{-1}-a_c Z^2 A^{-1/3}+\phi(A,Z)$$

Here, the total binding energy B(A,Z) is given as the sum of the volume, surface, symmetry, Coulomb and pairing energies in the successive terms above (a_v, a_s, a_{sym} and a_c are empirical coefficients). The deviations of energy values calculated from this crude formula from those obtained from experiments are of the order of 5MeV, which is fairly good because this is only of the order of one per cent of the total binding energies involved. However, the fission barrier for heavy elements is of the order of these deviations ($B(^{235}U)$=5MeV).

An improvment to this formula was provided by addition of a correction energy term due to the existence of shells in the nuclear structure to the energy term of the liquid drop.

II-2-2 The macroscopic approach with shell corrections

The "droplet model" of Myers and Swiatecki is a two-part model, made up of a smooth macroscopic part corresponding to the liquid drop approach, and an oscillating microscopic part corresponding to a shell model calculation. Although, both parts contain shape dependent parameters the effects of the deformation is mainly accounted for by the shell correction term (Mye-66).

It is the shell correction term that accounts for the main difference between the various existing droplet model mass equations.

Seeger and Howard (See-75) have devised a shell-correction term based on a microscopic Nilsson-model calculation (Nil-69). The result is then normalized to the macroscopic part using Strutinsky's procedure (Str-68).

II-2-3 Shell model calculations

Liran and Zeldes (Lir-76) have devised a shell-model semi-empirical mass equation where the total energy of the nucleus is the sum of strong-pairing, deformation and Coulomb energies. According to the shell configuration of the valence protons or neutrons this approach gives rise to different equations.

In order to obtain the semi-empirical coefficients, each of the 15 different shell regions is treated separately. The number of these coefficients is usually very large (a few hundreds) (Lir-76).

II-2-4 Mass Relations

While all of the above calculations were constructed on theoretical models, Garvey and Kelson (Gar-69) have derived relationships between the masses of neighbouring nuclei where very few assumptions about nuclear structure are necessary. The agreement with experimental data of the "transverse" relation (see NDT-76) is very good, the average deviation being about 100 keV.

The danger of such a method is the possibility of small systematic errors which can accumulate in the repeated application of the relationships for nuclei far from stability (Wes-72). To prevent such errors in large extrapolations, generalized relationships including an effective neutron-proton interaction have been derived (Jan-76a). The number of parameters, which have to be deduced, reaches 500.

II-2-5 Self-consistent calculations

The first approximation consists of describing the nucleon-nucleon interaction by a potential function, V(r), where r is the distance between the two nucleons. Once V(r) is provided, the problem is to modify this function in order to take into account the fact that nucleons are not free in the nucleus but depend upon all the others. The resulting new interaction is called an "effective nucleon-nucleon interaction". The nucleus is then described as a many body system in which each particle moves in an average potential set by all the others. This approach corresponds to the Hartree-Fock treatment of the nucleus (Bei-76).

Because of the poor agreement between experimental data and the calculations derived from this approach, self-consistent calculations will not be considered further.

Table I taken from (Ale-77) gives a brief summary of the main features of the mass expressions briefly reviewed above. It is worth noting that these mass formulas give rather good fits to known masses, i.e, masses of nuclides in and near the valley of beta stability. This is not surprising since the parameters used in these formulas are adjusted from a fit to these known masses. Thus, new experimental data is needed to test these models further by allowing a comparison of the theoretically predicted masses with new mass data in regions away from stability.

Table I. Summary of the main features of the mass formulas used in the comparison between theoretical predictions and experimental results.

Authors	Ref	Features	No of Coeff	Fitted to	Goodness of fit for Mex (MeV)
Myers	Mye 76	Improvement of droplet model. Fermi-gas level-bunching with deformation attenuation	16	Wap 71	see NDT-76, fig.3 page 415
Seeger, Howard	See 75	Shell and deformation energies from Nilsson model and BCS pairing	9	Wap 71	$\sigma = 0.704$[a,b]
Liran, Zeldes	Lir 76	Sum of strong pairing, deformation, and Coulomb energies	178	Wap 77	$\sigma = 0.276$[a]
Garvey, Gerace, Jaffe, Talmi, Kelson	Gar 69	Transverse Garvey-Kelson mass relationships	477	Mat 65	$\sigma = 0.092$[a]
Comay, Kelson	Com 76	Average values and uncertainties from ensembles of G-K mass tables	subsets of known masses	Wap 77	$\langle \lvert M-M_{exp} \rvert \rangle = 0.102$

[a]Root-mean-square error, $\left[\sum_i (x_i - \bar{x})^2/n\right]^{1/2}$.

[b]For binding energies.

II-3 Mass measurements

II-3-1 Definitions

The atomic mass is defined as

$$M(atomic) = M(nuclear) + (Z.m_e - B(Z))$$

where m_e is the mass of the electron and B(Z) is the binding energy of the Z electrons in the neutral atom. One unit of atomic mass has been internationally defined as being 1/12 of the mass of a ^{12}C atom and this has set a reference scale for mass measurements.

A nucleus is made up of Z protons and N neutrons but its actual mass is not the sum of the individual nucleon masses. The difference is the total nuclear binding energy which can be written as

$$B(Z,N) = Z.M(H) + N.M_n - M(Z,N)$$

where the masses are those of the corresponding neutral atoms.

If the masses are expressed in mass units, then this relation can be written as

$$Mex(Z,N) = M(Z,N) - A$$

where Mex(Z,N) is the so-called mass excess. Generally, nuclear masses are expressed as mass excess values.

The difference between the mass excesses of two isobaric nuclides, related through beta decay, defines the Q_β-value or beta total decay energy of the parent nuclide. The successive addition of these mass differences to the well established masses of the stable nuclei can then lead to the determination of the masses of any radioactive nuclei.

II-3-2 Techniques of mass measurements of radioactive nuclides

a- Direct mass measurement

A mass spectrometer is an instrument in which a combination of electric and magnetic fields is used to separate ions of different masses, and measure their masses.

In the case of light nuclei (A<40), it has been shown that with a single stage mass spectrometer one can measure on-line masses of sodium isotopes with relatively good precision, i.e. 100keV for A=30 (Thi-75).

To maintain the same accuracy (≃ 100keV) for heavier nuclei (A>100) requires the use of "double focussing" mass spectrometers (Eph-79). To compensate for the associated low transmission (1% for Na) of such machines, one requires an adequate intensity of the radioactive species of interest. This is the case at the ISOLDE Isotope Separator at CERN for a number of chemical elements (Rav-76, Car-78).

Actual measurements are done on-line by comparative studies (Kla-74), that is, a mass M1 is determined relatively to one or several well known reference masses (M2,M3,...).

Along with the restriction of their use to a few elements, such systems are expensive and elaborate.

The mass spectrometric arrangement called an "isotope separator" coupled with new on-line techniques is, indeed, one of the most powerful tools of investigation in nuclear science. However, its mass separation only serves as an identification system and no actual masses are directly measured.

b- Mass measurements from nuclear reactions

Near the bottom of the valley of beta-stability a very good precision (in the order of 1keV) can generally be achieved in the measurement of masses through nuclear reactions.

Actually, most of the known masses have been derived from the "Q's" of nuclear reactions such as (p,α), (d, He) or (t, He). The high precision is a consequence of the high precision achieved in the measurement of the kinetic energies of charged particles.

c- Q_β-value determination

Another traditional approach to mass measurements is the determination of Q_β-values. Generally, Q_β-values are obtained by summing the maximum energy of the beta particles of the decaying nuclide and the excitation energy of the level populated in the daughter nuclide. (The recoil energy of a nucleus of A=100 emitting a beta particle of 10MeV is in the order of 500eV. Thus, recoil energies are considered in this study as negligible, the experimental errors being in the order of 50-200keV). Such determinations require a good knowledge of the parent decay scheme and level structure of the daughter nuclide.

Experimentally, coincidence methods are, in general, required if such determinations are to be made with a high degree of confidence. When the beta branching of the parent is known, a beta-gamma coincidence experiment where specific beta end-point energies are measured to be in coincidence with specific gamma-rays of the daughter nuclide determine uniquely the Q_β-value associated with this decay.

Generally the achieved precision is in the order of 100keV. The difficulties lie in the determination of the end-point energy of continuous beta spectra and in the decay scheme construction.

Beta-ray spectrometers, plastic scintillators, Si(Li) and recently intrinsic Ge detectors have been used for the measurement of the energies of beta-rays. Si(Li) detectors have very good resolution. Their main disadvantage is that they are very difficult to make thick enough to stop high energy electrons (>3MeV).

However, special arrangements can be found (Ale-77) which extend the range of commercial Si(Li) detectors to beta energies up to 10MeV.

Intrinsic Ge of high purity is the newest detector material and is still under development. These new counters should have high efficiency as well as good resolution (Gou-74). However, one of their present disavantage is the relatively high sensitivity to the "bremsstrahlung" process which increases as Z^2 (Z is the atomic number of the detection material) and distorts the response of the detector at high electron kinetic energy.

Plastic scintillators are inexpensive. They can be bought in large sheets and can be machined in nearly any desired shape. They represent an extremely useful and versatile tool. Owing to their large sensitive volume, their total counting efficiency can approach 100 percent. This feature conjoined with their excellent time resolution (decay time in the order of 1-10ns), renders them particularly valuable for coincidence experiments. However, due to the several statistical processes involved in producing the output electronic signal the energy resolution of scintillation counters is limited.

A plastic scintillator counter has been chosen as the means of measuring the energy of beta-rays in all beta-gamma coincidence experiments of the present study.

III- SPECTROSCOPY

III-1 General

Even-even nuclei in regions of deformation have very characteristic excited states. The ground-state is obviously 0+(J^{π}). The first excited level is a 2+ state and its energy is very low, typically 50-100keV for nuclei near A=160. Theoretically, in a way very similar to molecular rotation, the low-lying energy levels can arise from the rotation of the deformed nucleus. Thus, a series of energy levels with spin and parities 0+,2+,4+,6+,..., is predicted for deformed nuclei. Such series are called rotational bands (Mar-70). In most regions, the energies of the first 2+ excited state change smoothly when varying the neutron number N, keeping Z constant and vice-versa (Che-74). The transition from spherical to deformed behaviour is characterized by a rapid drop in the energy of the first 2+ level and an increase in the E4+/E2+ energy ratio. As this ratio approaches 3.33, the value for a rigid rotator, the energy of the first 2+ state changes less and less from isotope to isotope (Boh-75).

III-2 A=100 Mass-Region

If strong changes in the energy of the first 2+ levels may be regarded as indicative of transition from the vibrational to rotational modes and of a strong change in nuclear softness, then it appears that this transition occurs between neutron numbers 58-60 for the light fission fragments from uranium. The energies of the lowest 2+ state and the ratios E4+/E2+ for the nuclei in the mass region near A=100 are shown in fig.3 (Mfa-74). The most striking case is that of the Zirconium isotopes (Z=40). The abrupt change in E2+ and E4+/E2+ values between ^{98}Zr and ^{100}Zr is much sharper than the corresponding change between ^{150}Sm and ^{152}Sm, which shows the well-known discontinuity for N=88 and N=90 isotopes. In the neighbouring Mo(Z=42) isotopes, the change in the first 2+ level energies between N=58 and 60 is again much less abrupt and in Ru(Z=44) the transition to rotational behaviour is relatively smooth and gradual. A recent publication (Wol-77) has reported a very abrupt change in similar energies between ^{96}Sr and ^{98}Sr.

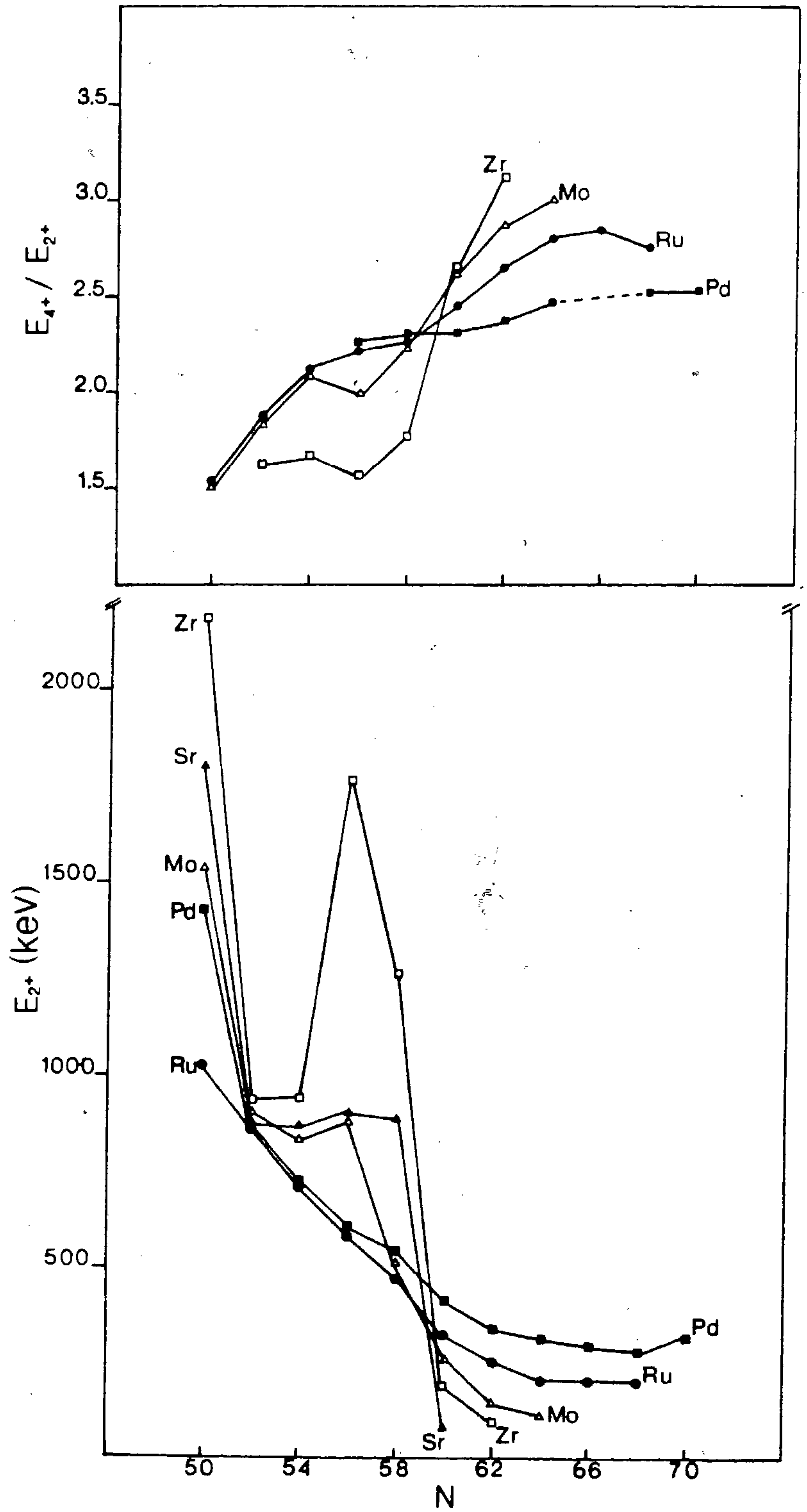

Figure 3. Energies of E_{2+} and E_{4+}/E_{2+} for neutron-rich nuclides of masses near A = 100

Theoretical calculations for deformations in the light fission product region have been carried out by several authors (She-72,Ars-69,Fae-74). However, none of these calculations predict the existence of a sharp transition region for the Zr isotopes. The transition in the calculations is very smooth when compared with the data. Experimentally the nucleus ^{96}Zr appears to have extra stability due to the closing of two subshells: the $2p_{1/2}$ proton level at Z=40 and the $2d_{5/2}$ neutron level of N=56. This stability apparently is quite localized since the addition of four neutrons brings on a rapid onset of deformation. The calculations do not reproduce the increased stability for 96 Zr and therefore predict the onset of deformation to be more gradual than observed. A recent publication (Kha-78) reports good agreement of the experimental level energies with postulated triaxial deformation for ^{100}Zr. However, more data are needed to reveal the intriguing nuclear structure in this region near mass 100.

III-3 The "Pandemonium" effect

By creating the fictional nuclide, Pandemonium and studying its beta-decay J.C. Hardy et al have demonstrated that beta-decay branching ratios and ft-values extracted from gamma intensities must be regarded as doubtful for most beta-transitions in complex decay schemes (Har-77).

The nuclides under investigation in the present study lie far from the valley of beta stability and therefore exhibit generally high total beta decay energies. As a consequence, many beta transitions may contribute to the decay of these nuclides. Hence, a beta spectrum in coincidence with a gamma line of deexcitation of a low energy level in the daughter nuclide may be the result of the summation of many beta transitions of weak intensities. Such a spectrum can then be regarded as the result of the statistical population of a sea of highly excited states.

At excitation energies of the order of a few MeV the traditional spectroscopic description of the nuclear states as discrete energy levels loses its significance. The beta strength function as defined in ref.(Han-74,Ale-75) permits a more adequate description of the behavior of these excited nuclides.

However, low lying energy levels in daughter nuclides are not as bunched as high excited states (especially in even-even nuclides), and therefore beta transitions populating such levels should generate electron spectra whose end-point energies could be in principle well differentiated.

IV- EXPERIMENTAL TECHNIQUES

IV-1 Production methods

The neutron-rich nuclides of interest were produced using induced fission of natural uranium (foil of 270mg/cm^2) either with fast neutrons at SFU or with high energy (480MeV) protons at TRIUMF.

The Texas Nuclear Corp., model 9900 neutron generator, located at Simon Fraser University, produces 14-MeV neutrons using the T(D,n)α reaction. The flux is typically of the order of 5×10^7 n/(cm^2.s).

At TRIUMF the availability of the intense, intermediate energy proton beam was utilized to induce fission in a similar uranium foil.

TRIUMF is a sector-focussed isochronous cyclotron which accelerates H- ions. Stripping of the H- ion at appropriate beam orbits leads to essentially 100% extraction of an external proton beam of a pre-selected energy. This machine is capable of delivering simultaneously two proton beams of different energies, each individually variable from 180MeV to 525MeV.

Fig.4 displays schematically the cyclotron and the "proton hall" where the present experimental set-up is located.

The SFU gas-jet facility is situated near the end of the 4A beam-line, which is shielded for an ultimate beam intensity of 10microamperes. For most of the experiments described below, the energy of the proton beam was either 480MeV or 442MeV with a typical current of a few hundred nanoamperes. Some gamma-gamma coincidence experiments were performed with a beam current of about 1microampere at 485MeV.

The mass, charge distributions and yield of fission fragments produced from the two processes are expected to be different (Lef-66). However, these differences do not affect spectroscopic properties of produced isotopes.

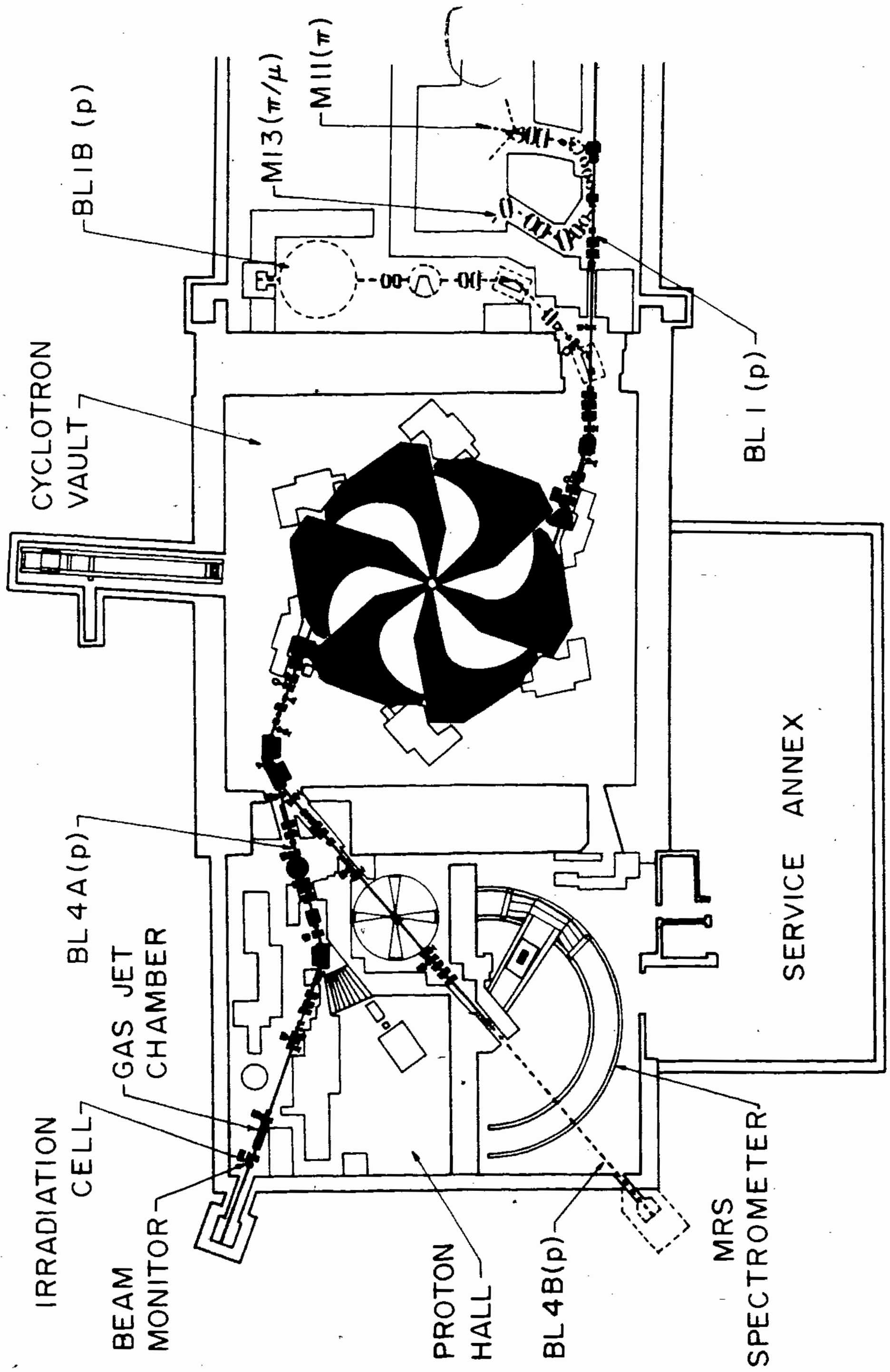

Figure 4. The proton area of TRIUMF

IV-2 The gas-jet transport system

An ideal method for studying properties of nuclei far from stability is an on-line isotope separator (ISOL). It can provide A and Z selection of a particular species from among a large number of reaction products. Such devices, however are expensive and sophisticated. Athough, great improvments have been made in the recent years, there still are elements which can not be delivered by ISOL machines (Rav-76).

An alternate approach which complements studies at ISOL facilities is the gas jet recoil transport method. It can be used to transport essentially any reaction product from point of production to a detection area of low radiation background, rapidly (∿ 1s), efficiently (∿70%) and over a long distance (∿ 30m).

The gas jet system also produces very thin active sources allowing alpha or beta ray measurements.

Such systems are much less expensive, and largely not chemically limited but it is imperative that some selectivity be achieved through the detection system if specific isotopes from the large number produced are to be studied. This is the approach taken in the present study.

In a gas jet system, nuclei recoiling from nuclear reactions leave the target and are slowed down in a gas before being transported through a capillary tube at close to sonic velocity to a region of low radiation background. The gas jet emerging into vacuum from the end of the capillary and carrying the recoils, is allowed to impinge on a solid collector (fig.5).

It has been shown by several research groups (Mfa-74) including the S.F.U. Group (Wie-73) that the presence of gas-phase molecular clusters as carriers is a necessary component for efficient transport of radioactive products.

In most reported applications helium has been used as a carrier gas to transport activities over short distances (50-100cm). When suitable molecular clusters are added to the helium, the distance of transport can reach several tens of meters with very little loss of activity.

The gas jet system was initially developed at SFU using fast-neutron-induced fission of uranium to provide a source of radioactive species. In this system ethylene gas was used as both the source of the necessary clusters as well as the carrier gas. Complete details of these studies can be found elsewhere (Dau-73).

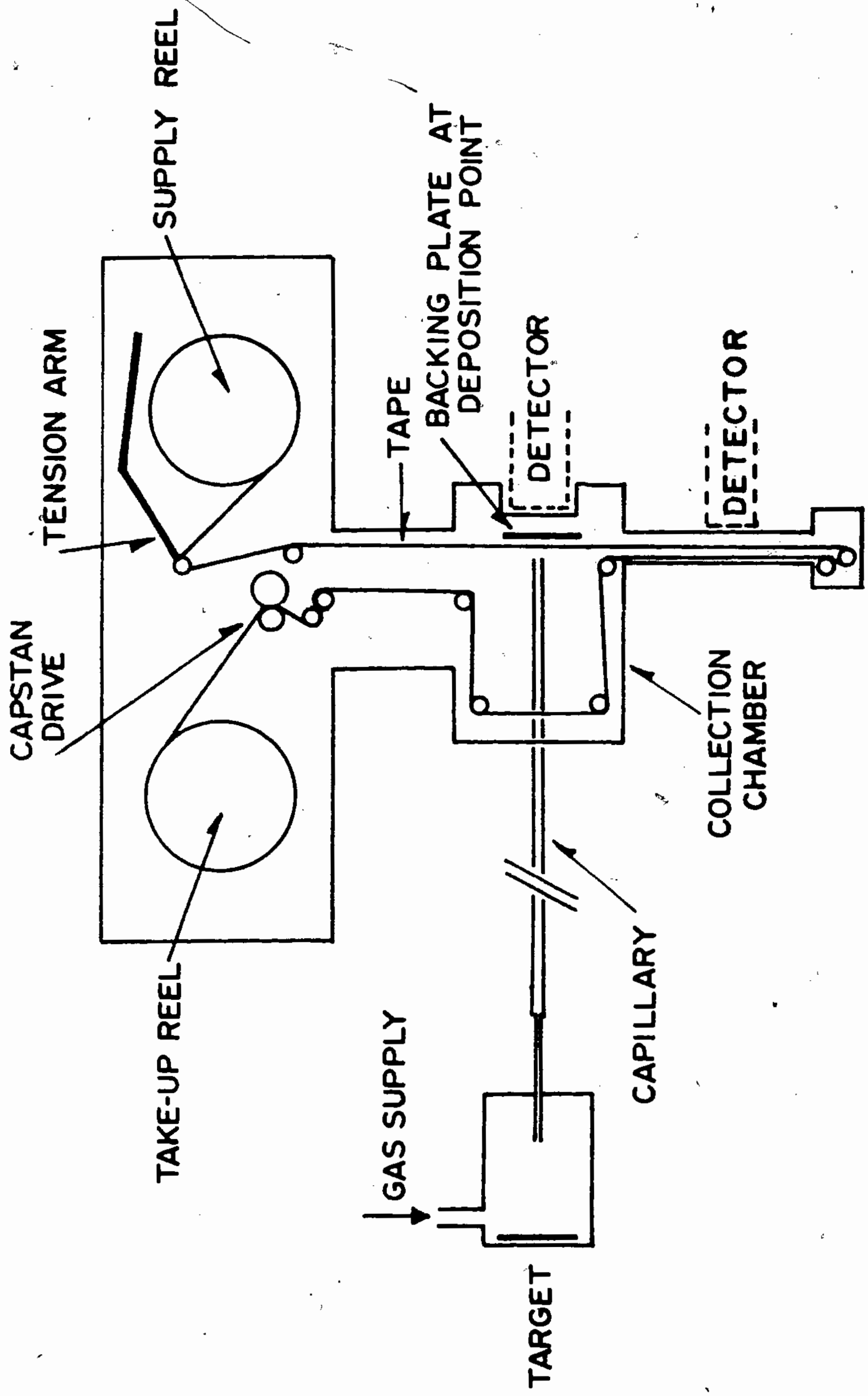

Figure 5. The gas jet transport system

The overall efficiency of the system at SFU was measured (Dau-73) to be about 75% for fission fragment transportation. However calculations (Wie-75c) have shown that 20-30% of losses occur in the production chamber where recoils reach the side walls before being thermalized. Thus, the measured overall efficiency reflects little loss in the transport process itself.

The present arrangment of the target cell of the SFU gas-jet transport system is schematically depicted in fig.6. The length of the production chamber can be adjusted to match the mean recoil energy of the reaction products. For the fission reaction the length was 8cm corresponding to a volume of 160cm^3. To reduce activation between experiments, the whole chamber can remotely be lifted up out of the beam-line. Also, the target ladder can be moved up and down by remote control and thus, six different targets may be used in one run. The flow rate of the helium gas at an outlet pressure of about two atmospheres was in the order of 40cm^3/s leading to a pressure in the production chamber of about 1 atmosphere and a pressure in the collection chamber of about 1.5mm of mercury.

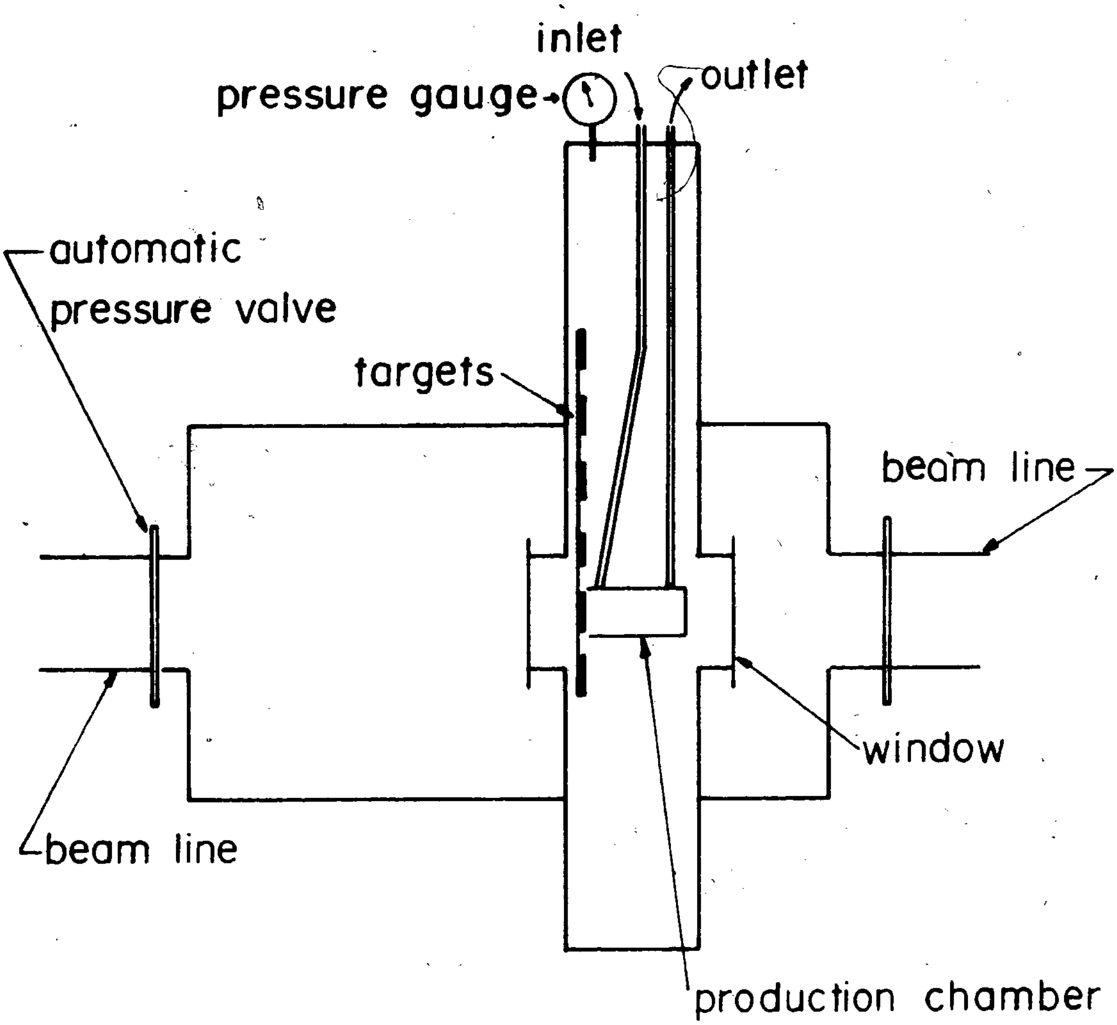

Figure 6. The target cell

A beam of 500nA with such a flow rate of helium, typically provides, for a collection of three seconds, an active spot with a counting rate of 5000 counts per second using the X-ray counter described in section V-1.

The gas carrying the radioactivity was allowed to impinge onto a discarded computer magnetic tape in an externally controlled movable tape system (fig.5). After a collection time of typically 3-10 seconds, the tape was moved a pre-determined distance to bring the collected sample of radioactivity to a position located between an appropriate combination of detectors, for a counting period which varied between 3 and 60 seconds. The timing of the different sequences was controlled by the computer associated to the data acquisition system.

IV-3 Chemical selectivity

IV-3-1 The ethylene system

The studies described below were undertaken to test the dependence of the Z of the fission products on the transport efficiency of the ethylene gas-jet system.

An energy spectrum between 5 and 150keV was recorded for each different flow rate of ethylene gas containing clusters. Two reservoirs of ethylene gas were used. One was capable of supplying clusters whereas the gas in the second reservoir was kept at a pressure under the critical pressure, thus preventing the formation of clusters. Both reservoirs were coupled together in order to keep constant the total inlet gas flow. The relative yield of most of the intense peaks, normalized to the 137.7keV gamma line was observed to remain about constant throughout the flow-rate variation studied (Wie-75a).

A striking features of all those spectra was the lack of X-ray lines corresponding to Te, I and Xe X-ray energies. Comparison of the X-ray spectrum obtained from a catcher foil placed directly behind the uranium target (no gas-jet was used) with that obtained through the same procedure of irradiation, delay and counting periods but using the gas-jet system proves that some elements such as Sb, Te and I are not collected by the gas-jet system. An interpretation is that uncollected products are formed either in the gas phase or form gaseous compounds with the transporting clusters and thus do not "stick" on the collector. The relative intensities of all other major peaks, corresponding to collected elements, normalized to the same Sb k_{α} X-ray line, have been determined for both spectra. These intensities appear to remain about constant for the two spectra. Thus, while the ethylene gas jet system may act as a selector for certain elements, for collected species the efficiency is largely independent of Z.

IV-3-2 Different transporting media

The purpose of the following studies was twofold, namely to a) find other efficient transporting media to replace ethylene which, under bombardment with charged particles, might undergo polymerisation and b) to determine whether other materials would provide any form of selectivity when used as transporting media in a gas-jet system.

In this investigation the usual ethylene clusters were replaced by clusters generated by "atomisation" of selected liquids. Fig.7 shows the design of the aerosol generator (Wie-75b).

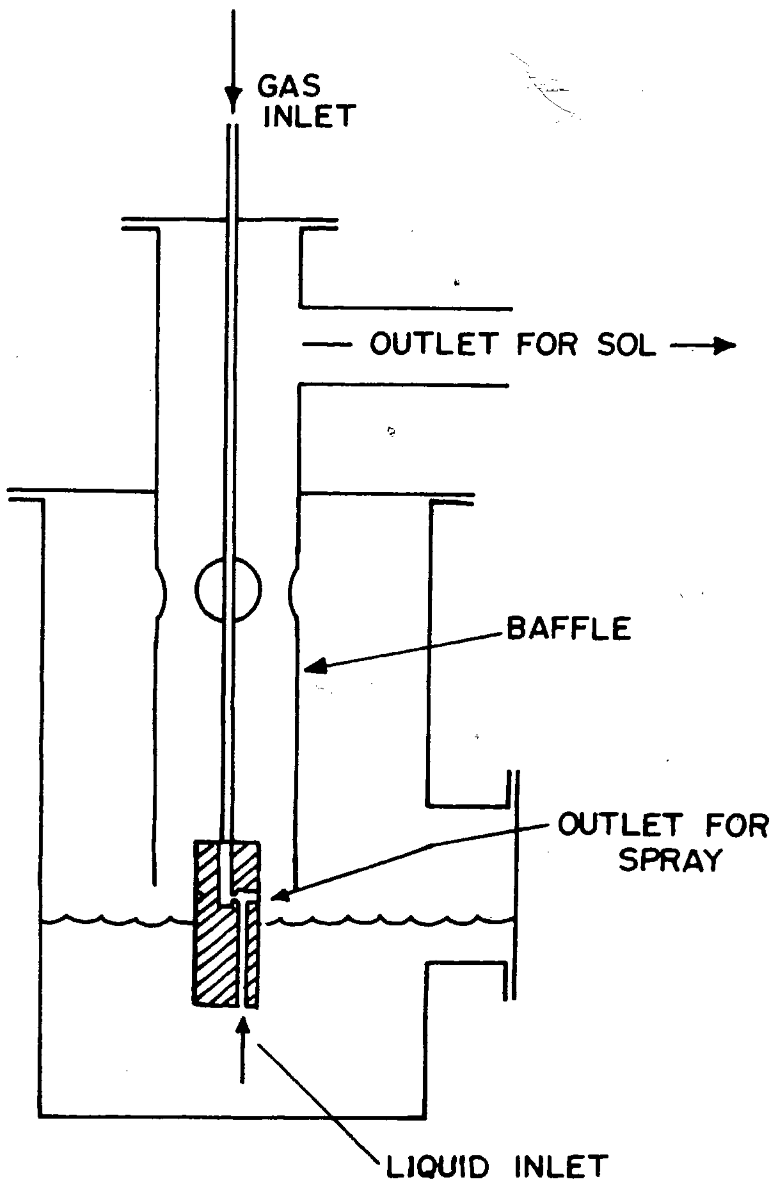

Figure 7. The aerosol generator

Clusters were made in each case by blowing nitrogen gas through the "atomiser". The cluster density was varied by changing the amount of nitrogen entering the atomiser. The total gas flow through the capillary was kept constant by accordingly changing the amount of nitrogen supplied by the second reservoir (see fig.8). Between two runs of different liquids, the system was "flushed" with nitrogen alone to eliminate traces of any remaining liquid. An identical experimental procedure was followed for each liquid. The yield curve for each individual liquid was then obtained by integrating the collected activity between 5 and 150keV (fig.9).

The comparison between the X-ray spectra of fission fragments transported via a given liquid indicates, as already seen for ethylene, that the variation of the cluster concentration does not cause a variation of the pattern of the spectrum, i.e., the relative peak areas remained constant through the flow-rate variations studied.

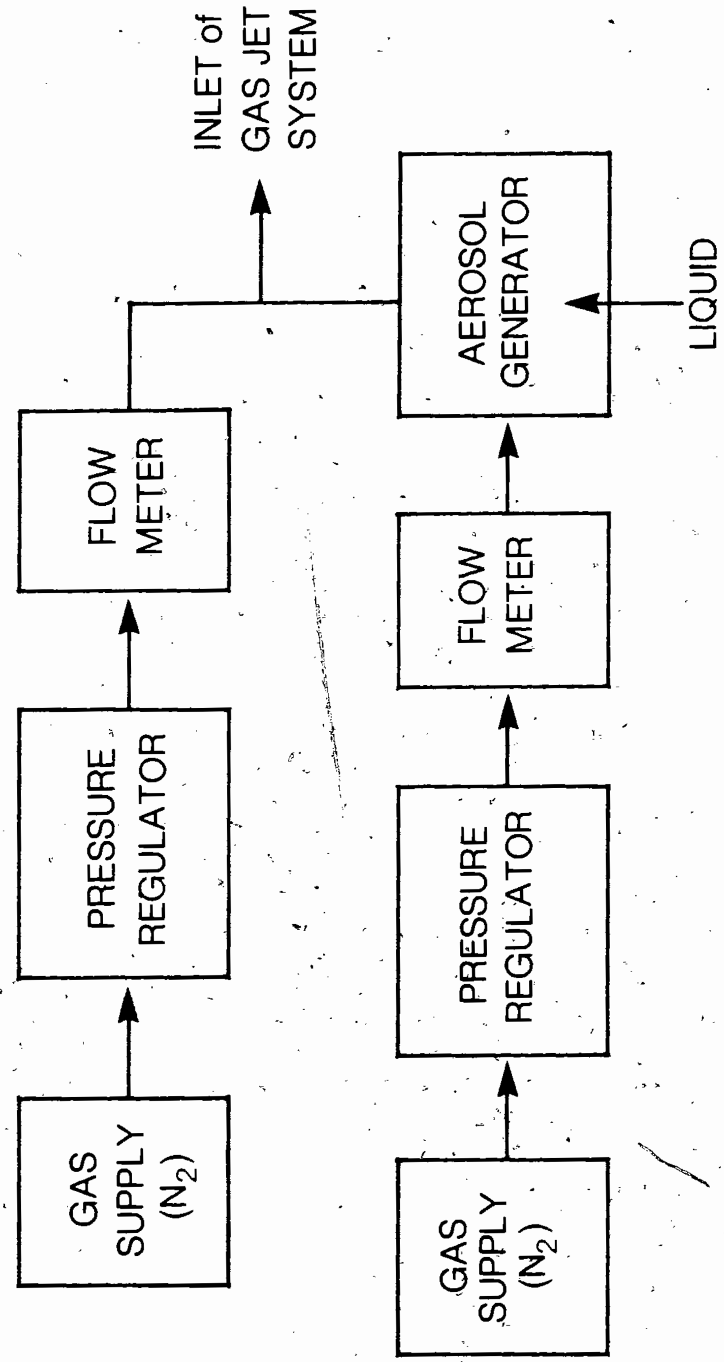

Figure 8. The gas supply set-up

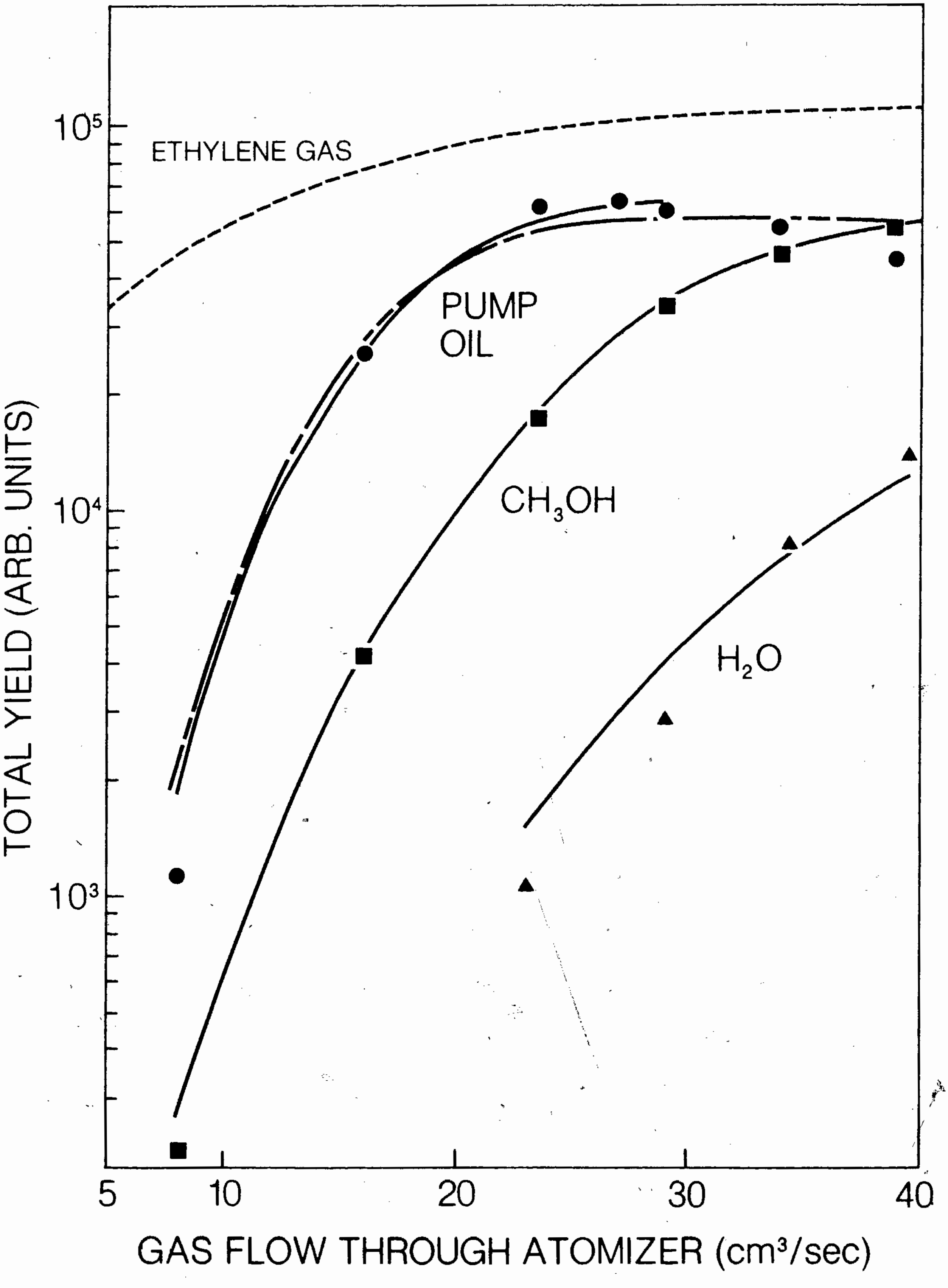

10⁵
10⁴
10³
ETHYLENE GAS
PUMP OIL
CH3OH
H2O
TOTAL YIELD (ARB. UNITS)
5
10
20
30
40
GAS FLOW THROUGH ATOMIZER (cm³/sec)

Figure 9

Chemistry between transporting clusters and recoiling nuclei has been shown to be a means of an on-line selection system (Kos-75, Cab-75). At TRIUMF, similar chemical selection has been observed when using an argon gas target (Bis-76).

In the first part of the experiment, the argon and the ethylene-gas, with clusters, were mixed together before entering the production chamber. In the second part, nitrogen gas was injected into the atomiser containing methanol. Ar-gas was then added to the mixture at the outlet of the atomiser. Fig.10 displays the two gamma-spectra collected using a Ge(Li) counter at the end of the gas jet system. The tape-drive collection system was used to collect the transported activity. The sequence of 10s-collection/10s-counting was repeated continuously until adequate statistics were obtained. It can be seen that halogen products are only collected when methanol was used.

This selectivity was used to collect $^{20-21}F$ from the spallation reactions induced by 480MeV protons on natural aluminium. The end-point energies of the beta spectra associated with the decay of these isotopes were used as high energy points in the calibration of the beta telescope.

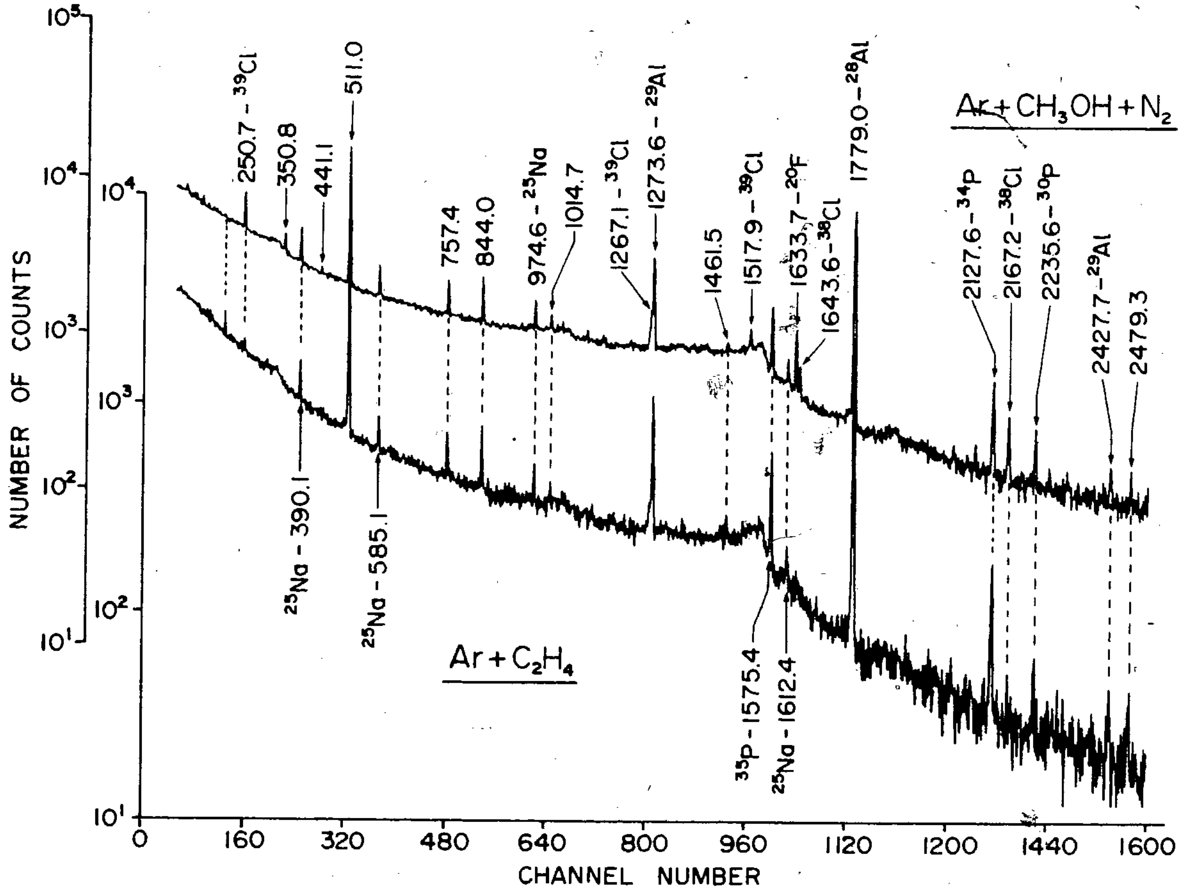

Figure 10. Gamma spectra collected from an Ar target

Although, no trace of polymerisation has been observed in the TRIUMF system with ethylene, it has been preferred to use helium-gas carrier of methanol droplets for all spectroscopic studies of fission products. The main reason for such a choice was the high intensity in the collected gamma-spectra of the annhilation gamma-line at 511keV (arising from beta-plus decay of low Z nuclear reaction products of C or N) when using ethylene or nitrogen.

V- DETECTION, DATA ACQUISITION AND DATA ANALYSIS TECHNIQUES

V-1 Gamma detection

The low energy gamma counter employed in this work was a 0.5cm^3 coaxial Ge(Li) detector which had an energy resolution of 0.50keV for 14.4keV gamma-rays. The high energy gamma detection system consisted of 2 Ge(Li) detectors. One of 40cm^3 with an energy resolution of 2.6keV for 1.33MeV gamma-ray and an efficiency of about 5% (relative to a 3"x3" NaI(Tl) crystal). The other was a 60cm^3 counter with an energy resolution of 1.9keV for the 1.33MeV gamma-ray and an efficiency of about 18%.

The energy calibration of these gamma counters was performed by using standard sources. ^{241}Am and ^{60}Co were used for the X-ray counter and ^{226}Ra and ^{22}Na for the gamma counters. The effiency of the Ge(Li) gamma systems as a function of energy was determined using the ^{226}Ra source (Bow-74) while the ^{226}Ra, ^{57}Co and ^{241}Am sources were used for the Ge(Li) X-ray systems.

The absolute efficiencies of the Ge(Li) counters used in beta-gamma experiments have been measured at a source-window distance corresponding to the experimental conditions (.5cm). A calibrated source of ^{241}Am was used for the low energy gamma detector while a calibrated source of ^{60}Co was used for the high energy gamma detector. 6.5% efficiency was measured for the .5cm ^{3} Ge(Li) detector at 59.5keV while for the 60cm^3 Ge(Li) detector an efficiency of 5.5% was measured at 1332keV.

V-2 Beta detection

V-2-1 Description

The detector used to measure the kinetic energy of beta particles is a DE-E plastic scintillator counter made of NE102A plastic. Such a arrangement helps to reduce the effects of background radiation, e.g., from the nearby collection spot, to minimize the gamma sensitivity of the detector and to lower backscattering effects (Bec-69). Also, it acts as a collimator by reducing the solid angle of detection, thus allowing for removal of most of the events corresponding to beta-rays escaping the E-detector and not depositing their full energy.

The DE detector is a 1mm thick disc, 2.54cm in diameter. The E counter is a cylinder 5.08cm in diameter and 5.08cm deep. A discriminator was set on the DE signal as shown schemattically in fig.11. Also displayed in fig.11 is the variation of the energy loss versus the kinetic energy for electrons in plastic.
The low energy cut-off permits the exclusion of low

Figure 11.

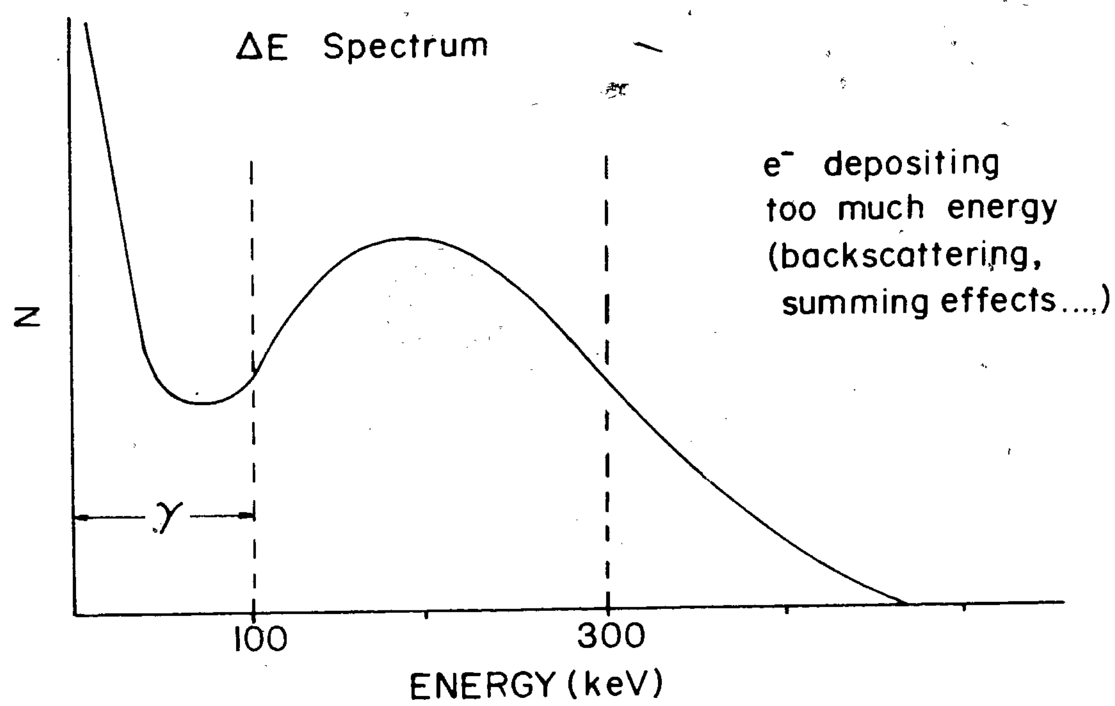
ΔE Spectrum
e⁻ depositing
too much energy
(backscattering,
summing effects....)
N
γ
100
300
ENERGY (keV)

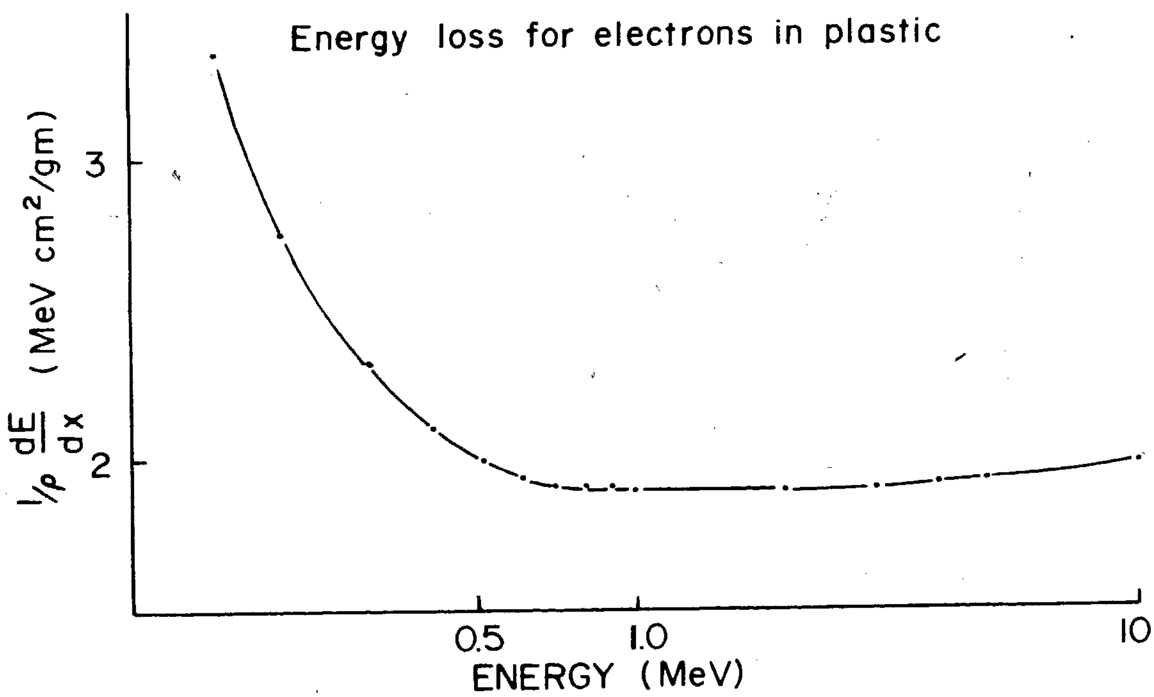
Energy loss for electrons in plastic
1/ρ dE/dx (MeV cm²/gm)
3
2
0.5
1.0
10
ENERGY (MeV)

amplitude signals associated with gamma-rays losing a little energy (mainly, by Compton interactions) in the DE counter. A high percentage of signals corresponding to events depositing too much energy is excluded by the high amplitude cut-off. Such events are mainly due to summing effects (see below) and electrons backscattered in the main counter. Thus, only DE signals corresponding to deposited energies between 100 and 300 keV were used in the DE-E coincidence requirements. A coincidence output was generated when such a defined signal was coincident with a signal coming from the E counter.

V-2-2 Calibration

The calibration of the DE-E system was done using the following beta standards:

The beta end-point energies from:

^{32}P E =1.7104 ± 0.0014 MeV (Wap-77)
^{90}Y E =2.289 ± 0.003 MeV (Wap-77)
^{144}Pr E =2.996 ± 0.011 MeV (Wap-77)
^{106}Rh E =3.541 ± 0.015 MeV (Wap-77)

Two other calibration points were obtained from the beta spectra in coincidence with the 976keV and 1633keV gamma lines in the decays of ^{25}Na and ^{20}F, respectively. These isotopes were produced via the following nuclear reactions on an aluminium foil:

$$^{27}Al\ (p,3p)\ ^{25}Na \quad \text{and} \quad ^{27}Al\ (p,5p3n)\ ^{20}F$$

The associated beta end-point energies are:

^{25}Na (976keV)	E=2858 ± 7 keV	(Wap-77)
^{20}F (1633keV)	E=5398 ± 6 keV	(Wap-77)

Beta-rays from the active spot have to go through the thin plastic wall (1/32") of the collection arm before penetrating the telescope (fig.5). To take this effect into account a piece of the same plastic was placed before the DE counter during the calibration measurements with the beta standards. The calibration was achieved by an iterative procedure. First, a simple Kurie-plot (Mar-70) analysis was performed to obtain a first estimate of the end-point channel of each of four standard beta spectra.

A first calibration line, energy versus channel, was thus derived. This line was then used to analyze each calibration beta spectrum with the "KURIE" code (see section V-6) with the response function (see section V-6) folded in. The process was repeated in an iterative manner until self-consistent results were obtained.

Then, a linear least-square fit was performed on the six points (4 from the beta standards and 2 from the beta spectra obtained from the nuclear reactions on aluminium) to get the final beta calibration line with the associated errors. The fig.12 displays the final energy calibration of the beta telescope.

The high energy point corresponding to the end-point energy of the beta transition populating the first excited state in ^{11}B from the decay of ^{11}Be has not been included in this calibration (see section V-6).

Sum-events occur when two events of energies E1 and E2, respectively are "seen" by a detection system as one event of energy E1+E2. This effect arises when the time interval between the two events is short compared with the duration of the individual signal associated with an event. These sum-events are also referred to as "pile-up" events. A counting rate restricted to a

Figure 12. The calibration of the telescope

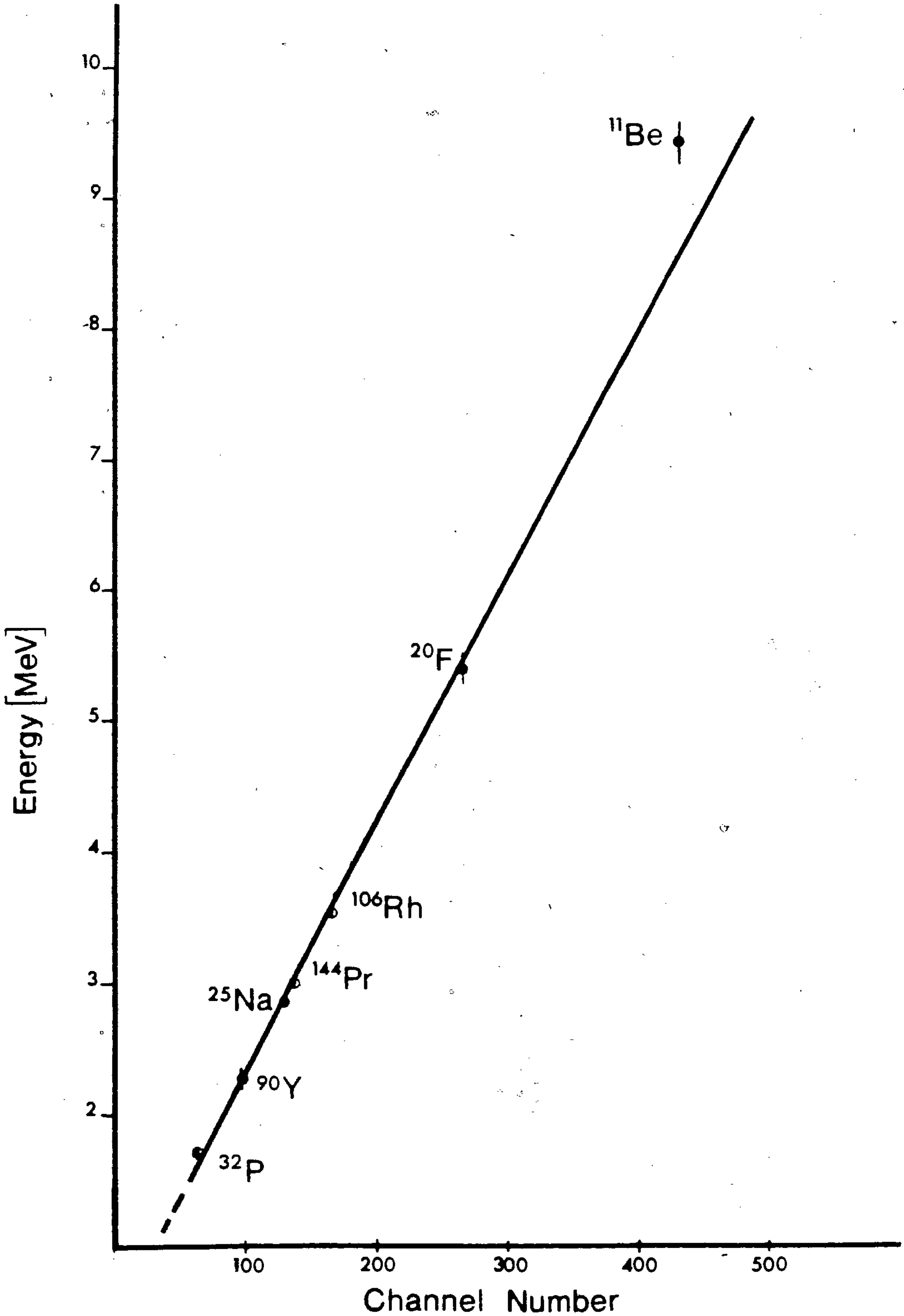

maximum of about 5000c/s was adequate to allow for this effect to be less than 1% and thus considered negligible.

The absolute efficiency of the beta-telescope has been measured for two transitions, namely, the beta transition in coincidence with the 622keV gamma line in the decay of Rh and that in coincidence with the 1633keV gamma line in the decay of F. For the first transition (Emax=2.41MeV) the efficiency was of the order of 1% whereas for the second one (Emax=5.42MeV) it was about 2.3%.

The calculated solid angle of the telescope system was about 15%. The DE-E coincidence requirement was measured to decrease the efficiency by a factor of about 2. If one assumes an intrinsic efficiency of the counters near 100%, the total efficiency of the beta telescope should be about 7%. Thus, the experimental values seem lower than expected. However, electrons go through the plastic wall of the tape-collection system (fig.5) and also through the material used for preventing light leakage. This extra material traps a large number of low enegy electrons. It was then assumed that such losses can account for much of the initial discrepancy.

V-3 Electronic configurations

In addition to "singles" types of experiments when only one detector is used, it has been necessary to set up several combinations of detectors and perform coincidence studies. Schematic block representations of the electronic systems used are displayed in fig.13.

The statistical variation of the time interval between two events in coincidence can be recorded as a "time-spectrum". True coincidence between "fast" events (here "fast" means that the time between two events is less than 5ns) generate signals of which the amplitudes are distributed around a specific time and thus give rise to the so-called prompt-peak in a "time spectrum". False coincidence events result in a "background" of signals spread at random over the entire spectrum.

In general, to differenciate between these two kind of events, a gate or window is set up on the time-peak so that only events whose time intervals generate signals inside this gate are recorded.

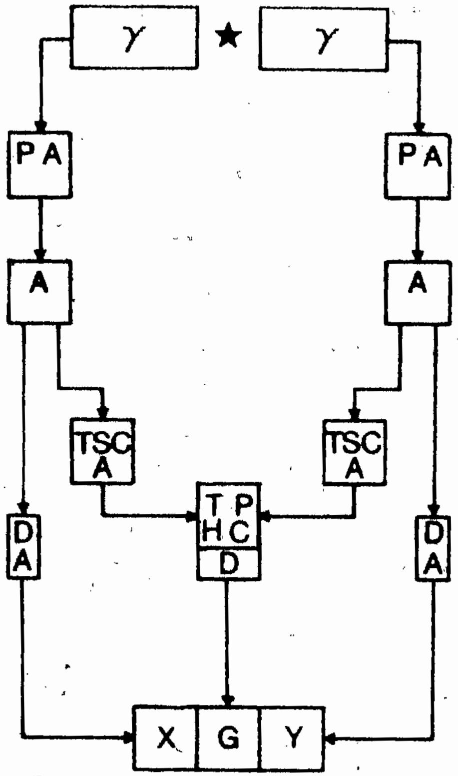

PA = Pre-Amplifier
A = Amplifier
DA = Delay-Amplifier
TSCA = Timing Single Channel Analyser
TPHC = Time-to-pulse Height Converter
D = Discriminator
G = Gate
CFD = Constant Fraction Discriminator
FD = Fast Discriminator
RM = Ratemeter

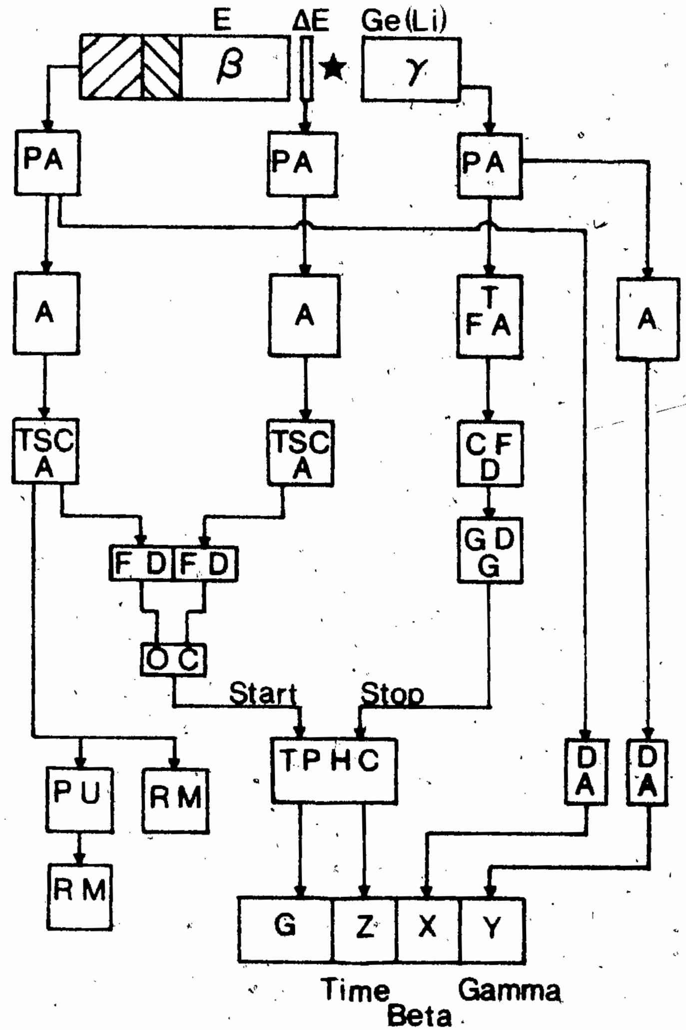

GDG = Gate Delay Generator
PU = Pile-up
OC = Overlap Coincidence

Figure 13. Coincidence systems

The intrinsic time resolution of a coincidence system is then the full width at half maximum of this peak. However, the time window corresponding to the electronic gate set at the bottom of the same peak defines the time requirement of the coincidence system and therefore represents the experimental time resolution.

In system "a",the time resolution was about 30ns and the time window used about 50ns. The system "b" has a time-resolution of 12 ns and the time-window was about 20ns. This resolution was measured for energies above 40keV for the low energy gamma-lines(10-300keV) and above 400 keV for the high energy gamma-lines (150-2000keV). These regions correspond to energy ranges for which constant-fraction discriminators (ORTEC-463) have a time-response independent of the amplitude of input signals. For low amplitude signals corresponding to low energy events the time-response of such discriminators depends strongly on the amplitude and therefore alters the resolution of the coincidence systems.

The resolution achieved in system "b" permits the determination, by the slope-method, of nuclear state lifetimes of about 10ns to about 200ns (Mfa-74). The slope method consists of fitting a simple exponential function to the slope of the peak in the time-spectrum.

In the beta-gamma coincidence experiments only the energy deposited in the E-detector was recorded. The energy loss occuring in the DE counter was treated as constant for particles with energies deposited in the E-counter above 1MeV (fig.11).

V-4 Data acquisition system

The data acquisition system is formed by eight equivalent 2048 channel "stretchers" coupled together via a multiplexer unit to a single ADC (Tennelec-series 620). The system stores incoming signals up to an amplitude of 8 volts if the gate in the multiplexer has been activated. A PDP15 computer is associated with this system. A general code, mainly written in focal language and called FOLDAP (Fol-73) handles all operations between the computer and the ADC's. Events are stored event by event in the "buffer-tape" mode.

Further, extension programs (Dau-79) allow one to record events according to special configurations such as in the multispectra mode. For instance, subsequent off-line analysis can generate a series of gamma spectra in coincidence with a particular X-ray line as a function of time, following interruption of the collection of activity.

V-5 Experimental conditions

The collection tape system described in section (IV-6) has been used for all experiments in the present study. The distance between the collection spot and the centroid of the detection system is adjusted mechanically. The speed of travel of the tape could also be adjusted, and the time for such a travel was typically about .7s. A stepping motor provided a rapid and reliable means of controlling the tape movement. The computer associated to the data acquisistion system controlled the motion of the collection tape in time sequences defined prior to experiment. A typical sequence was as follows (with the gas jet running continuously):

1-the collection tape moves to present a clean spot before the tip of the capillary

2-the collection period starts and lasts for a pre-selected time T1 (3-10s)

3-the tape moves to bring the active spot between the selected combination of detectors. The end of the motion starts the data acquisition.

4-the counting period lasts a time T2 (typically 10 to 60s). In multispectra mode this time is divided in n intervals such as nxt=T2 (typically t=1s)

5-At the end of the counting period the tape moves twice to present again a clean collection spot.

Such a sequence was repeated to accumulate adequate statistics. During off-line analysis the n coincidence spectra were retrieved, with the possibility of addition. For instance, to improve the counting statistics of long-lived nuclides, 60 intervals of 1 second were typically retrieved as 10 spectra of 1s intervals follow by 10 spectra of 2s intervals and finally 6 spectra of 5s intervals. Thus, 26 points could be obtained for most decay curves.

Also, in the off-line analysis it was possible to set energy thresholds on beta spectra of interest and then follow, separately, the decay of the total spectrum and of the high energy part only.

These times were chosen so that half-lives in the range of 1 to 60s could be obtained with good precision even in the presence of a complex decay curve and in particular in case of a parent-daughter relationship.

V-6 Data analysis systems

V-6-1 Gamma analysis

Photon spectrum data were analyzed using the SAMPO (Rou-69) and GAMANAL (Gun-72) Computer codes. (the latter being preferred for its more accurate analysis of complex peaks). The analysis generates gamma energies and peak areas with associated errors.

In X-gamma and gamma-gamma experiments, equal energy windows were set on the peak of interest and preferably on the near Compton continuum of higher energy gamma lines to extract, by subtraction, the true net coincidence gamma spectrum.

The electronic system "a" was used in the set-up of such experiments and the 50ns time window corresponded to a measured contribution from random coincidences of the order of 1%.

Fig.14 shows a total gamma spectrum collected using the 60cm^3 Ge(Li) detector, in coincidence with all beta-rays detected by the plastic telescope. The spectrum has been divided into 4 energy sections. The total energy range is from about 120keV to 2200keV. The accumulation corresponds to a one week run with a proton beam of 50-100nA at 480MeV.

Fig.15 shows the total low energy gamma spectrum in coincidence with all high energy gamma-rays of energies between 120keV and 2000keV. This spectrum was collected for a two shift period (2x12hours) with a proton beam of about 1micro-ampere at 480MeV.

Fig.16 displays four typical low energy gamma spectra in coincidence with four different X-ray gates, respectively. The gamma lines are labelled by the mass number of the isotope to which they have been assigned.

The following tables display the total resolutions achieved in the gamma detection system during typical beta-gamma experiments. These numbers are generated by the GAMANAL code during gamma spectrum analysis.

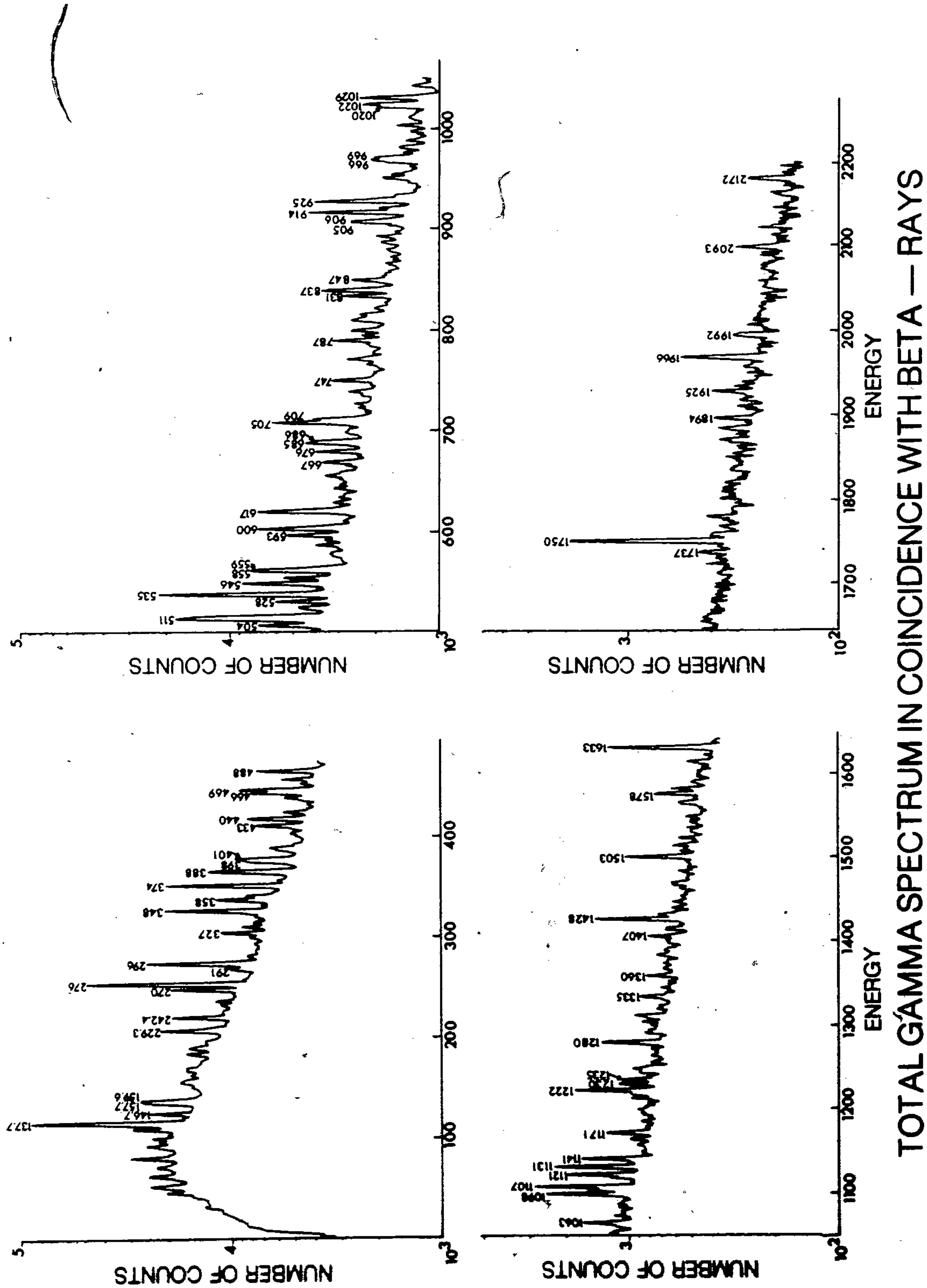
TOTAL GAMMA SPECTRUM IN COINCIDENCE WITH BETA — RAYS
ENERGY
ENERGY
NUMBER OF COUNTS
NUMBER OF COUNTS
NUMBER OF COUNTS
NUMBER OF COUNTS

Figure 14.

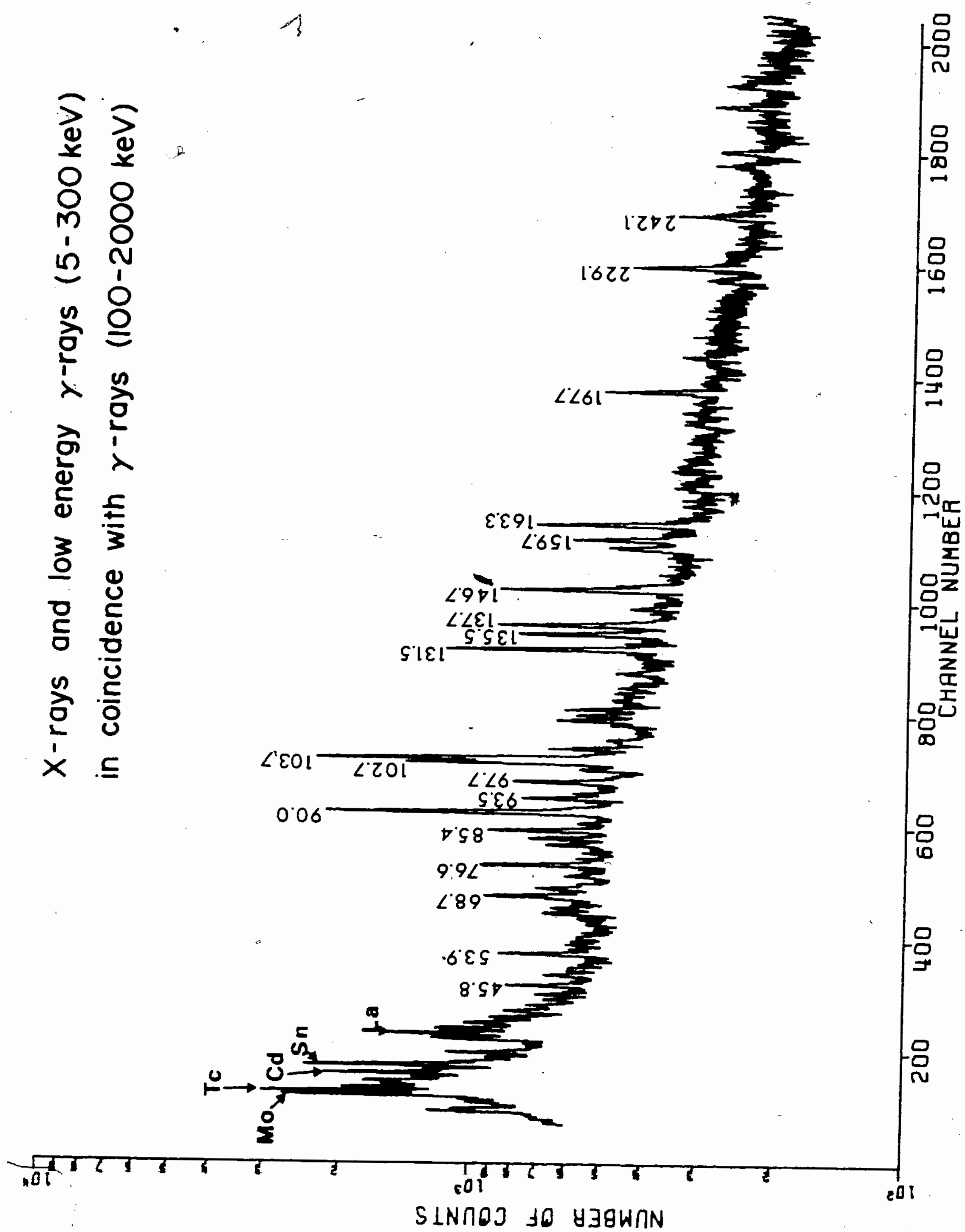
X-rays and low energy γ-rays (5-300 keV)
in coincidence with γ-rays (100-2000 keV)
Mo
Tc
Cd
Sn
La
45.8
53.9
68.7
76.6
85.4
90.0
93.5
97.7
102.7
103.7
131.5
135.5
137.7
146.7
159.7
163.3
197.7
229.1
242.1
CHANNEL NUMBER
NUMBER OF COUNTS

Figure 15.

Figure 16.

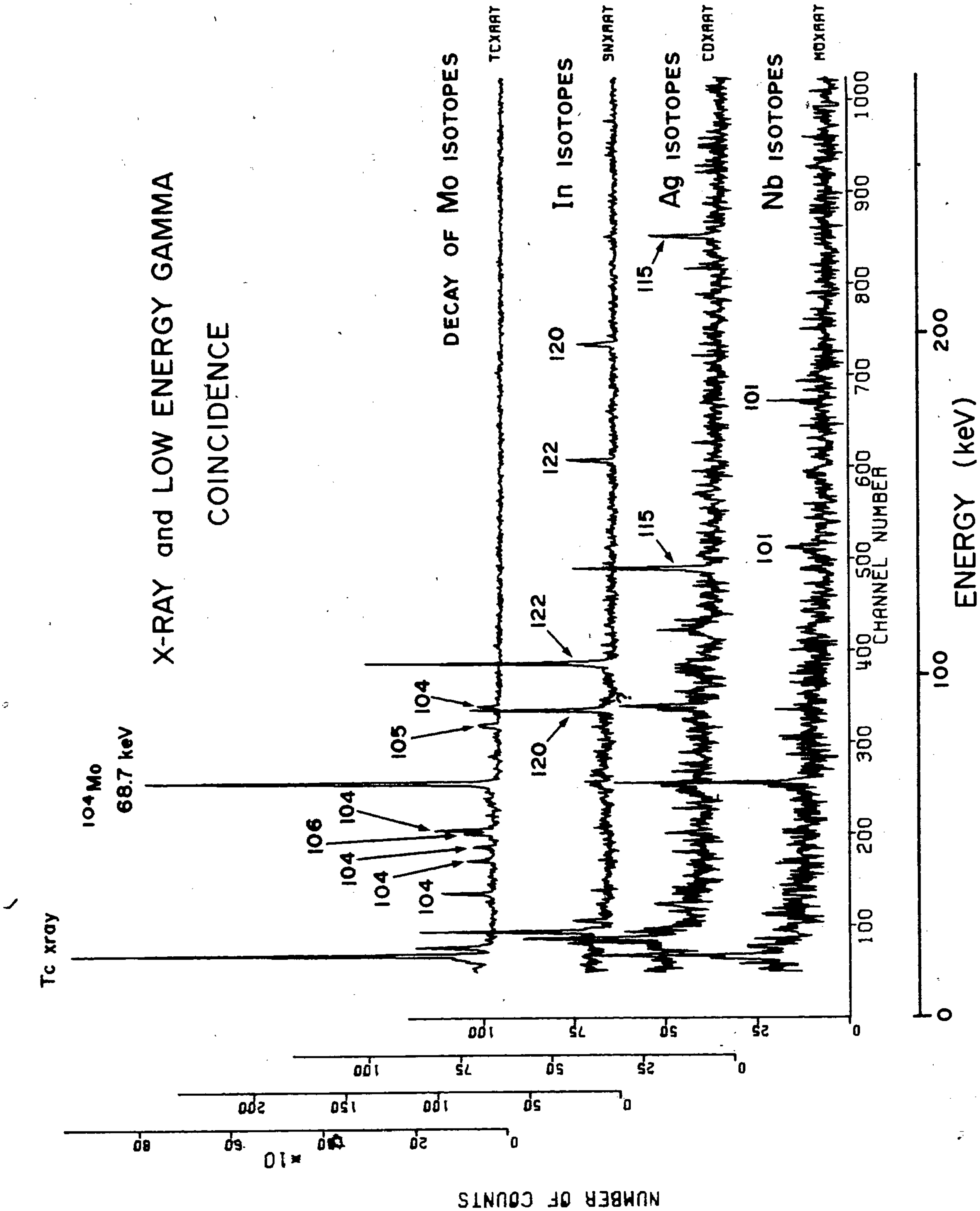
X-RAY and LOW ENERGY GAMMA
COINCIDENCE
DECAY OF Mo ISOTOPES
In ISOTOPES
Ag ISOTOPES
Nb ISOTOPES
TCXRAT
SNXRAT
CDXRAT
MOXRAT
Tc xray
^{104}Mo
68.7 keV
CHANNEL NUMBER
ENERGY (keV)
NUMBER OF COUNTS
x10

$0.5cm^3$ Ge(Li)	
gamma energy	resolution
53.9 keV	0.42 keV
93.6	0.49
137.7	0.57
229.0	0.73

$60cm^3$ Ge(Li)	
gamma energy	resolution
229 keV	2.3 keV
535	2.3
837	2.7
1334	2.9
1750	3.0

V-6-2 Decay curves analysis

In the single detector experiments, where the counting rate involved is usually high, data were recorded with a constant rate pulser signal entering the pre-amplifier of the detector. From the difference between the number of counts in the pulser peak and the number of pulses delivered, one can obtain an estimate of the dead-time of the data acquisition system and subsequently perform the appropriate correction.

Half-lives presented in this work were extracted using a least-square fit program allowing for parent-daughter relationships. The code "FITTIM", written by W. Wiesehahn (Wie-76), uses a regular iterative least square fitting procedure. The fit is, however, corrected for the finite bin width of the time intervals. It allows for either a fit of the sum of up to three different exponential decays with a constant background or for a fit of 1parent-1daughter decay relationship.

The nuclear half-lives of 20 delayed excited states have been determined (table-III). The time spectra of beta-gamma coincident events associated with chosen gamma gates contain contribution from the Compton part of gamma transitions of higher energies. This contribution was corrected for by subtracting the time spectra corresponding to gamma gates set on the near continuum. A simple exponential function was fitted to the slope of the resulting spectrum (Fos-74). Fig.17 displays two typical examples of decay curves obtained from such an analysis.

When coincident events are detected in two different counters of different energy ranges, each of the counters is associated with one side of the time-peak. Therefore, it is possible to deduce the relative position, in time, of the two events in coincidence. One event corresponds to the population of the "delayed state" while the other corresponds to its deexcitation.

Figure 17.

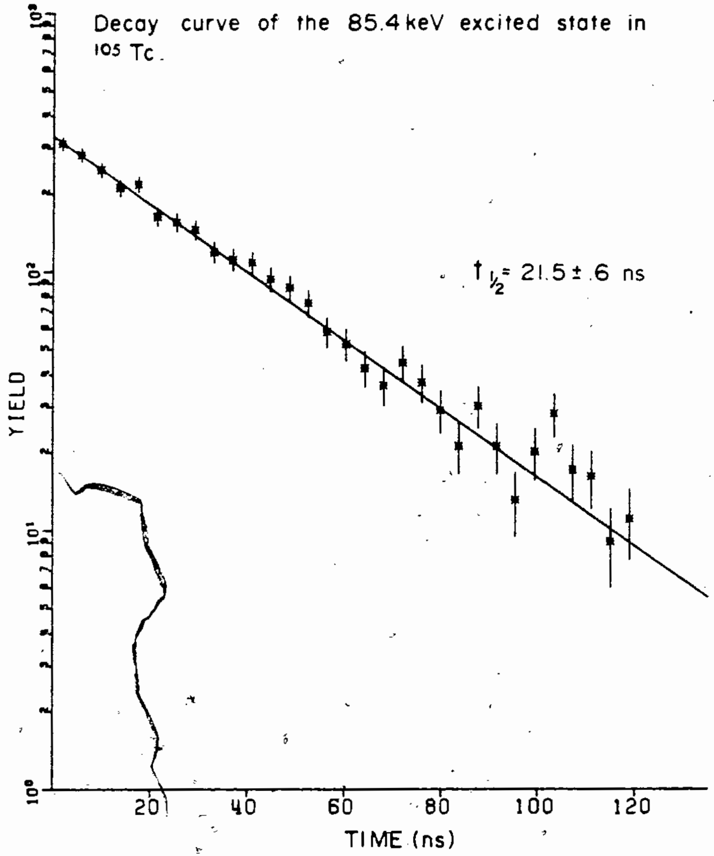
Decay curve of the 85.4 keV excited state in
105 Tc.
t½= 21.5 ± .6 ns
YIELD
TIME (ns)

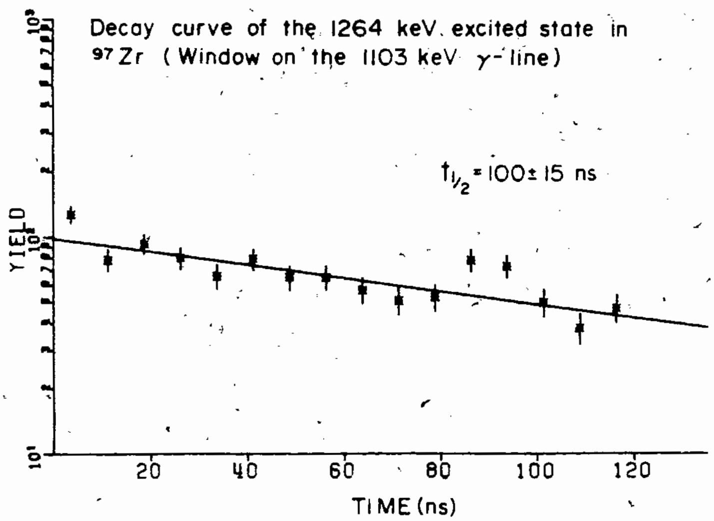
Decay curve of the 1264 keV excited state in
97 Zr (Window on the 1103 keV γ-line)
t½ = 100± 15 ns
YIELD
TIME (ns)

V-6-3 Beta analysis

Beta spectrum data were analysed using the computer code, "KURIE", written by P. Rogers (Rog-65b) and modified by W. Wiesehahn to allow it to be used on the SFU IBM370 computer.

Beta spectra collected by the data acquisition system in 2048 channels were summed every 4,8 or 16 channels to reduce spectra to 512, 256 or 128 channels respectively, and thus, to increase counting statistics before analysis. The resulting reduction in the energy resolution is considered negligible when compared with the errors associated with the determination of end-point beta energies. Before the summation, a beta spectrum in coincidence with a gamma gate set as close as possible to the peak of interest was subtracted from the beta spectrum in direct coincidence with this specific peak.

The "KURIE" program first transforms a total theoretical spectrum, with end-point energies supplied as first estimates (which may contain several components), into a corresponding detector pulse amplitude spectrum and then compares the latter with the experimental one (Woh-72). For the conversion, a response-function of the detector (fig.18) is inserted into the computer code. Such a function defines the response of the detector for mono-energetic electrons. The lack of accessible mono-energetic electron sources in the energy range of interest has not permitted an experimental investigation of the actual response-function of the telescope and the mathematical expression of ref.(Rog-65b) has been utilized.

Values of the parameters b and W (fig.18) were initially taken as b=1% and W=5 % as suggested in refs.(Rog.65b, Sti-78). These parameters were then varied in the fitting of ^{32}P and ^{144}Pr beta spectra, respectively until lowest "chi" squares were obtained. Following an iterative procedure to attain best fits, a value of 8% of the centroid-energy at 5MeV was selected for W. The energy dependence of this width (W) has been taken as a linear function of the square-root of the electron kinetic energy. The height of the tail has been taken as 1% of the peak height of the distribution.

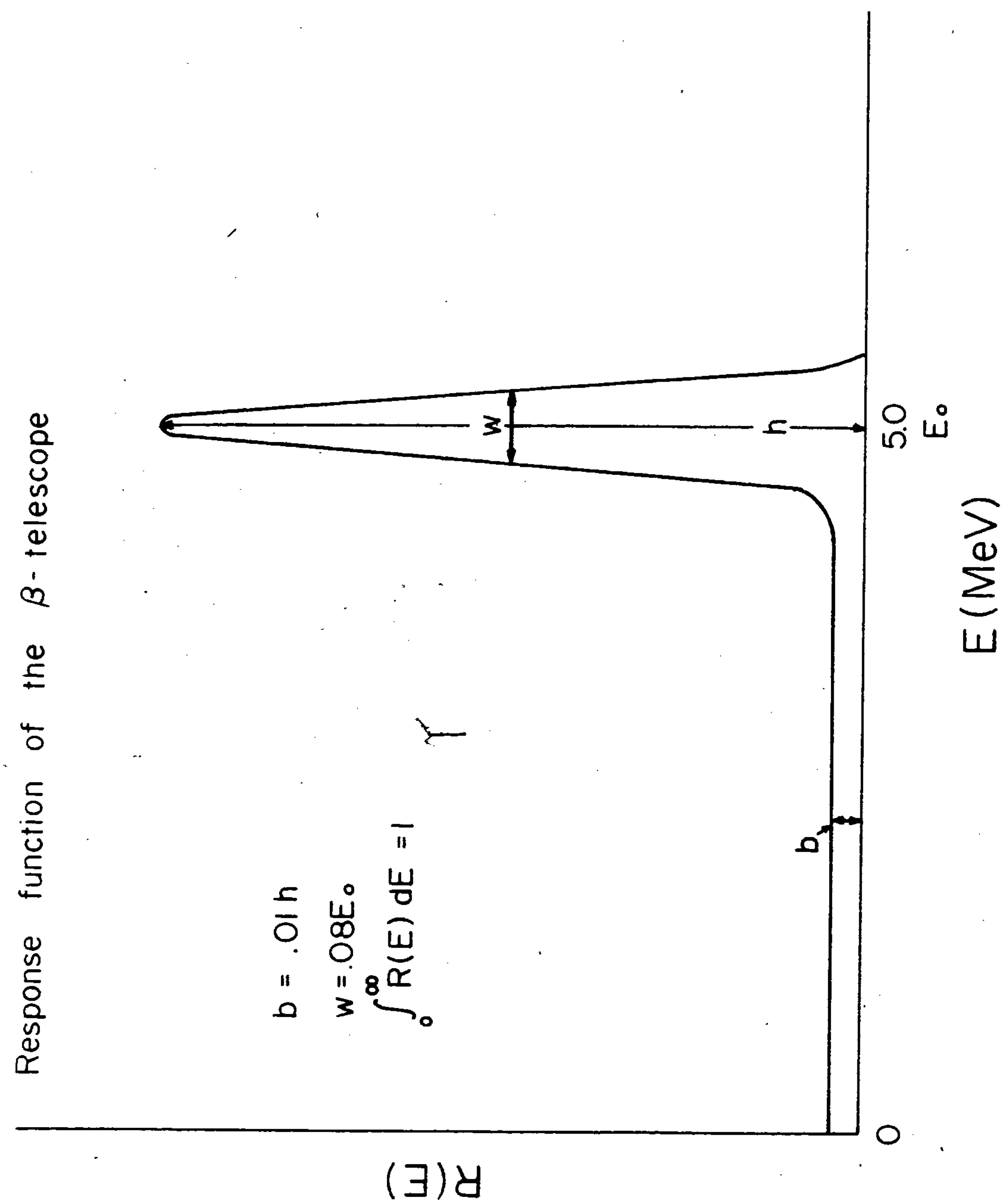
Response function of the β- telescope
b = .01 h
w = .08E₀
∫₀^∞ R(E) dE = 1
w
h
b
R(E)
0
5.0
E₀
E (MeV)

Figure 18.

The KURIE code permits the fitting of spectra with several components and analyses of allowed as well as first forbidden shape spectra. The program generates a "Kurie-plot" for the total spectrum as well as for each component. These curves serve as checks for the existence of unpredicted branches. The error associated with the end-point energies are generated through the fitting routine. These errors are then multiplied by the square root of the normalized "chi" square (X^2/d.f., d.f.=degree of freedom). To these individual errors the calibration error (see section V-2-2) is quadratically added. Since the energy loss in the DE counter remains approximately constant (fig.11) for electrons of kinetic energies greater than 1MeV, analyses of beta spectra were only performed for energies above this threshold.

For the ^{11}Be beta spectrum a reasonable fit could not be obtained with "KURIE" when using the usual parameters. A good fit was, however, arrived at with b=5% and W=5% The increase in b is consistent with very recent studies of similar beta telescopes (Ott-79). Since the decrease in W could not be easily explained, the beta spectrum of ^{11}Be was not used for energy calibration purposes.

In view of these results the ^{20}F and ^{25}Na spectra were re-analysed varying the fitting parameters (b and W). The best fits were obtained with b=1% and W=8% for ^{25}Na and with b=3% and W=8% for ^{20}F. The end-point energy of the ^{20}F spectrum was raised by 80keV which is within the experimental error. It has then been assumed that most of the error introduced by the empirical response function is accounted for in the calibration.

These preliminary results call for further investigations and especially for experiments to determine the behavior of the response function of the telescope at high energies (>8MeV) for which the finite size of the E counter becomes an important factor.

The KURIE code generates, for each individual beta spectrum component, the associated logft-value. This value is a function of the matrix element associated with the beta transition and depends upon the spins and parities of the initial and final states involved. Thus, experimental determination of the logft-value associated with a specific beta transition could provide information about spins and parities of the nuclear states involved (Mar-70).

In the present study only the A and the total half-life of the decaying nuclide were entered as input parameters in these calculations and, subsequently, only maximum logft-values were generated.

A program called "BETAS" has been written to generate simulated experimental beta spectra. The code generates a beta spectrum which may be the result of the summation of several spectra whose end-point energies as well as the total integrated number of counts can be chosen a priori, individually. Each individual theoretical spectrum is corrected for the effect of the response function of the detector before summation. This part of the program was taken directly from the KURIE code. The effect of Poisson counting statistics is then superimposed on the sum-spectrum so that the counts per channel could be distributed as experimental data. Due to the statistical nature of beta transitions the determination of end-point energies using the KURIE code has been found to be 100% reliable only above a certain statistical limit. Above an average of 20 counts per channel the analysis was found independent of the total number of counts in the spectrum as well as of the chosen bin width. Under this limit, measured end-point energies were usually too low. With an average of 2 counts per channel measured energies may be as much as 150keV lower than the actual value of 4.5MeV.

However, measured end-point energies were found closer to the actual values with increasing bin width. Therefore, all beta spectra were analysed with different bin widths and when disagreement occured the highest end-point energy prevailed. In the case of a large disagreement, the "chi" squares values were high (>5) and, generally, the analysis was rejected.

All complex beta spectra were analyzed as two component spectra where the low energy branch does not have, in general, any realistic significance. This low energy branch generally represents an average of several beta transitions populating higher levels (Pandemonium effect).

Above the limit of 20 counts per channel per branch the determination of the high end-point energies was found to be very reliable. Under this limit problems arise. Depending on the relative intensity and the separation energy of the the two branches, the high energy branch may be missed by the program.

The assumption taken when analysing complex beta spectra with only two component spectra has been proven to be reasonable one only above the statistical limit of 20c/ch. and for end-point energies separated by at least 500keV.

For the present experimental results, the statistical limit of 20counts per channel (overall average) corresponds to about 1count per keV. Thus, for a spectrum with an end-point energy of 4MeV this limit corresponds to an integrated number of counts of 4000. Under this limit, the fitting routine can lead to end-point energies lower than the true value. The difference mainly depends upon the statistics and the bin widths chosen for the analysis. The difference between the true value and the result of KURIE was plotted for several total statistics and several bin widths. For single component beta spectra where the integrated number of counts is easily known these curves help to assess a systematic error to the end-point energy determined by the KURIE code. This procedure introduces a new source of error which was estimated from the above curves and directly added to the error generated by KURIE.

For complex beta spectra, other parameters such as the end-point separation energy and the relative intensities of the two branches render more difficult the determination of the systematic error on the high energy end-point. Also, an estimate of the number of counts in this high energy branch becomes difficult to assess.

Several tests were performed with the BETAS simulation program on two component spectra. An important result was that for separation energies greater than 1.5MeV and for an intensity of the high energy branch even as low as 1% of the low energy branch, the true end-point values were within the quoted errors. This would apply as long as there was at least an overall average of 20c/ch in the high energy branch. In the present study all complex spectra analyzed as 2 component spectra have end-point separation energies greater than 1.5MeV. However, the constraint imposed on the number of components could mean that components with intermediate end-point energies were not "seen" by KURIE. Obviously, this is also true for high energy branches whose relative intensity is low with respect to lower energy branches.

Tests on a simplified beta decay of ^{102}Nb have been conducted using the simulation program BETAS. The sum-spectrum of 3 transitions with end-point energies of 4.3(B1), 6.4(B2) and 7.0(B3) has been analysed by KURIE as a 2 component spectrum for several relative intensities. A reasonable end-point energy for the B3 branch was obtained when the average number of counts in this branch was over 20c/ch and the relative intensities in the ratio B1=10, B2=1, B3=10. For a higher B2/B3 intensity ratio the high energy end-point was measured to be between 6.64 and 6.79MeV. Reducing the average number of counts in B3 to under 20c/ch and with different B2/B3 ratios the high energy end-point ranged from 6.4 (the B3 component was not seen) and 6.72MeV.

From the above studies, it has been concluded that it was not feasible to assess accurately the systematic error due to low statistics. A weak high energy branch may have been missed by KURIE. Therefore, for nuclides of unknown decay schemes, the measured end-point energies and corresponding deduced Q_{β}-value may only represent a lower limit.

Each individual beta spectral analysis was checked both visually and for the generated "chi-square" value. Occasionally, analyses produced high chi-square values (>3) but visual inspection indicated that the poor fit occurred generally in the low energy region.

V-7 Isotopic assignment and decay scheme construction

Identification of most of the observed gamma-lines has been achieved by comparing experimental energies and half-lives with those available in the literature. Coincidence X-gamma data help in the identification in Z of the gamma-lines of energies between 40 and about 2000keV. The comparison between literature and experimental half-lives most often gave the final identification (Z and A). In some cases, gamma-lines were not in coincidence with any X-ray or statistics were too poor to permit determination of a precise decay constant. In these cases, gamma-gamma coincidence data were sometimes helpful, especially when unknown lines were determined to be in coincidence with an already assigned line.

Coincidence relationships between different lines were also required to start the construction of decay schemes. Relative intensity data for gamma lines observed in "singles" or in beta coincidence were normalized and corrected for detector efficiencies.

Large discrepancies between "singles" and beta coincidence data indicate that an intermediate long-lived state has been populated in the decay process.

The most intense line in a specific coincidence relationship has been assumed to depopulate the lowest energy level. Further, low-energy gamma-gamma delayed coincidence data can sometimes lead directly, as discussed earlier, to the relative position in the decay scheme of the two gamma lines under consideration.

Relative intensities are only reported for gamma lines whose identification was straightfoward (measured half-lives corresponding to the decay of the isotope of interest). These intensities were measured from the beta-gamma coincidence experiments. The values are generated by the gamma fitting routine. In the absence of interfering gamma lines, the calculated relative intensities are believed to be within 10% (see the decays of ^{96m}Y and ^{116m}Ag for examples). High discrepancies between the literature and these values are therefore indicative of interfering gamma lines (see the discussion about the 617keV gamma line in ^{96m}Y).

VI- RESULTS

A total of 40 isotopic decays have been investigated through the present study. The nuclides concerned cover a range from Z=37 to Z=49 and from A=91 to A=123. Many of these nuclides have two isomeric states, and in a few cases it has been possible to determine the relative position in energy of the isomers (fig.19).

Table-II presents a comparison between recent end-point energy measurements and corresponding results obtained in this study. The general good agreement shows the feasibility of the technique used to derive beta end-point energies.

Table-III presents the half-lives of some long-lived excited nuclear states derived from the beta-gamma coincidence experiments.

Table-IV presents a comparison between Q_β-values obtained in this study and corresponding total beta decay energies predicted from current mass formulas.

Table-V compiled the end-point beta energies and associated Q_β-values of the nuclides studied.

Table-VI lists all observed gamma lines with their half-lives, coincidence data, associated beta end-point energies and their isotopic assignments.

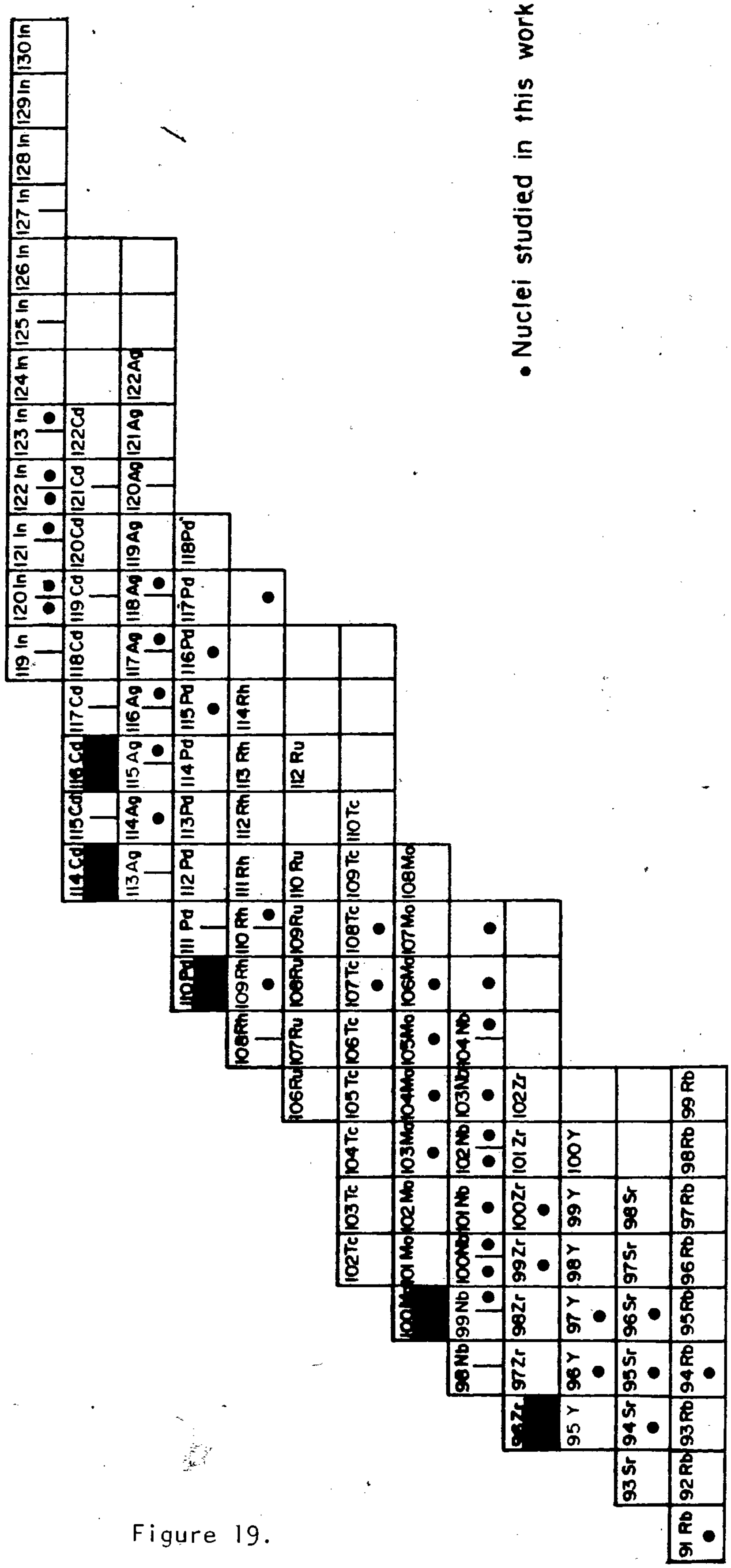
• Nuclei studied in this work
119 In 120 In 121 In 122 In 123 In 124 In 125 In 126 In 127 In 128 In 129 In 130 In
114 Cd 115 Cd 116 Cd 117 Cd 118 Cd 119 Cd 120 Cd 121 Cd 122 Cd
113 Ag 114 Ag 115 Ag 116 Ag 117 Ag 118 Ag 119 Ag 120 Ag 121 Ag 122 Ag
110 Pd 111 Pd 112 Pd 113 Pd 114 Pd 115 Pd 116 Pd 117 Pd 118 Pd
108 Rh 109 Rh 110 Rh 111 Rh 112 Rh 113 Rh 114 Rh
106 Ru 107 Ru 108 Ru 109 Ru 110 Ru 112 Ru
102 Tc 103 Tc 104 Tc 105 Tc 106 Tc 107 Tc 108 Tc 109 Tc 110 Tc
100 Mo 101 Mo 102 Mo 103 Mo 104 Mo 105 Mo 106 Mo 107 Mo 108 Mo
98 Nb 99 Nb 100 Nb 101 Nb 102 Nb 103 Nb 104 Nb
96 Zr 97 Zr 98 Zr 99 Zr 100 Zr 101 Zr 102 Zr
95 Y 96 Y 97 Y 98 Y 99 Y 100 Y
93 Sr 94 Sr 95 Sr 96 Sr 97 Sr 98 Sr
91 Rb 92 Rb 93 Rb 94 Rb 95 Rb 96 Rb 97 Rb 98 Rb 99 Rb

Figure 19.

VII- DISCUSSION OF RESULTS

VII-1 Test measurements

The beta-gamma coincidence system was initially tested using a ^{106}Ru-^{106}Rh source. A beta-gamma coincidence experiment was performed during and after the on-line experiments. The beta spectra in coincidence with the 512 and 622keV gamma-rays of ^{106}Rh exhibited end-point energies of 3.02 ±.14MeV (higher energy branch) and 2.42 ±.12MeV, respectively. The deduced average Q_{β}-value is 3.54 ±.10MeV in excellent agreement with the accepted value of 3.54 ±.01MeV (Wap-77).

Errors on the energies of excited states are considered to be negligible when compared with errors on end-point energies of beta spectra. Therefore, the error associated with a specific Q_{β}-value is, in general the same as that associated with the corresponding beta end-point energy. However, when an average Q_{β}-value is obtained from measurements corresponding to different decay paths of a particular isotope, this mean value is given as follows:

$$\overline{Q}=\frac{\Sigma\ \omega_i\ Q_i}{\Sigma\ \omega_i} \qquad \text{with } \Delta\overline{Q}=(\overline{\sigma}^2+\sigma_{cal}^2)^{1/2}$$

where $\omega_i=\sigma_i^{-2}$

σ_i =uncertainty on the end-point energy

$\overline{\sigma}=(\Sigma\ \sigma_i^{-2})^{1/2}$

σ_{cal}=variance of the calibration

Table-II shows the general good agreement between end-point beta energies measured in the present work and literature values.

The excellent agreement between the half-lives of the long-lived 93.5keV and 2245keV excited states in ^{91}Rb and ^{122}In, repectively, measured in the present study and the previous reported values (table-III) demonstrate the reliability of the method of analysis of the time-spectrum data for half-lives in the order of 10-150ns. The 103.6keV gamma line was identified as being an unresolved doublet. One transition depopulates the 2245keV level in ^{122}In and the other the 504keV level in ^{100}Zr. The relative intensity of the 104keV line in ^{100} Zr is very low (TI-78) and therefore, after comparison with the intensities of other lines in ^{100}Zr and ^{122}In, the delayed part of the time spectrum associated with the 103.6keV gamma line has been assigned to ^{122}In.

VII-2 Discussion of results for individual mass

A=91

The main features of the decay scheme (Gla-76) of ^{91}Rb are depicted on fig.20. This nuclide had been studied (Cli-73) and, recently Glascock et al (Gla-76) performed a further in-depth investigation.

In the present study, weak coincidences are observed between the 93.5keV gamma-ray and the 2564keV and 3600keV gamma-lines. The decay curve associated with the 93.5keV line is displayed in fig.21. From the fit it was possible to extract the half-life of ^{91}Rb as well as that of the parent ^{91}Kr (65 ±8s and 7 ±3s respectively). These values are in good agreement with previously measured values (Gla-76) of 58.2 ±.2 and 8.57±.04s for ^{91}Rb and ^{91}Kr, respectively. The assignment of the 93.5keV gamma-line to the decay of ^{91}Rb is further supported by the measurement of the half-life of the first excited state in ^{91}Sr. The value determined in the present work is 87.4± 3.6ns, in very good agreement with values from previous measurements (Gla-76) (table-III).

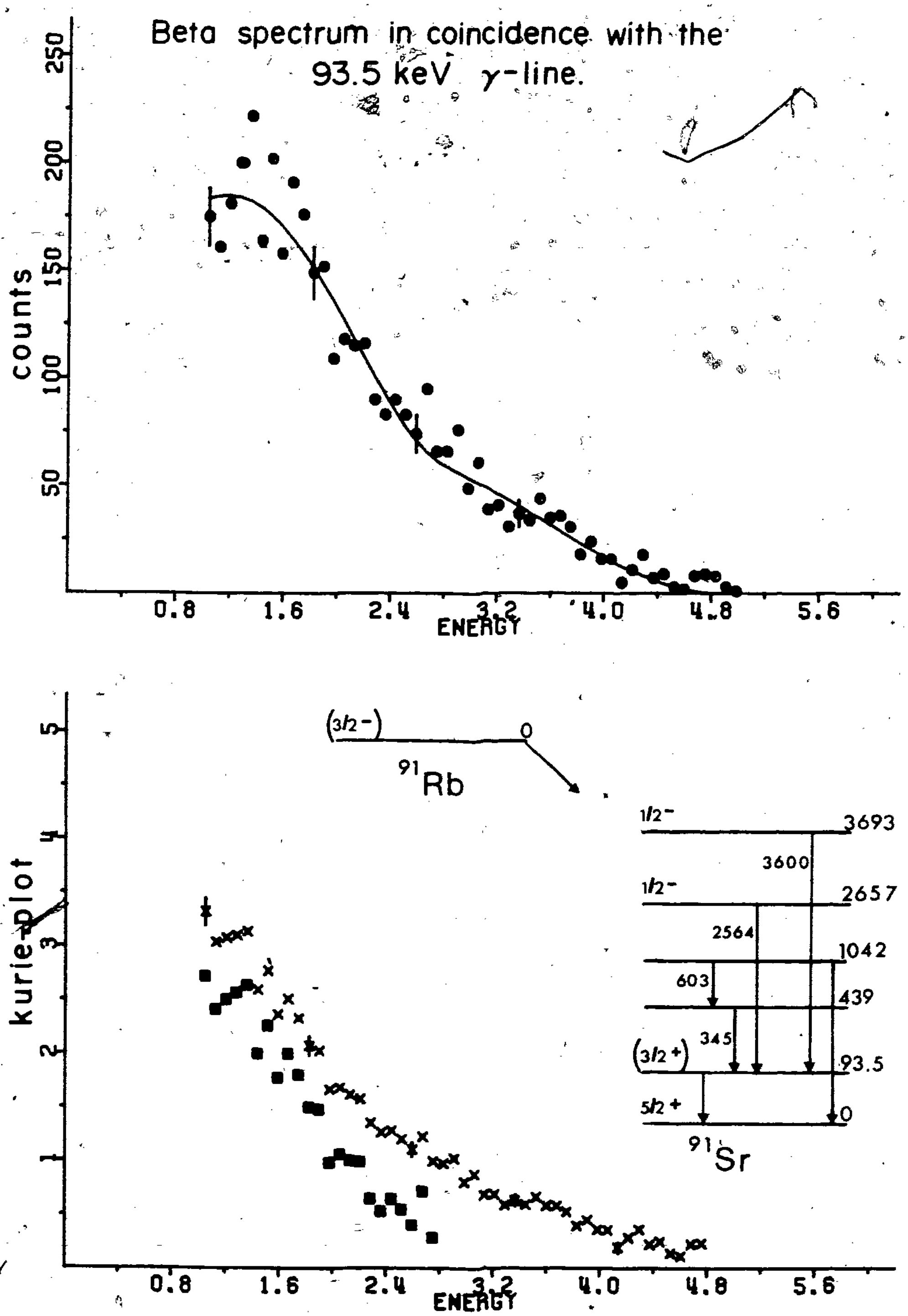
Beta spectrum in coincidence with the
93.5 keV γ-line.
counts
250
200
150
100
50
0.8
1.6
2.4
3.2
4.0
4.8
5.6
ENERGY
kurie-plot
5
4
3
2
1
(3/2−)
0
91Rb
1/2−
3693
3600
1/2−
2657
2564
1042
603
439
(3/2+)
345
93.5
5/2+
0
91Sr
0.8
1.6
2.4
3.2
4.0
4.8
5.6
ENERGY

Figure 20.

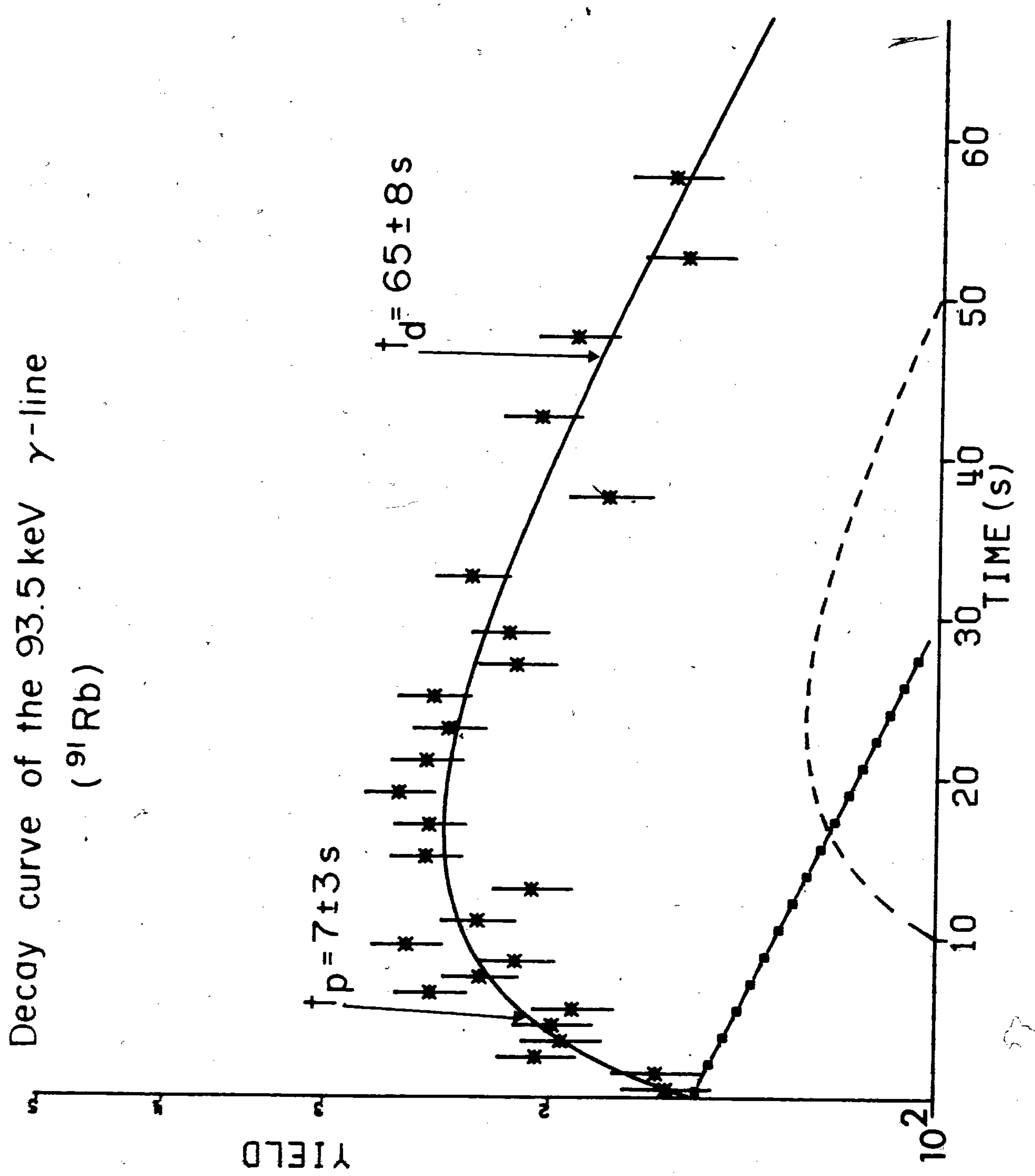
Decay curve of the 93.5 keV γ-line
(91Rb)
tp=7±3 s
td=65±8 s
YIELD
10²
10
20
30
40
50
60
TIME (s)

Figure 21.

The analysis of the total beta spectrum in coincidence with this line gives an end-point energy of 4.93±.12MeV. The maximum associated logft-value is 5.9. If one derives the Q_β-value associated with the decay of ^{91}Rb according to the decay scheme of Gla-76 one finds a value of 4.93 +.09=5.02MeV which is about 800keV less than the previous determinations (Cli-73, Wun-78).

The observation of a buildup in the decay curve of the 93.5keV line rules out the presence of an isomer state of similar half-life in ^{91}Rb. The Q_β-value of ^{91}Rb has been measured by different authors (Cli-73, Wun-78, Woh-78). Most of these determinations involved the measurement of the end-point energy of the single beta spectrum observed after mass separation. The measurement of Cli-73 involved gamma-beta coincidence techniques but the gamma lines chosen for the coincidence gates were not listed. A large Ge(Li) was used and thus, it seems improbable that these authors set a gamma gate on the 93.5keV line. These authors show the beta spectrum in coincidence with the 603keV gamma line which exhibits an end-point energy near 4.9MeV. This energy corresponds to a transition which should populate the 1042keV level in ^{91}Sr. A similar population would reconcile the measurement of the present study with the other Q_β determinations.

However, it would be in violent contradiction with the decay scheme of Gla-76. The study of ref.(Gla-76) is very complete and the discrepancy between their derived beta branching and the end-point energy of the beta spectrum in coincidence with the 93.5keV gamma line measured in this work can not be explained presently.

It should be pointed out that the beta transition intensities derived in Gla-76 are based entirely on relative gamma and the difficulties, as described in ref.(Har-77), with such a procedure could introduce significant errors.

A=94

No decay scheme has been published for ^{94}Rb. Only two main gamma-lines (837keV and 1578keV) are listed in the literature and the half-life has been determined from delayed neutron studies to be 2.73±.02s (Ris-79).

In the present study, the 1578keV gamma-line decays with a 2.5±0.2s half-life while the 837keV line exhibits 2 components: one of 17±2s and the other of 2.6±0.2s. Moreover the beta-rays of energies greater than 4.5MeV in coincidence with the 837keV gamma-line decay with a 2.7±0.3s half-life.

In the beta-gamma experiment the centroid position of the 837keV gamma-line exhibits an energy shift of about 1keV during the counting period. The initial peak at 836.9keV decays while a 837.9keV peak grows in and becomes the dominant peak. This latter peak associated with the 18s half-life could not be assigned. This shifting (of about one channel) was not observed for any other gamma-line in the spectrum.

^{94}Rb mainly decays to ^{94}Sr by beta-minus decay (about 9% of the decay is known to take place by delayed neutron emission) (Ris-79). The relative intensities (fig.22) of the 837 and 1578keV gamma-lines measured in the present work are in agreement with the values reported in ref.(N94-73).

A search for a growth in the decay curve of ^{94}Sr was undertaken but (as detailed below) no growth was actually observed (fig.23). The beta spectra in coincidence with the 837 and 1578keV lines are each fitted by 2 components (fig.24). For both spectra, the high energy branch exhibits a similar end-point energy of about 6.30MeV (fig.24) with a maximum logft-value of about 5.0 which is specific of an allowed beta transition.

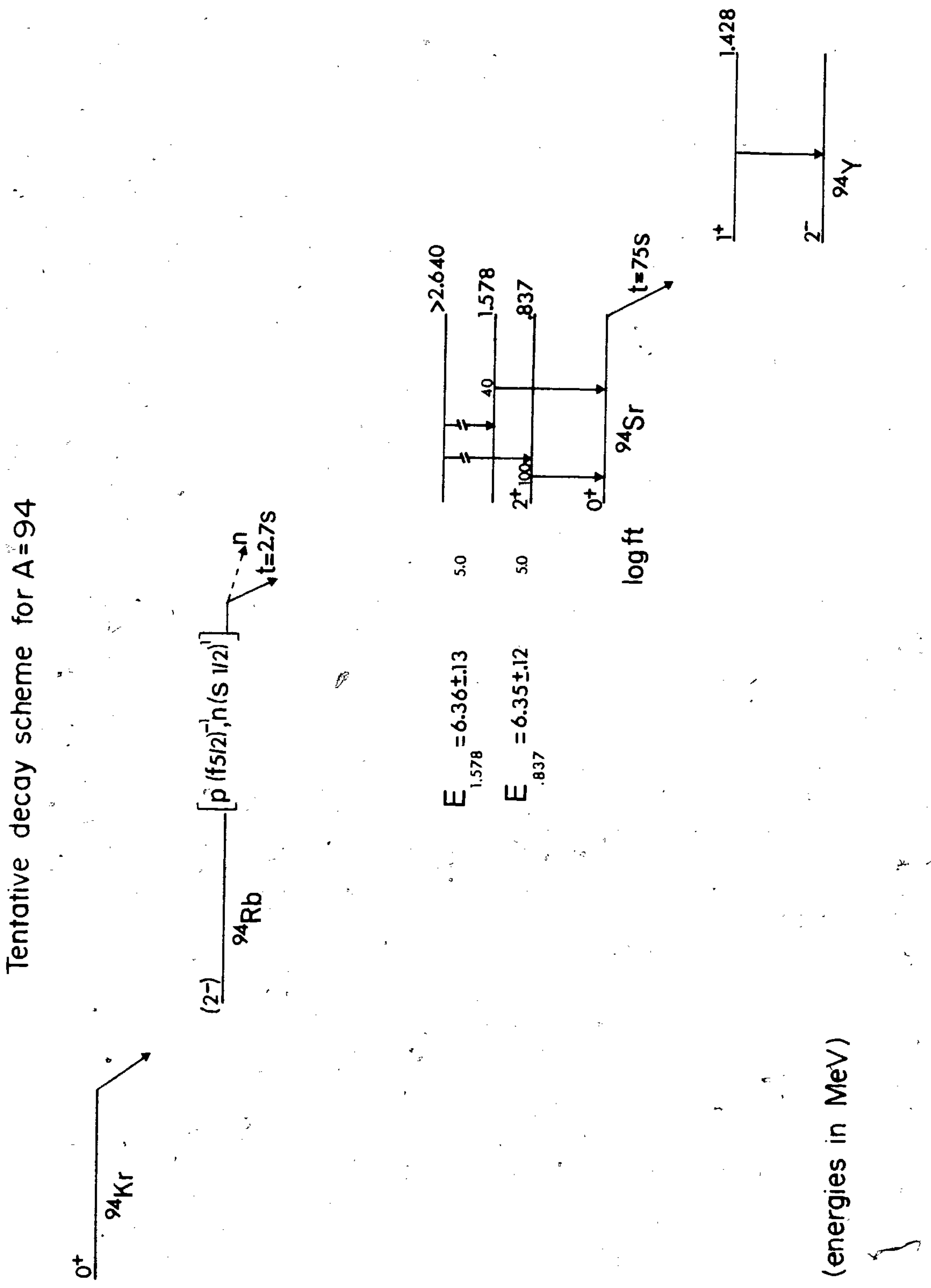

Tentative decay scheme for A=94
0+
94Kr
(2-)
94Rb
[p(f5/2)-1, n(S 1/2)1]
n
t=2.7S
>2.640
1.578
.837
2+
0+
94Sr
t=75S
40
100
5.0
5.0
log ft
E1.578 =6.36±.13
E.837 =6.35±.12
1.428
1+
2-
94Y
(energies in MeV)

Figure 22.

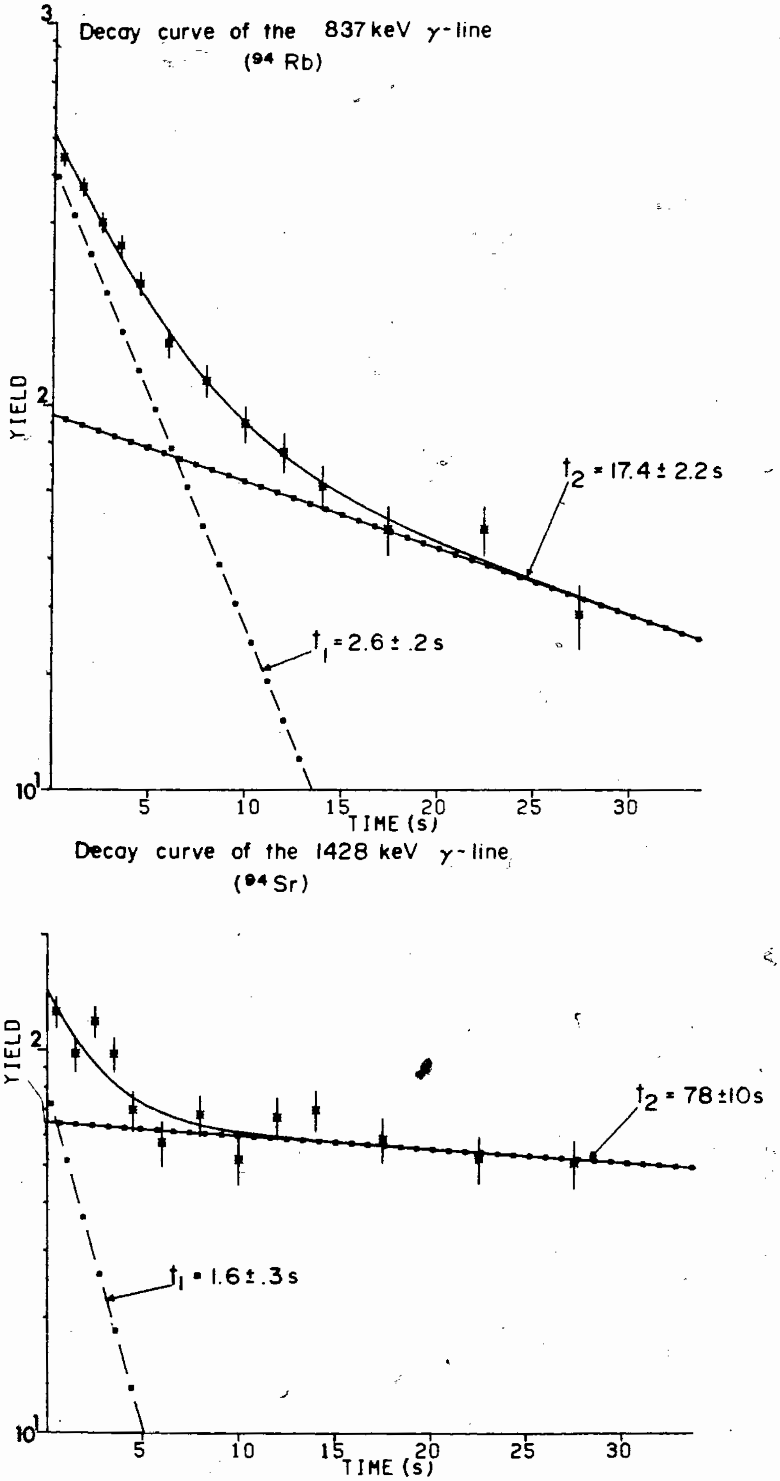
Decay curve of the 837 keV γ-line
(94 Rb)
YIELD
3
2
10 1
t2 = 17.4 ± 2.2 s
t1 = 2.6 ± .2 s
5
10
15
20
25
30
TIME (s)
Decay curve of the 1428 keV γ-line
(94 Sr)
YIELD
2
10 1
t2 = 78 ±10 s
t1 = 1.6 ± .3 s
5
10
15
20
25
30
TIME (s)

Figure 23.

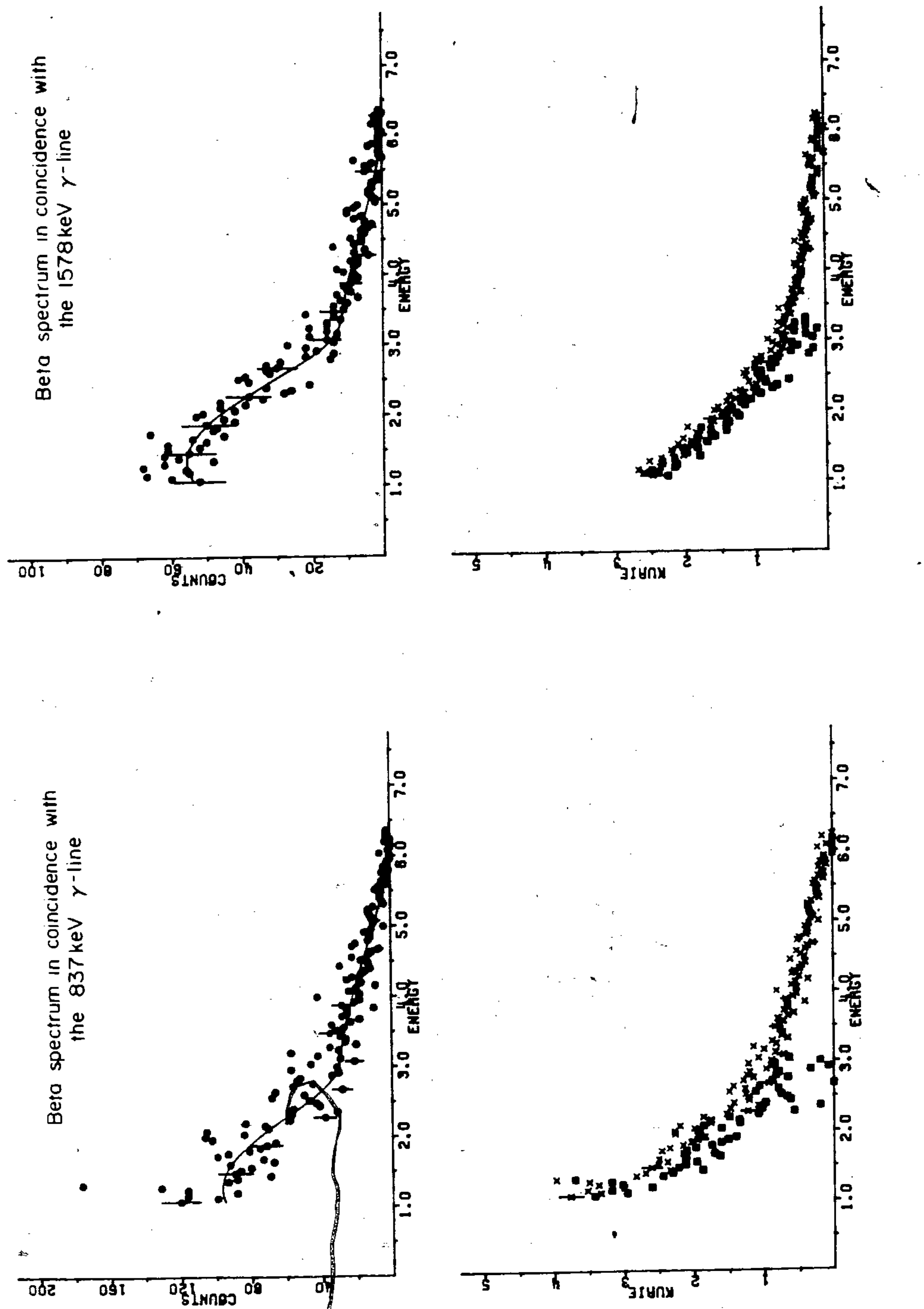
Beta spectrum in coincidence with the 1578keV γ-line
COUNTS
ENERGY
KURIE
Beta spectrum in coincidence with the 837keV γ-line
COUNTS
ENERGY
KURIE

Figure 24.

In the gamma-gamma coincidence data, there is some evidence for the non-existence of a coincidence relationship between the 837 and 1578keV gamma lines. However, owing to poor statistics it was not possible to exclude completly such a relationship. If it is assumed that these two lines are not in coincidence, a lower limit for the energy of the level populated by the beta transition of about 6.4MeV end-point can then be calculated. An energy of 1800keV corresponding to the upper energy limit in the gamma-gamma coincidence experiments is thus added to the 837keV of the main gamma line to give an excitation energy of about 2600keV (1800+837).

This interpretation is in contradiction with the results of Wun-78 where the authors report a end-point energy of 7.89±.06MeV for a beta transition populating a 2413keV level (837+1578=2415) in ^{94}Sr. However, these authors do not indicate that a beta-gamma coincidence experiment was performed. If the interpretation of Wun-78 is correct it is possible that the authors observed a beta transition which would have been missed in the present study. This last interpretation is supported in the present work by the fact that the gamma spectrum in coincidence with beta-rays of energies greater than 6.5MeV exhibits the 837 and 1578keV peaks (fig.25). A more intense transition, with a 6.4MeV end-point energy, could then be postulated to populate an excited state of higher energy in ^{94}Sr (~4MeV).

The interpretation of beta population of high energy levels in ^{94}Sr does not agree with the results of ref.(Ale-75) where the beta-strength of the decay of ^{94}Rb is distributed for over 60% between 1 and 3MeV. However, the assumptions underlying the data analysis procedures of that reference, namely that the gamma decay of the levels excited following beta decay can be treated statistically, may not be valid in this case where the daughter nuclide, ^{94}Sr, is an even-even isotope with supposively well separated low energy excited levels.

The decay of ^{94}Sr has been well studied (N94-73) and it is known to populate almost exclusively the 1428keV excited level in ^{94}Y. A half-life of 75.7±.5s was measured previously (N94-73). The decay data for the 1428keV gamma-line in the gamma-beta coincidence experiment of the present work could only be fitted with two decay constants (fig.23) corresponding to half-lives of 1.6±.3s and 78±10s. Furthermore, the associated beta spectrum exhibits two components of which the high

Figure 25.

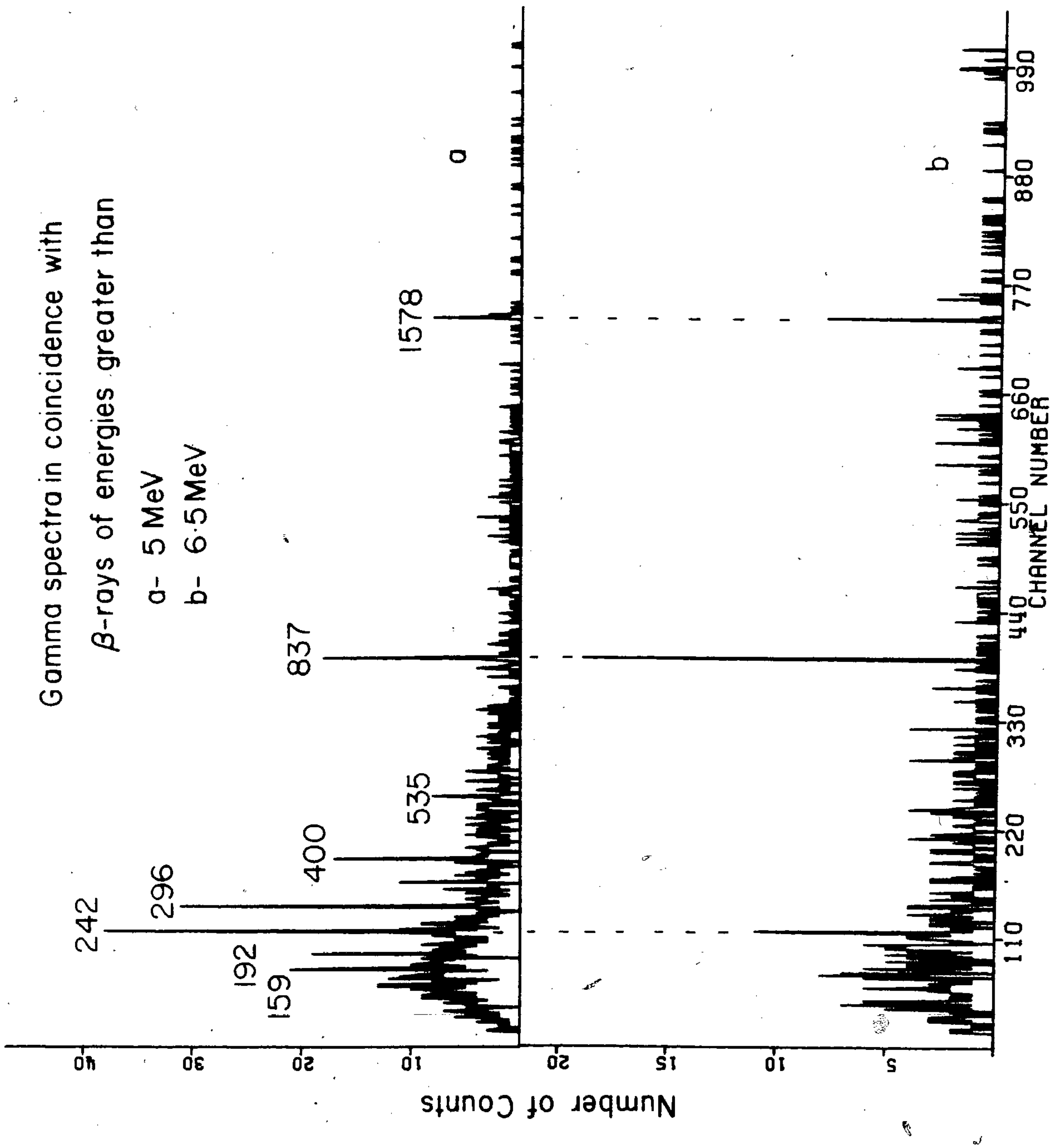
Gamma spectra in coincidence with
β-rays of energies greater than
a- 5 MeV
b- 6.5 MeV
242
296
192
159
400
535
837
1578
a
b
Number of Counts
CHANNEL NUMBER
110
220
330
440
550
660
770
880
990

energy one decays with a 2±2s half-life. The end-point energy of the low energy branch (E=2.14±.10MeV) leads to a Q_β -value of 3.57 ±.10MeV for the decay of ^{94}Sr (table-V). Such a value is within the experimental error of that in ref.(Wap-77). No assignment could be made for the short-lived component.

An isomer state in the even-even ^{94}Sr is not expected in regard to the systematics in this region. This new line is more likely to come from another nuclide. Since there is a large difference in half-lives, it should be possible to enhance the observation of the short-lived species with respect to ^{94}Sr in further investigations.

A=95

The higher energy gamma-line of a doublet observed at 685-687keV in the beta-gamma coincidence experiments was assigned to the decay of ^{95}Sr from ref.(Mon-76). If the high energy branch is assumed to populate directly the 687keV level in ^{95}Y, a Q_β -value of 6.15±.20MeV can be derived (table-V). This value is in agreement with the published value of Sti-78.

A=96

A weak gamma-line at 122.1keV has been assigned from ref.(Sis-76) to the decay of ^{96}Sr. The half-life of 1.1±0.4s, measured from from the data of single detector experiments, is in agreement with the accepted value of 1.0±0.1s (Sis-76). The end-point energy of the associated beta spectrum has been determined to be 4.8±.2MeV. Since the decay scheme is known (Sis-76) a Q_β-value of 5.7±.2MeV can be deduced (table-V). This is somewhat higher than the 5.35±.10MeV value of Sti-78. This discrepancy is believed to be mainly due to the poor statistics in the gamma spectrum of the present study.

Fig.26 displays the decay scheme associated only with the decay of the isomeric state of ^{96}Y. The main essential features of this decay were taken from ref.(Sad-75). This isomeric state is assumed to decay only to the energy levels 4390keV (90%) and 3773keV (10%) in ^{96}Zr. Stippler et al (Sti-78) reported results which are not in agreement with such a beta branching ratio and attributed a stronger branch to the 3773keV level. In the latter report the sources were mass-separated (as in the first one) but due to poor statistics the contribution of all gamma-peaks of higher energies than the peak of interest (Compton effect) was not taken into account.

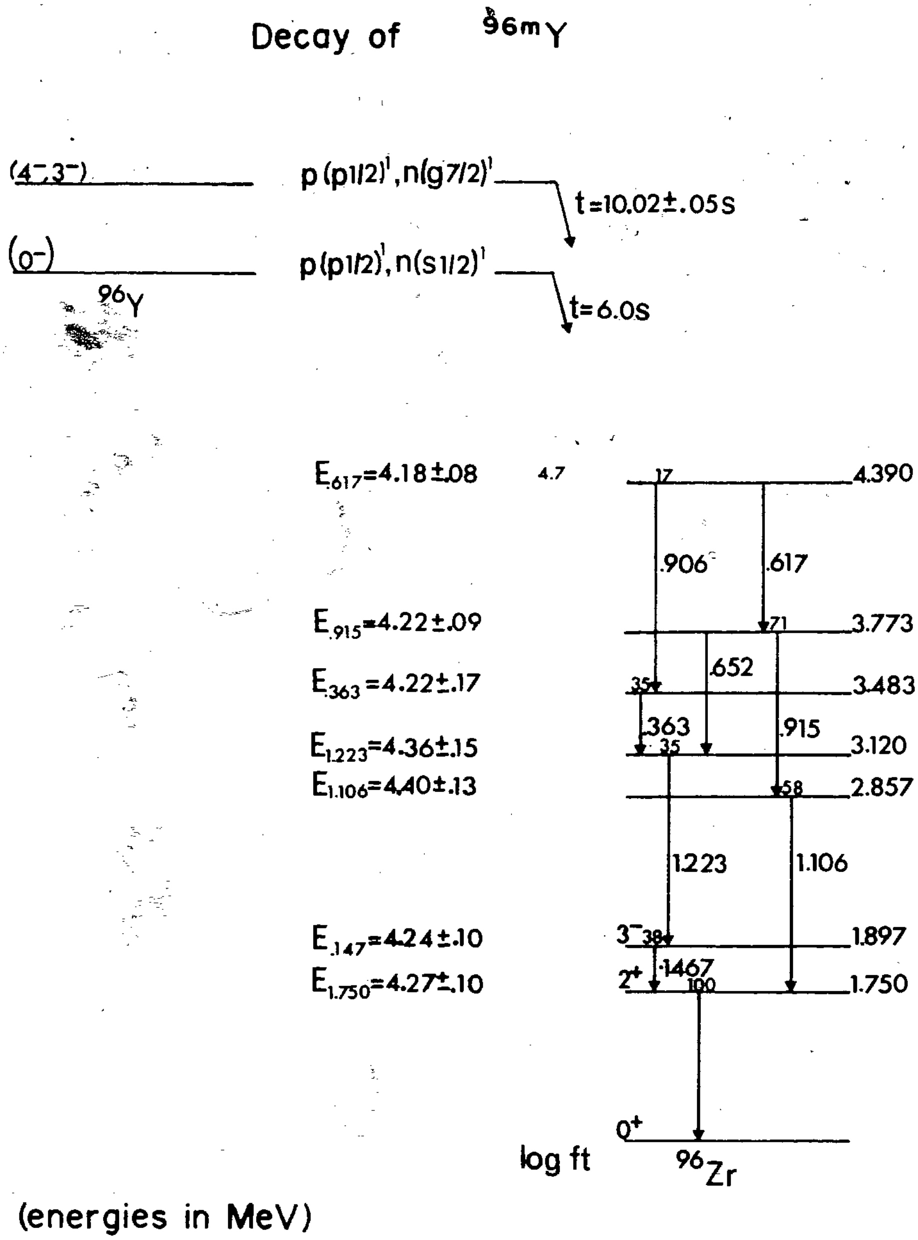

Decay of ^{96m}Y
(4⁻,3⁻)
p(p1/2)¹,n(g7/2)¹
t=10.02±.05s
(0⁻)
p(p1/2)¹,n(s1/2)¹
t=6.0s
96Y
E.617=4.18±.08
4.7
17
4.390
.906
.617
E.915=4.22±.09
71
3.773
.652
E363=4.22±.17
35
3.483
.363
.915
E1.223=4.36±.15
35
3.120
E1.106=4.40±.13
58
2.857
1.223
1.106
E.147=4.24±.10
3⁻
38
1.897
E1.750=4.27±.10
2⁺
.1467
100
1.750
0⁺
log ft
96Zr
(energies in MeV)

Figure 26.

The half-lives corresponding to the main 6 gamma-peaks have been measured in the present study and a mean value of 10.02±.08s has been obtained. Such a result is in excellent agreement with previous determinations (Sis-76,Sad-75). The gamma-gamma coincidence data (table-VI) also agree with the published decay scheme. The relative intensities of the major gamma peaks calculated from the gamma-beta coincidence data are compared with the values obtained in ref.(Sad-75) in the following table:

energies (keV)	% present work	% literature Sad-75
146.7	38±2	40.5
363	35±3	25
617	(100±4)*	62.1
906	17±5	20.4
915	71±5	66.5
1106	58±2	54.4
1223	35±4	29.3
1750	100±2	100

* see text

The contradiction observed for the relative intensity of the 617keV gamma line can be partially explained by the presence of an unresolved 618keV gamma line, decaying with a similar half-life and assigned to the decay of ^{106}Mo (table-VI).

Seven end-point energies (fig.27) have been measured and these lead to an average $Q\beta$ -value of $8.63\pm.05$MeV (table-V) for the high spin isomer of ^{96}Y. The ground-state $Q\beta$ -value has been reported to be $6.5\pm.5$MeV (Sis-76) and $7.03\pm.07$MeV (Sti-78). The 10s is supposed to lie 400 ± 200keV above the latter (Sad-75). These values lead to a $Q\beta$-value for the 10s isomer which is far less than that derived in the present work.

Stippler et al (Sti-78) obtained end-point energies in excellent agreement with these results. However, they also observed a high energy beta branch in coincidence with the 146.7keV gamma-line which led them to postulate a $Q\beta$-value of $8.03\pm.15$MeV. Such a branch has not been observed in the present study. Fig.28 displays the low energy gamma spectra in coincidence with the beta-rays of energies greater than 3.5 and

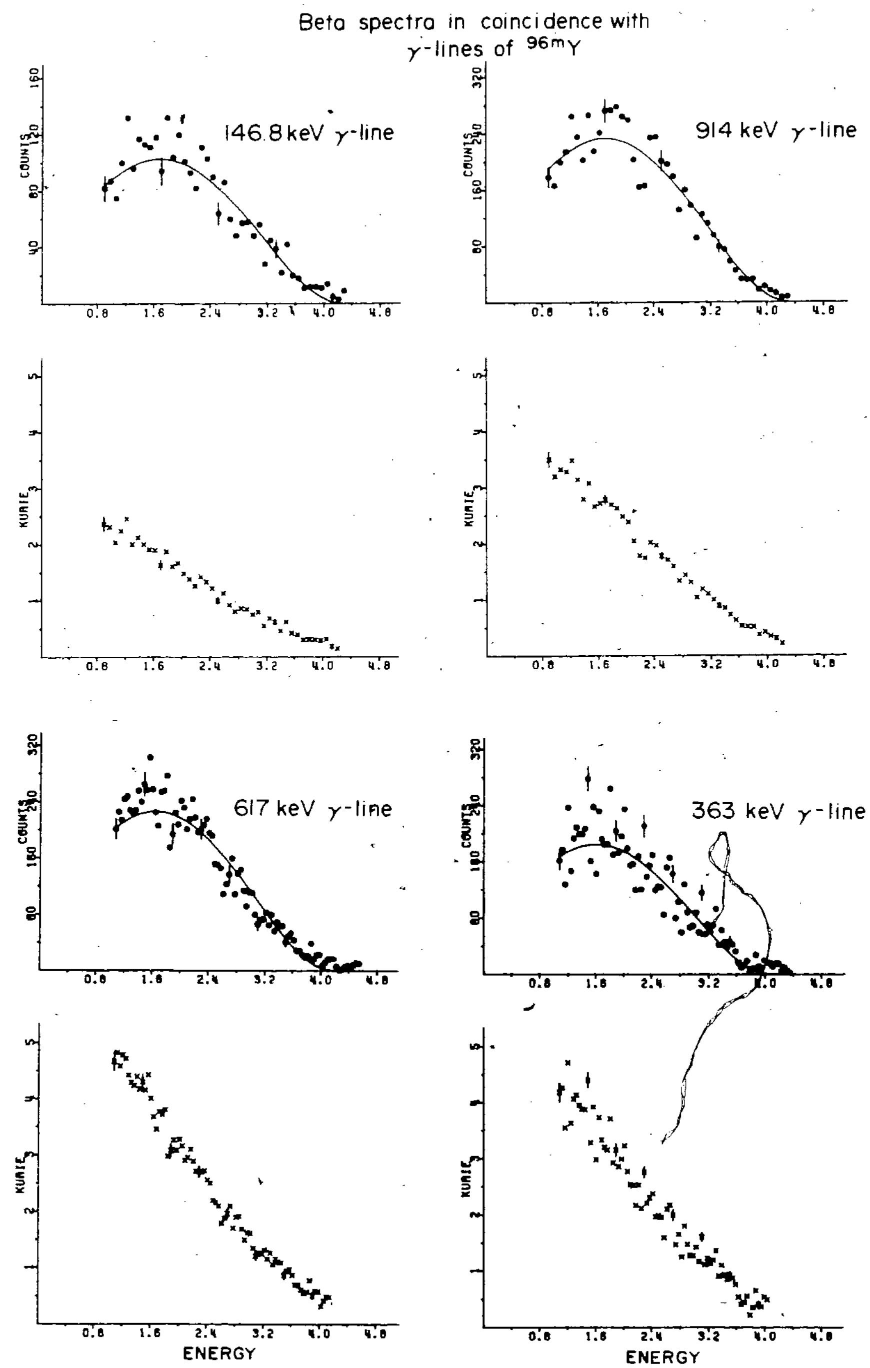
Beta spectra in coincidence with
γ-lines of 96mY
146.8 keV γ-line
914 keV γ-line
617 keV γ-line
363 keV γ-line
COUNTS
KURIE
ENERGY
0.8
1.6
2.4
3.2
4.0
4.8

Figure 27.

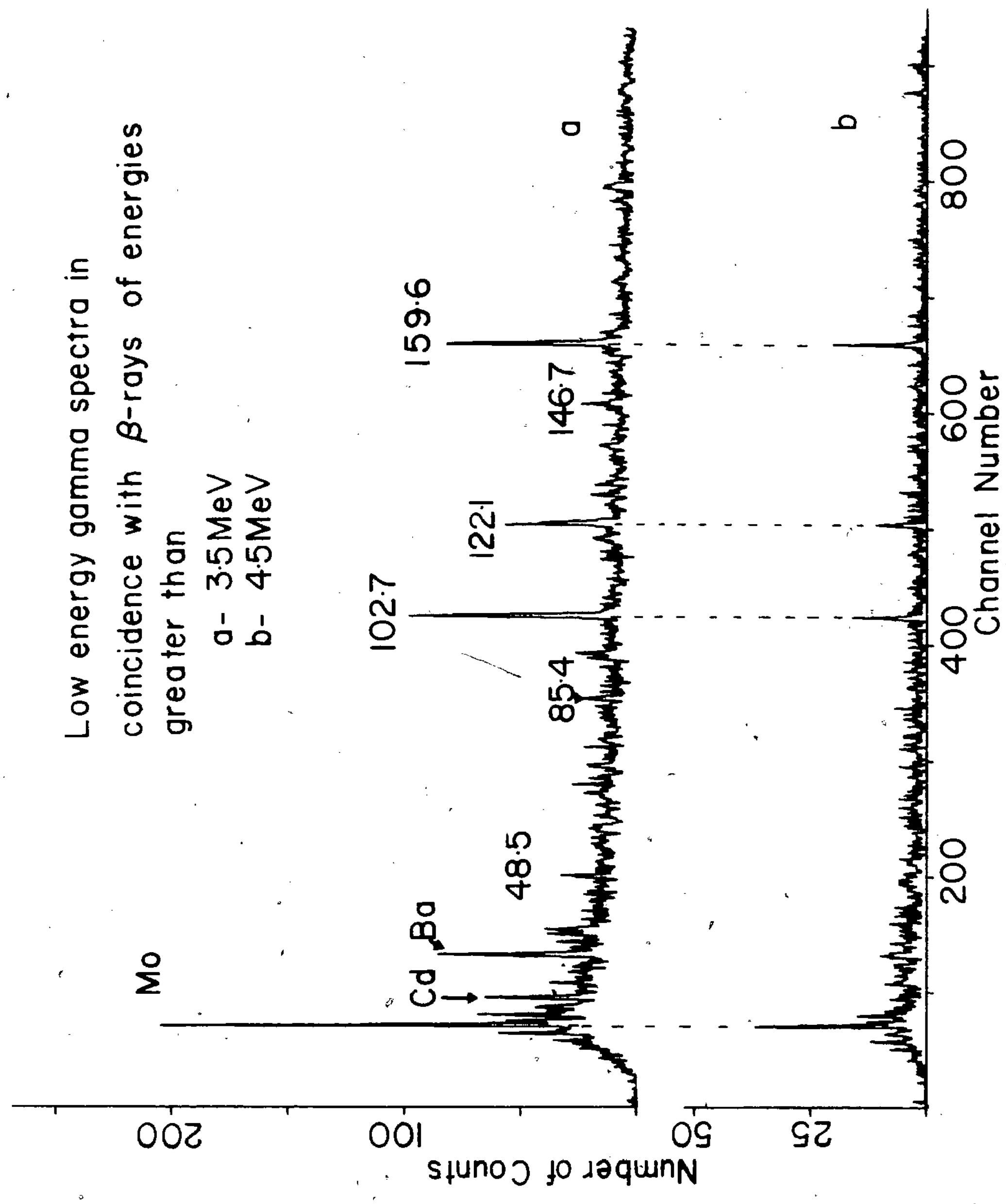
Low energy gamma spectra in coincidence with β-rays of energies greater than
a- 3.5MeV
b- 4.5MeV
Mo
Cd
Ba
48.5
85.4
102.7
122.1
146.7
159.6
a
b
200
100
50
25
Number of Counts
200
400
600
800
Channel Number

Figure 28.

4.5MeV. It can be seen that the 146.7keV line is only present in the low energy window spectrum. Therefore, the high energy branch observed in Sti-78 could be due to contamination from other isobars.
The interpretation of Stippler et al (Sti-78) assumed that the beta transition of 4.2MeV end-point energy in coincidence with the 617keV gamma-line populates the 3773keV rather than the 4390keV level in ^{96}Zr. The same authors assume that the high energy part of the spectrum came from the Compton contribution of higher energy gamma transitions. Since this contribution has been subtracted in the present study, this explanation does not hold and therefore, the 4.2MeV beta branch populates the 4390keV ~~level~~ ~~le~~ leading to a Q_β-value of $8.63 \pm .05$MeV (table-V).

The calculated logft-value (4.7) for the beta transition populating the 4390keV excited level in ^{96}Zr is specific to an allowed transition. The possible shell-model configurations of the two isomers are shown in fig.26.

A=97

The decay of ^{97m}Y has been investigated previously (Mon-76). Two gamma lines 968 and 1103keV have been assigned to this decay. A 163-1103keV gamma cascade deexcites the 1264keV delayed state in ^{97}Zr. The half-life of the 1264keV state was measured to be 100 ± 15ns (table-III) and this is in agreement with the 104 ± 5ns reported earlier (TI-78).

An end-point energy of $5.2 \pm .2$MeV was measured for the beta spectrum in coincidence with the 968keV gamma line. A Q_β-value of $7.4 \pm .2$MeV could then be derived for the high-spin isomer in ^{97}Y. Such a result is in agreement with the value that one can obtain from the reported ^{97}Y ground-state Q_β-value of $6.67 \pm .13$MeV (Sti-78) and the energy of the isomeric level of 667keV (Mon-76)($6.67+.67=7.34 \pm .13$MeV).

A=99

The data obtained in the present work (table-VI) for the decay of ^{99}Zr are in good agreement with the decay scheme in fig.29, reproduced from ref.(Mon-76).

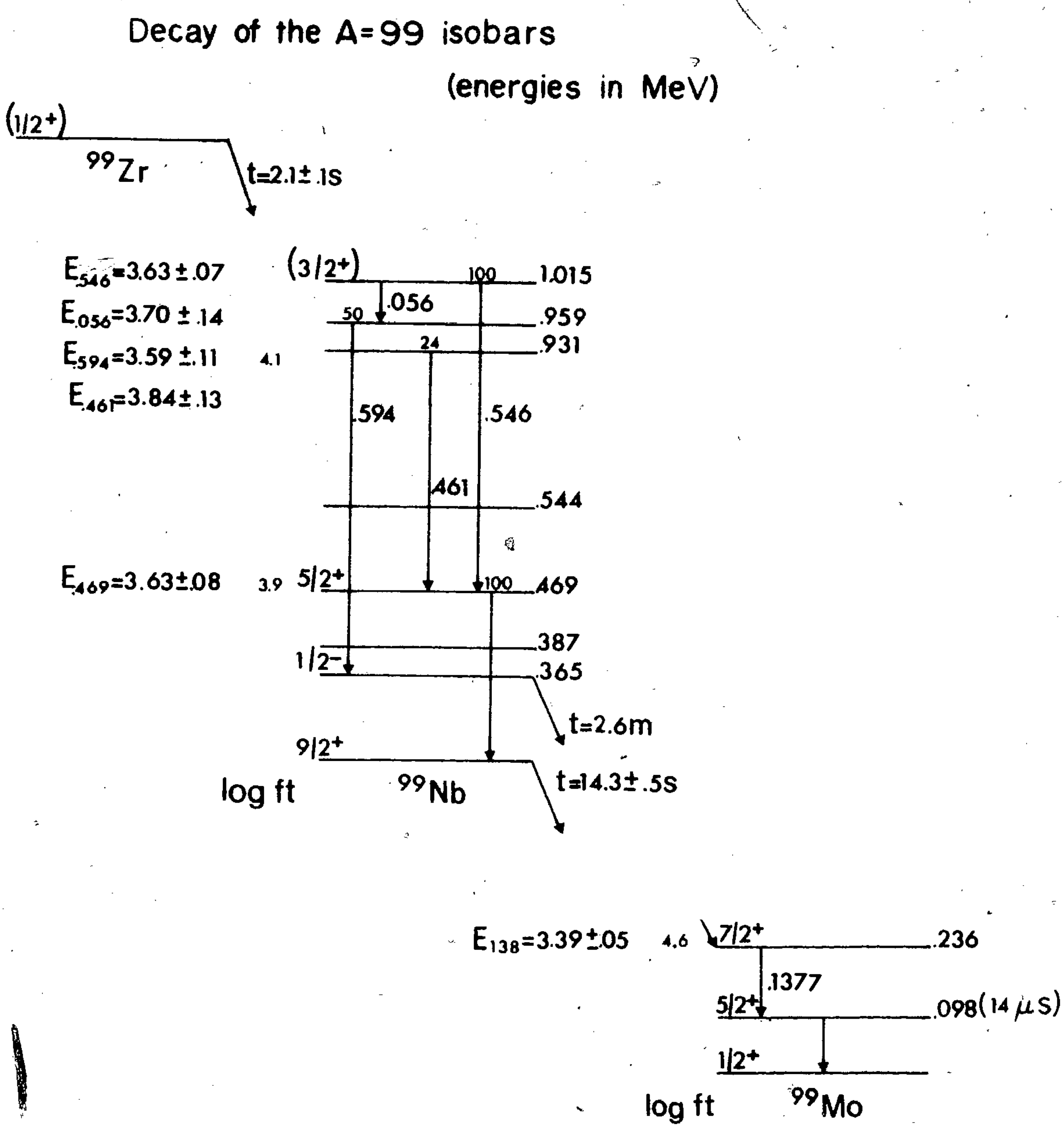

Decay of the A=99 isobars
(energies in MeV)
(1/2+)
99Zr
t=2.1±.1s
E.546=3.63±.07
E.056=3.70±.14
E.594=3.59±.11
E.461=3.84±.13
4.1
(3/2+)
100
1.015
.056
50
.959
24
.931
.594
.546
.461
.544
E.469=3.63±.08
3.9
5/2+
100
.469
.387
1/2−
.365
t=2.6m
9/2+
log ft
99Nb
t=14.3±.5s
E.138=3.39±.05
4.6
7/2+
.236
.1377
5/2+
.098(14 μs)
1/2+
log ft
99Mo

Figure 29.

The relative intensities measured in the present study are compared with the values of ref.(Sel-79) in the following table:

energies (keV)	% present work	% Sel-79
56.0	-	4
461	24±3	21
469	100±3	100
546	100±3	85
594	50±2	49

The high value obtained for the 546keV line suggests a possible weak interference from an unknown gamma transition of a similar energy.

The measured beta end-point energies lead to an average Q_β-value of 4.64±.06MeV which is in fair agreement with the value of 4.54±.12MeV reported in ref.(Sti-78).

The beta decay of the ground-state of ^{99}Nb is known to populate only the level at 235.5keV in ^{99}Mo (N99-74). The end-point energy of the beta spectrum in coincidence with the intense gamma-line of 137.7keV was determined to be 3.39±.05MeV. This leads to a Q_β-value of 3.62±.05MeV which is in excellent agreement with that of ref.(Wap-77).

A=100

The excited states at 504keV and 400keV in ^{100}Nb are the main levels assumed to be populated via the beta decay of ^{100}Zr (Sti-78). The 400keV gamma line is an unresolved multiplet and therefore, the relative intensity in fig.30 may be overestimated as it is suggested by the comparison with the value reported in TI-78. Since the relative intensity of the 104keV line was reported to be small (TI-78) this implies the direct individual beta population of the levels at 504 and 400keV, respectively. Since the maximum logft-values for these transitions are typical of allowed transitions, the populated levels are likely to be (1+) state. The beta spectrum in coincidence with the 400keV

Decay of the A=100 isobars

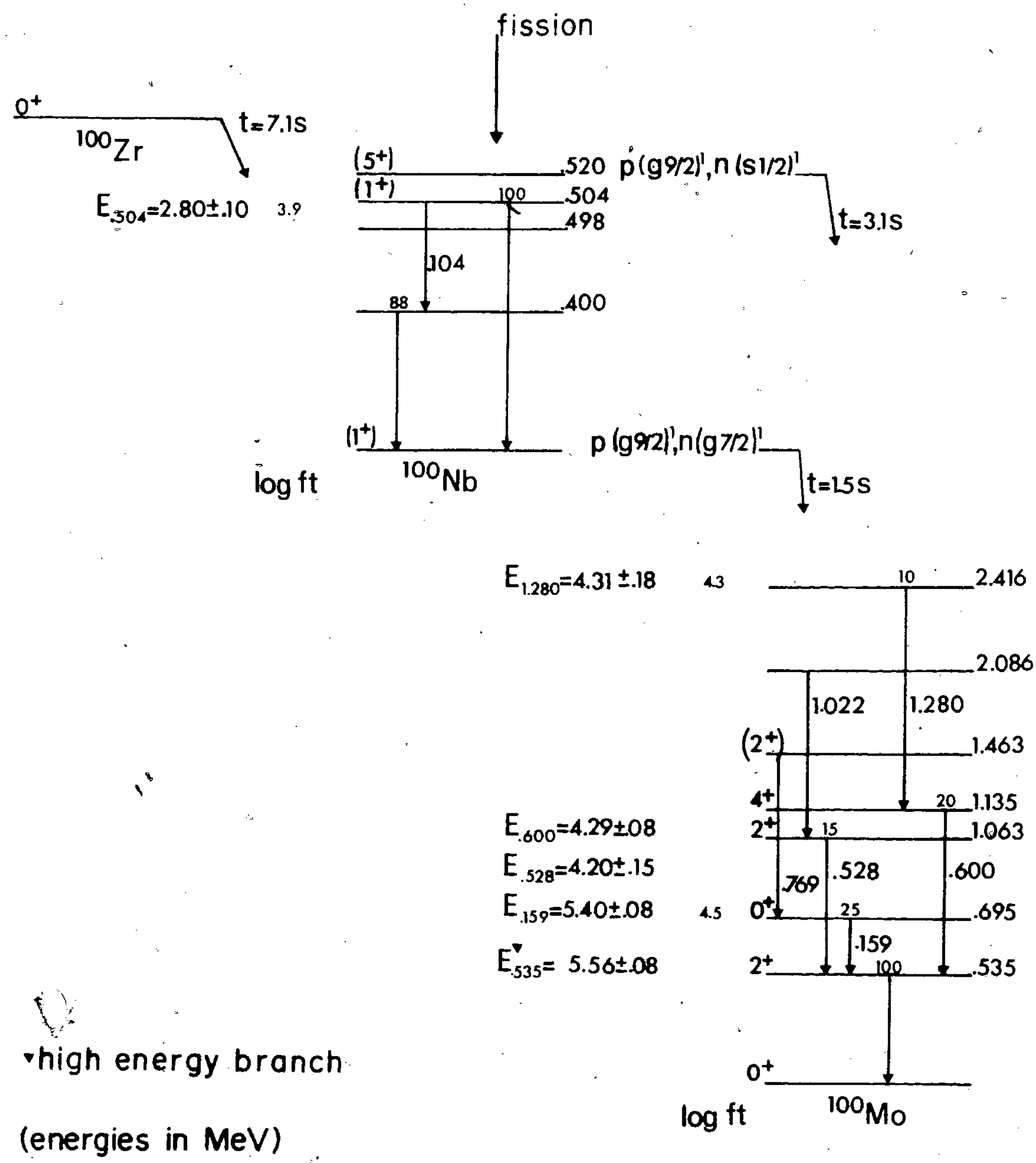

Figure 30.

gamma line is a complex spectrum. Although the low energy branch has a end-point energy consistent with that of the beta spectrum in coincidence with the 504keV gamma line, it has not been included in the Q_β determination. The measured half-life associated with the 400keV line seems to represent an average value between the 7.1s of ^{100}Zr and the 1.3s of ^{102}Nb (table-VI).

The coincidence results obtained in the present study (table-VI) confirm the decay scheme of ref.(N100-74) for the decay of the ^{100}Nb isomers. In the present investigation, beta-rays of energies greater than 4MeV in coincidence with the 535keV gamma-line have been measured to decay with a 6.5±1.0s half-life. Such a value agrees with the accepted value for the half-life of the parent nuclide ^{100}Zr which populatesthe low spin isomer in ^{100}Nb (N100-74).

The relative intensities measured in the present study do not agree with those reported in ref.(TI-78). However, the decay scheme of the latter reference has not been assigned to a specific isomer. In the present study both isomers were observed and the gamma relative intensities correspond to the sum of both decays.

It is assumed that the low spin isomer, mainly populated through the beta decay of ^{100}Zr, populates directly the two first excited levels in ^{100}Mo. The high spin isomer is assumed to mainly populate the 2416keV excited state (Sti-78). This is supported by the fact that the 1280keV gamma line which deexcites the 2416keV level was measured, in the present study, to decay with a 3.2±.5s half-life. The accepted value for this isomer being 3.1±.3s (Kaf-76a).

From the end-point energies of the beta spectra in coincidence with the 600 and 1280keV gamma transition an average Q_β-value of 6.69±.15MeV can be derived for the high spin isomer in ^{100}Nb (table-V). The high energy beta branch populating the 535keV level comes almost exclusively from the low spin isomer. The beta spectrum in coincidence with the 159keV gamma line was fitted by a single component spectrum suggesting a low contribution from the high spin isomer (fig.31). The end-point energies associated with these beta branches lead to a Q_β-value of 6.09±.06MeV (table-V).

Such a value is consistent with that of Sti-78. However, from the $^{100}Mo(t,{}^{3}He)^{100}Nb$ reaction a much higher value was obtained (Ajz-79). This 6709±30keV value is unexpectedly consistent with the Q_β-value derived in the present study for the high spin isomer.

Figure 31.

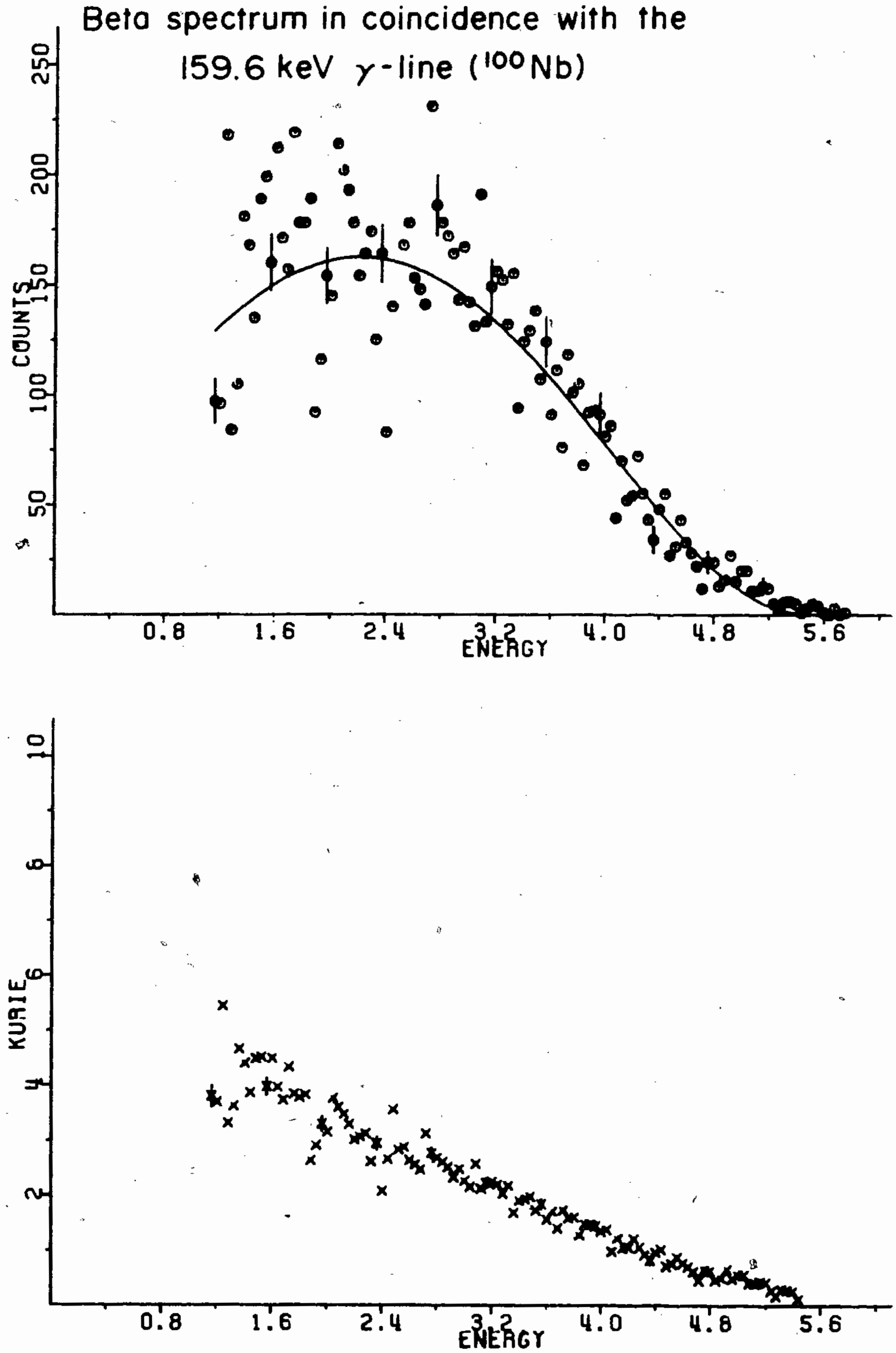
Beta spectrum in coincidence with the
159.6 keV γ-line (^{100}Nb)
COUNTS
250
200
150
100
50
0.8
1.6
2.4
3.2
4.0
4.8
5.6
ENERGY
KURIE
10
8
6
4
2
0.8
1.6
2.4
3.2
4.0
4.8
5.6
ENERGY

If the nuclear reaction value is confirmed the energy levels in ^{100} Mo would have to be revised.

The maximum logft-values associated with the above beta transitions (fig.30) imply that strong allowed beta transitions populated the 2416, 695 and 535keV levels in ^{100}Mo. The high spin isomer in ^{100}Nb lies 600±130keV (the difference in Q_β -values) above the ground-state. A possible single particle configuration is shown for each of these states in fig.30.

A=101

The coincidence data for the 118, 157 and the 276keV gamma-lines fit very well into the tentative decay scheme for ^{101}Nb in ref.(Kaf-76b).

The end-point energy of the high energy beta branch in coincidence with the 276keV gamma transition is consistent with a direct beta population to the 289keV level as reported in Sti-78. The end-point of the beta spectrum in coincidence with the 118keV gamma line supports this interpretation. A 157keV gamma line has been assigned as the main transition deexciting the 171keV level in ^{101}Mo. Owing to the associated large error, the end-point energy (4.20±.12MeV) of the beta spectrum in coincidence with this line is consistent with a direct beta population to either the 171 or the

289keV level. Although, this energy is somewhat lower than that of Sti-78 (4.35±.15MeV) it is within the experimental errors. The relative intensities of the 118 and 157keV gamma lines favor a direct beta population to the 171keV level in ^{101}Mo. An average Q_β-value of 4.47±.11MeV can be derived from the three measurements (table-V) and this is in agreement with the 4.57±.10MeV of Sti-78.

The half-life associated with the beta-gamma concident events of the 43.5keV gamma transition was measured to be greater than 300ns. The 43.5keV line deexcites the 57keV in ^{101}Mo (Kaf-76b). Since no other delayed coincidences have been found in the decay of ^{101}Mo, this half-life has been associated with the 57keV level.

A=102

Similar to ^{100}Nb, two isomers are known to exist for ^{102}Nb (Ahr-76). The decay of the two isomers has been investigated previously (Kaf-76a). Nevertheless, no relative intensities of the main gamma-lines associated with this decay have been reported. Thus the values in fig.32 are those measured in the present work.

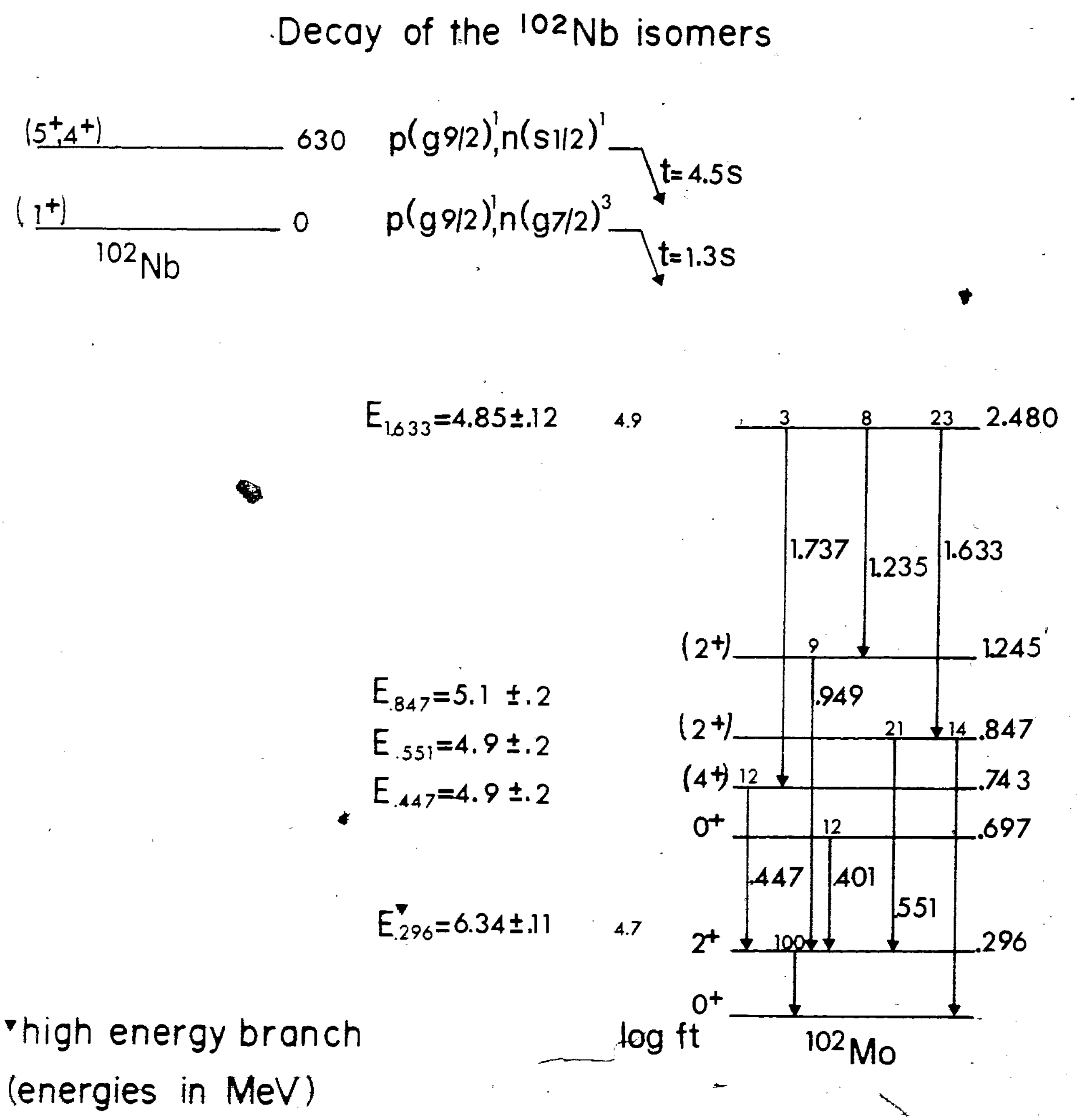
Decay of the ¹⁰²Nb isomers
(5⁺,4⁺) 630 p(g9/2)¹,n(s1/2)¹
t=4.5s
(1⁺) 0 p(g9/2)¹,n(g7/2)³
t=1.3s
102Nb
E1633=4.85±.12
4.9
3
8
23
2.480
1.737
1.235
1.633
(2⁺)
9
1.245
E847=5.1 ±.2
.949
(2⁺)
21
14
.847
E551=4.9 ±.2
(4⁺)
12
.743
E447=4.9 ±.2
0⁺
12
.697
.447
.401
.551
E296=6.34±.11
4.7
2⁺
100
.296
0⁺
▾high energy branch
(energies in MeV)
log ft
102Mo

Figure 32.

From the proposed scheme (Ahr-76) and the beta energies measured in the present study, two different Q_β -values have been obtained. The high-spin state is assumed to decay mainly to the 2480keV level of the daughter nuclide (^{102}Mo), via an allowed transition (logft=4.7). An average Q_β-value of 7.40±.09MeV (table-V) can then be derived and such a value is in agreement with that in ref.(Sti-78). The same authors observed an unassigned low energy component for the beta spectrum in coincidence with the 1633keV gamma-line. Such a branch was not observed in the present study (fig.33).

The low spin isomer should populate the energy levels of low spin in the first excited states in ^{102}Mo. The decay of all beta-rays in coincidence with the 296keV gamma line and of energies greater than 5MeV has been followed. Although no conclusive half-lives could be extracted the decay curve is complex. This suggests that weak beta transitions of high energy end-points (>5MeV) depopulate the high spin isomer in ^{102}Nb. In the present work, a 6.3MeV energy beta branch was measured in coincidence with the 296keV gamma-line. Such a branch was also observed in ref.(Sti-78).

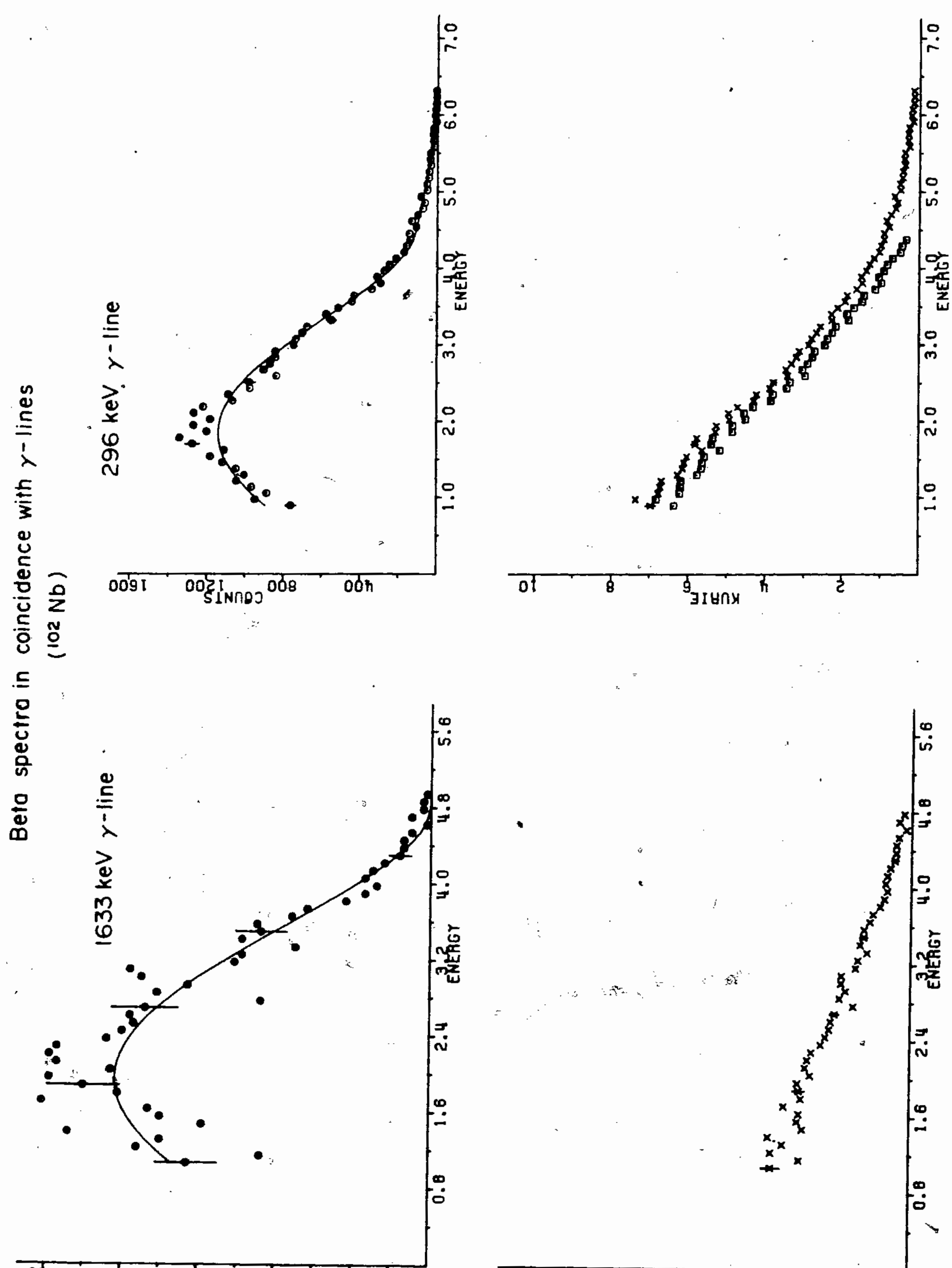
Beta spectra in coincidence with γ-lines
(102 Nb)
1633 keV γ-line
296 keV, γ-line
COUNTS
KURIE
ENERGY

Figure 33.

However the same authors reported a 7.1MeV branch in coincidence with the same gamma-line which was not observed in the present study (fig.33). Also, they measured the end-point energy (7.2MeV) of the single beta spectrum associated with A=102 and assigned this energy to the g.s.-g.s. transition.

The latter measurement represents a weak argument since beta-rays from the decay of other isobars may be present in the single beta spectrum associated with A=102. Fig.25 shows the gamma spectrum in coincidence with beta-rays of energies greater than 6.5MeV and a peak was not observed at 296keV. Since Stippler et al (Sti-78) did not subtract any background, their 7.1MeV beta branch could be due to the Compton contribution of higher energy gamma lines existing in nuclides of the A=102 chain. If it is assumed that all the counts in the 400keV gamma line come from ^{102}Nb, the 296keV line is still 3 times more intense. Thus it is postulated that the 6.4MeV beta branch populates directly the 296keV level in ^{102}Mo.

The Q_β-value (6.69$\pm$.13MeV) derived in the present work is then much less than that of Sti-78 (7.16$\pm$.15MeV). The difference in Q_β-values for the two isomers in ^{102}Nb implies that the high spin state lies 710$\pm$220keV above the low spin ground-state.

A=103

The observed gamma-line at 102.7keV contains contribution from the decays of both ^{103}Nb and ^{107}Tc (Kaf-76a). The beta spectrum in coincidence with this line exhibits two different half-lives, one short in the order of 2s and a longer one of about 20s (fig.34). Furthermore, the beta-rays of energy higher than 3MeV decay with the shorter half-life (2s)(table-VI). Since the reported half-life for ^{103}Nb is 1.8s (Kaf-76a), the higher end-point energy (4.86±.12MeV) has been assigned to the decay of ^{103}Nb (fig.35).

Berg et al (Ber-78) assigned three other gamma lines (641, 538 and 126keV) to the decay of ^{103}Nb. Their assignments were based on mass separation and half-life measurements. No gamma-gamma experiments were performed. The same authors measured an end-point energy for a beta transition postulated to populate a level at 641keV in ^{103}Mo which is consistent with the measurement of the present study. However, they observed a higher energy (5.34MeV) beta branch postulated to populate directly the 103keV level. Since neither the latter beta transition nor the new gamma lines were observed in the present study, the derived Q_β-value (4.99±.12MeV) has to be regarded as a lower limit.

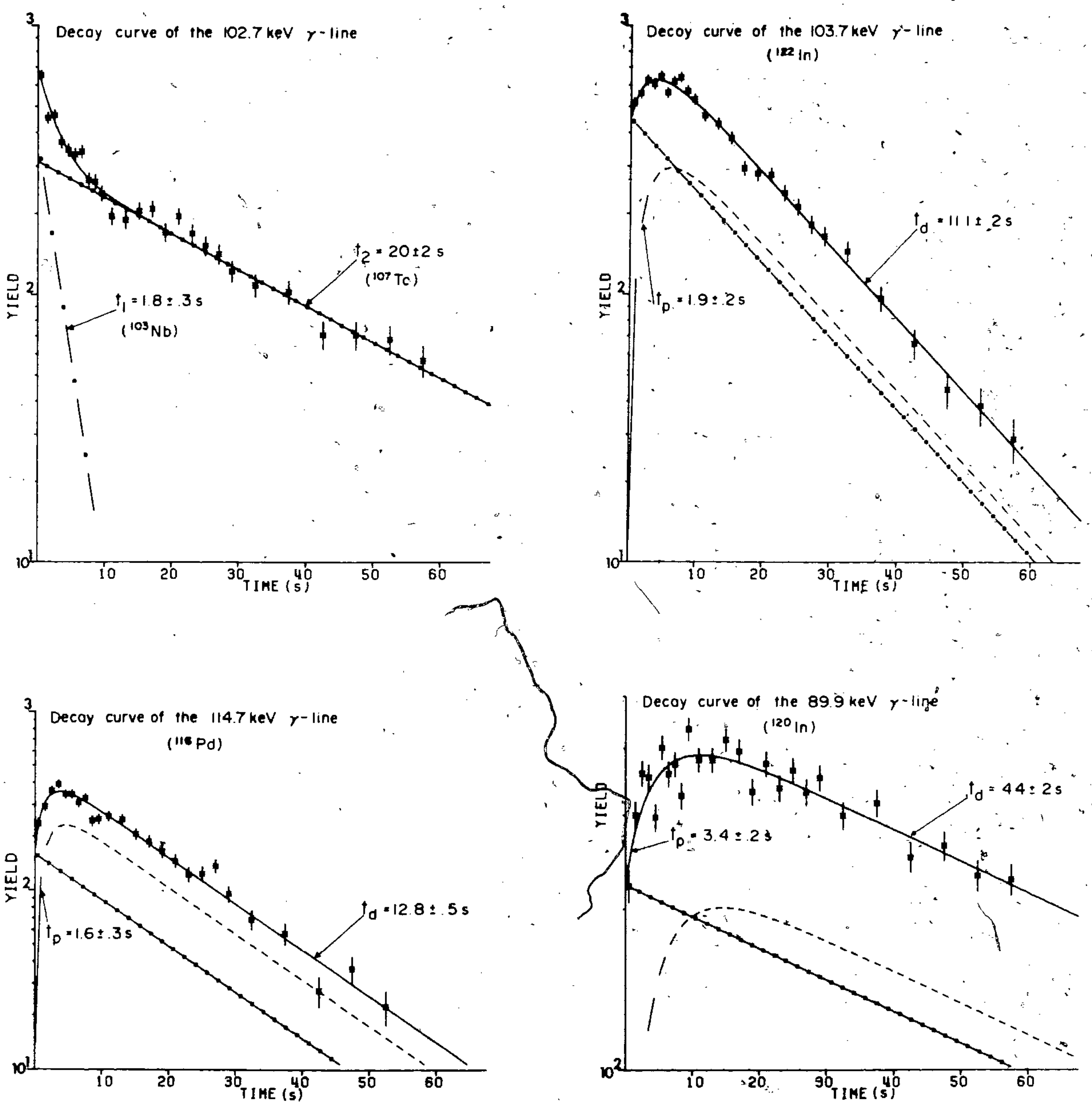
Decay curve of the 102.7 keV γ-line
t_2 = 20±2 s
(^{107}Tc)
t_1 = 1.8±.3 s
(^{103}Nb)
YIELD
TIME (s)
Decay curve of the 103.7 keV γ-line
(^{122}In)
t_d = 11.1±.2 s
t_p = 1.9±.2 s
YIELD
TIME (s)
Decay curve of the 114.7 keV γ-line
(^{116}Pd)
t_d = 12.8±.5 s
t_p = 1.6±.3 s
YIELD
TIME (s)
Decay curve of the 89.9 keV γ-line
(^{120}In)
t_d = 44±2 s
t_p = 3.4±.2 s
YIELD
TIME (s)

Figure 34.

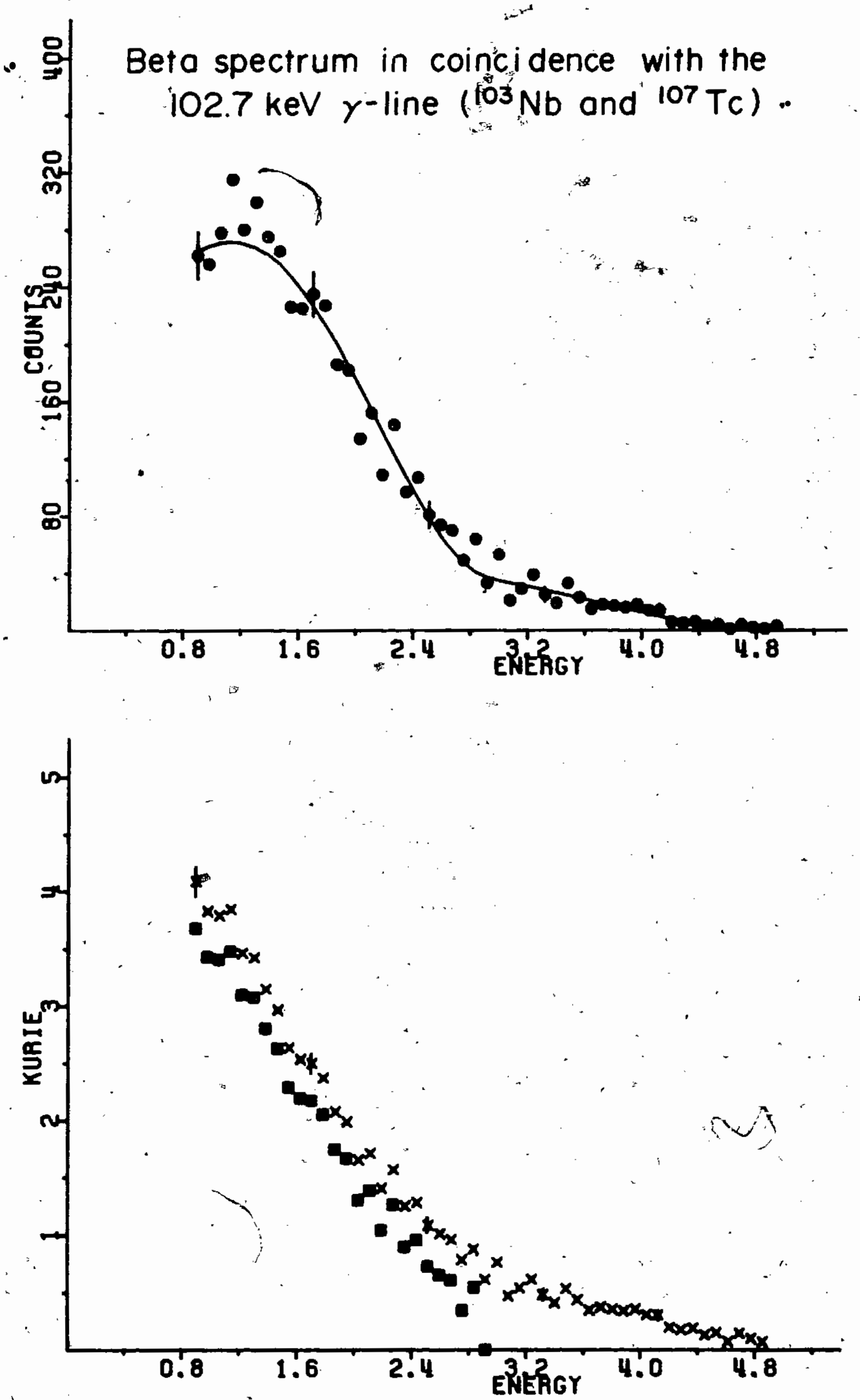

Beta spectrum in coincidence with the
102.7 keV γ-line (103Nb and 107Tc)
COUNTS
400
320
240
160
80
0.8
1.6
2.4
3.2
4.0
4.8
ENERGY
KURIE
5
4
3
2
1
0.8
1.6
2.4
3.2
4.0
4.8
ENERGY

Figure 35.

Although some information concerning the decay of ^{103}Mo can be found in ref.(Tit-76) a decay scheme has not been reported. In the present study a strong coincidence between the 45.8keV and the 423keV gamma-lines was observed. The half-life of the 45.8keV gamma-line was measured to be 65 ±3s which is in agreement with the value given in the previous reference. A 83.3keV gamma-line was also assigned to this decay in the same reference and such a line has also been observed in the present study, but no half-life determination could be made owing to poor statistics. The end-point energy of the beta spectrum in coincidence with the 45.8keV gamma-line has been measured to be 3.29± .17MeV (table-V). Since no gamma-line of greater energy than 423keV was detected in coincidence with the 45.8keV gamma-line it is assumed that the decay of ^{103}Mo populates mainly the 469keV (423+46) excited level in ^{103}Tc. This interpretation leads to a Q_β-value of 3.76± .17MeV for the decay of ^{103}Mo. Obviously, owing to the lack of information on the decay scheme of ^{103}Mo, this value has to be regarded as a tentative value.

A=104

The presence of the very neutron-rich nuclide ^{104}Nb has been observed in the present work. A 192keV gamma-line assigned to ^{104} Nb in ref.(Kaf-76a) was measured in the present study to decay with a 5 ±1s half-life. The value reported in the previous reference is 4.8±.4s for one the two known isomers.

The end-point energy of the beta spectrum in coincidence with this line leads to the determination of a lower limit of 5.7±.5MeV for the Q_{β}-value of ^{104} Nb. Due to the present lack of information concerning this decay no better Q_{β}-value could be obtained.

Some information about the decay of ^{104} Mo nuclide is available in ref.(Tit-76), but no decay scheme has been published. In the present study the gamma-gamma coincidence data (table-VI) can be separated in two groups. On the one hand, the 36.5,69.8,91.0 and the 375keV gamma-lines are all in coincidence with the 68.7keV gamma-line. On the other hand, the 50.0 and 55.0keV gamma-lines are in coincidence with each other and technetium x-rays, but not with transitions in the previous group, except for a weak coincidence between the 55 and 36keV gamma-lines. In the present study the average half-life obtained for ^{104}Mo through the decays of the 68.7(fig.36), 36.5, 50.0 and 55.0keV gamma-lines is 55±4s.

The Tc X-rays and the 36.5keV gamma line were observed in the gate spectrum of the 69.8keV gamma line in the gamma-gamma experiments (table-VI). However, these relationships were not confirmed by the gate spectra of either the 36.5keV or the Tc X-ray (fig.37). It is believed that the 69.8keV gate spectrum was contaminated by events from the tail of the very intense 68.7keV gamma line. A tentative decay scheme has been constructed (fig.38). The half-lives extracted from the beta-gamma delayed coincidence data (table-III) are consistent with the direct population of a delayed (7ns) state at 105keV in ^{104}Tc. The 36.5keV gamma line was part of a multiplet in the X-ray region and, consequently, the associated relative intensity may be overestimated. To be consistent with the decay scheme, it is assumed that this line is highly converted. This is a reasonable assumption with regard to the low energy involved and the delay of the depopulated state.

The measured end-point energies of the beta spectra in coincidence with the 68.7keV and the 55.0keV gamma-lines lead to an average Q_β-value of 2.12±.05MeV.

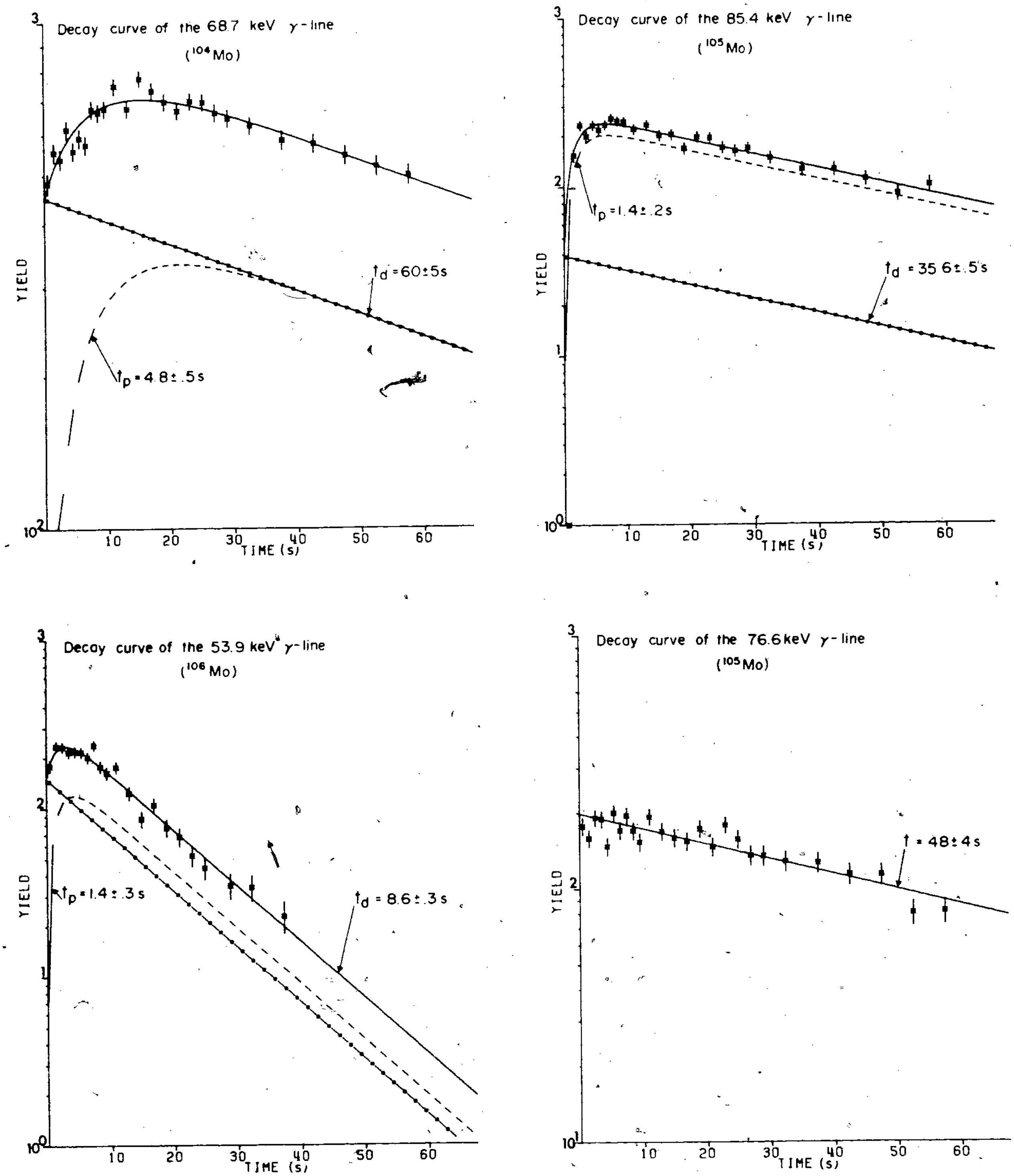
Decay curve of the 68.7 keV γ-line
(^{104}Mo)
t_d = 60±5s
t_p = 4.8±.5s
YIELD
TIME (s)
Decay curve of the 85.4 keV γ-line
(^{105}Mo)
t_p = 1.4±.2s
t_d = 35.6±.5s
YIELD
TIME (s)
Decay curve of the 53.9 keV γ-line
(^{106}Mo)
t_p = 1.4±.3s
t_d = 8.6±.3s
YIELD
TIME (s)
Decay curve of the 76.6keV γ-line
(^{105}Mo)
t = 48±4s
YIELD
TIME (s)

Figure 36.

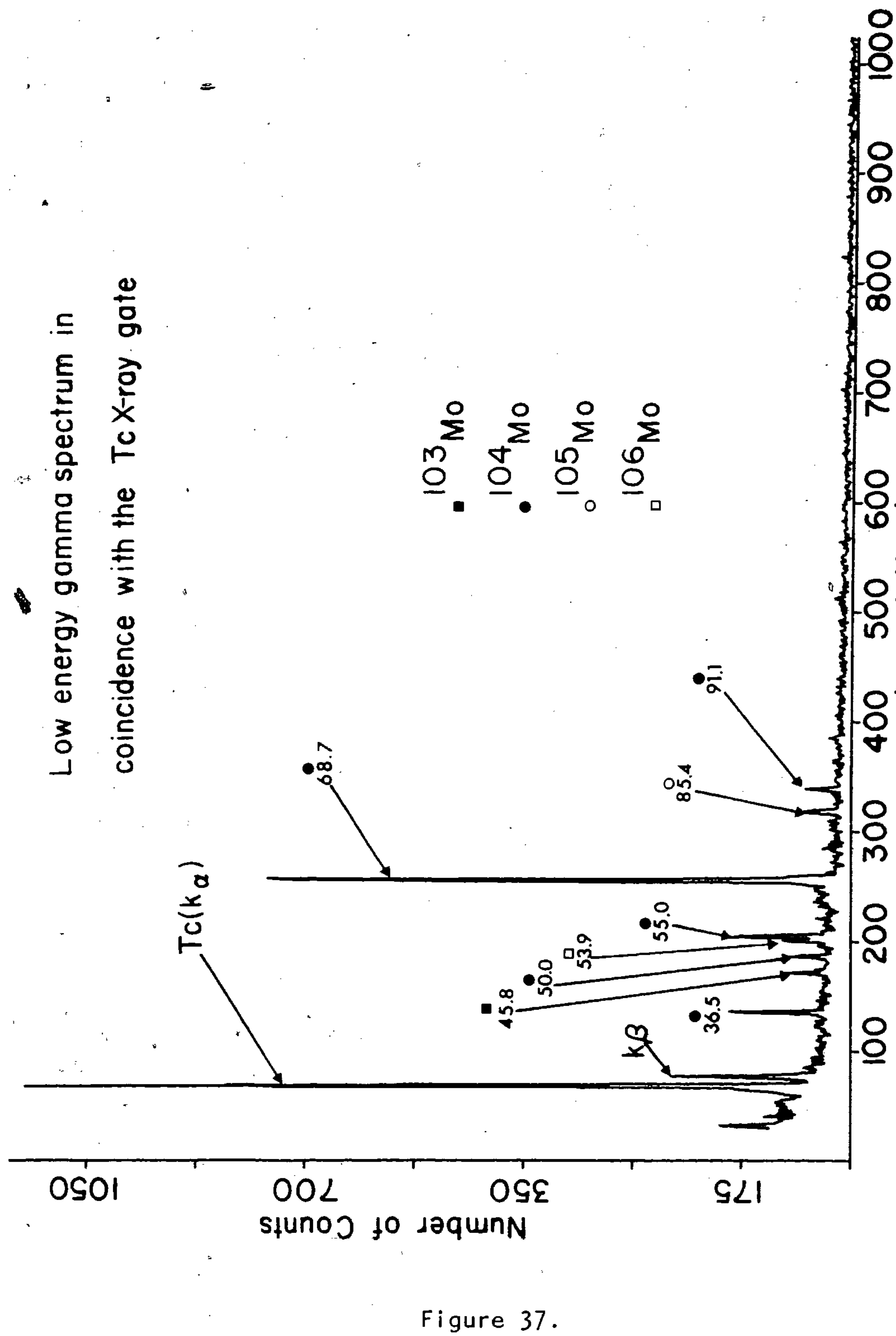

Low energy gamma spectrum in
coincidence with the Tc X-ray gate
103Mo
104Mo
105Mo
106Mo
Tc(kα)
kβ
68.7
45.8
50.0
53.9
55.0
36.5
85.4
91.1
Number of Counts
1050
700
350
175
Channel Number
100
200
300
400
500
600
700
800
900
1000

Figure 37.

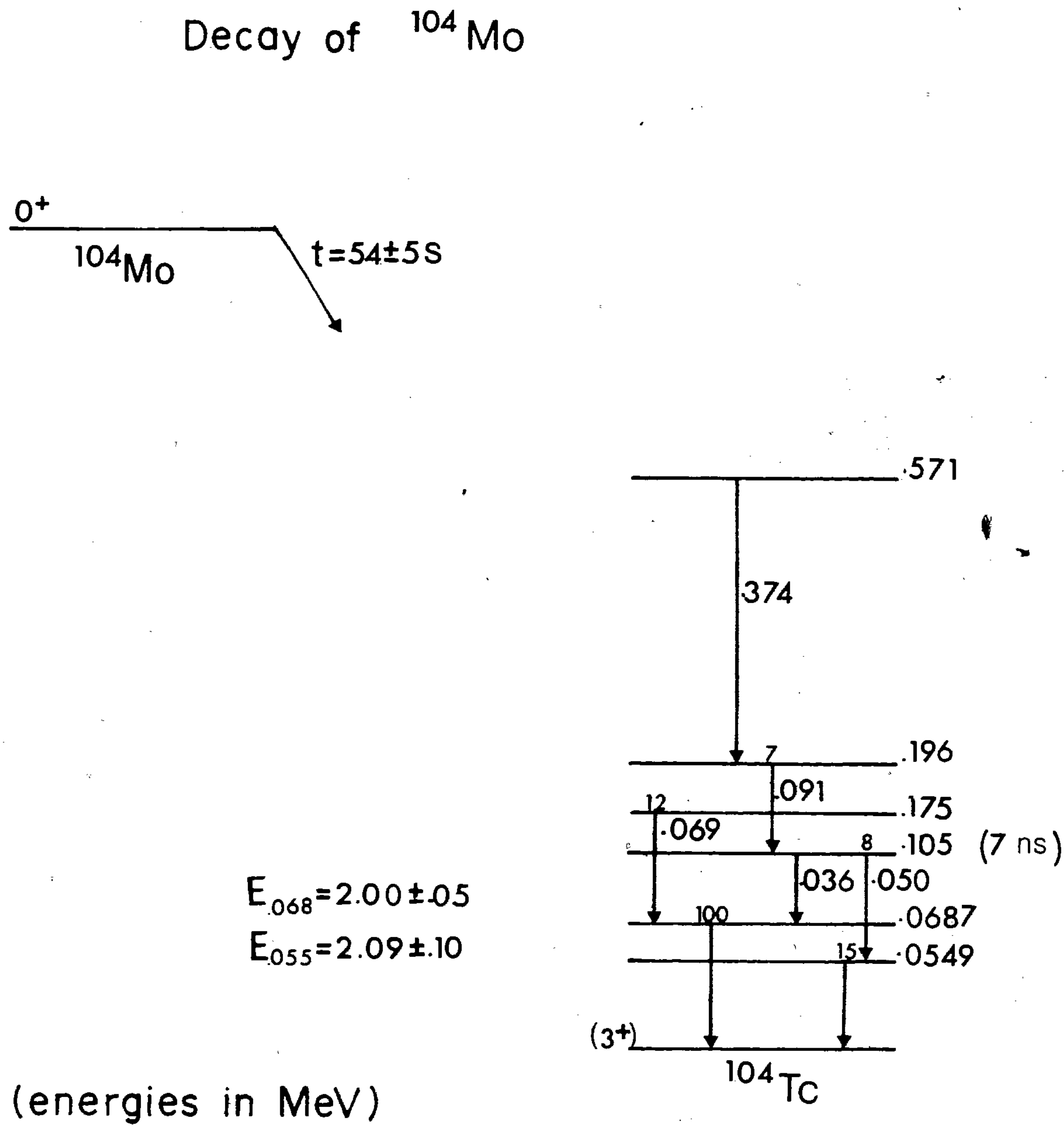

Decay of 104 Mo
0+
104Mo
t=54±5S
.571
374
.196
7
.091
12
.175
.069
8
.105 (7 ns)
.036
.050
100
.0687
15
.0549
(3+)
104Tc
E.068=2.00±.05
E.055=2.09±.10
(energies in MeV)

Figure 38.

A=105

A preliminary decay scheme exists for the decay of ^{105}Mo in ref.(Tit-77a). Coincidence data from the present work agree quite well with this scheme. Two main groups of gamma-lines can be separated. The first group contains all lines in coincidence with the 85.4keV line and whereas the second includes those in coincidence with the 76.6keV line. The 147.8keV and 85.4keV gamma-lines decay with a similar half-life. The 85.4keV line was measured in the present study to decay with a 35.6±.5s half-life. Such a value is, indeed in good agreement with the determination of ref.(Tit-77b). From "singles" and gamma-beta coincidence data from the present work, a half-life of 48±4s can be attributed to the 76.6keV gamma-line. This value is in disagreement with the measurements of ref.(Tit-77b). However, both half-lives are in agreement with the determinations of ref.(Kis-77). The presence of two states has been suggested very recently in ref.(N105-79).

However, the list of the gamma transitions with their relative intensities assigned to this decay in the latter reference is not consistent with either the present results or those in ref.(Tit-77b). In particular, the 69keV gamma line assigned to the decay of ^{105}Mo is believed to belong to the decay of ^{104}Mo. The half-life (58±1s) measured in Kis-77 supports this latter identification.

In fig.39 the main features of the decay scheme are reproduced from ref.(Tit-77a). Relative gamma intensities are those measured in the present work. As a growth is observed in the decay curve of the 85.4keV gamma line (fig.36) the half-life of ^{105}Nb can also be determined (T=1.4 ±.2s). The two different half-lives for the decay of ^{105} Mo imply the existence of an isomeric state. As no growth can be observed in the decay of the 76.6keV gamma-line (fig.36) one can deduce that this isomer is populated exclusively via fission and therefore, is likely to be a high spin state. The odd neutron in ^{105}Mo can either be in the $s_{1/2}$ or $g_{7/2}$ state according to the shell model suggesting a possible 1/2+ and 7/2+ spin assignment for the two isomers.

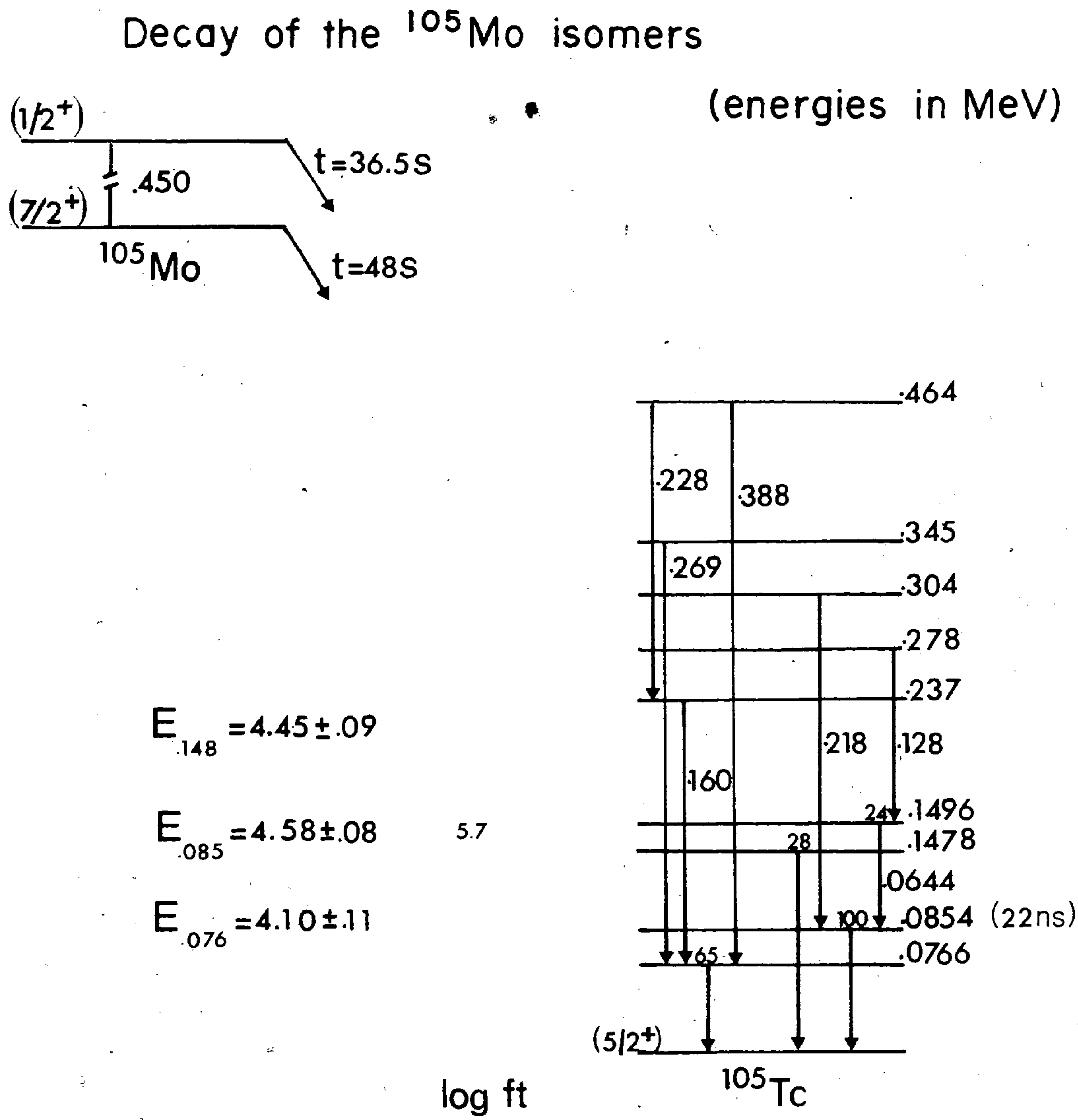
Decay of the 105Mo isomers
(energies in MeV)
(1/2+)
.450
(7/2+)
105Mo
t=36.5S
t=48S
.464
.228
.388
.345
.269
.304
.278
.237
.218
.128
.160
24
.1496
28
.1478
.0644
100
.0854 (22ns)
65
.0766
(5/2+)
105Tc
E.148 =4.45±.09
E.085 =4.58±.08
5.7
E.076 =4.10±.11
log ft

Figure 39.

The beta spectra in coincidence with the 85.4keV and 76.6keV gamma-lines are displayed in fig.40 with the associated Fermi-Kurie plots.

It is assumed direct beta transitions populate the excited levels at 85.4 and 147.8keV in ^{105}Tc (fig.35). These transitions are, furthermore, assumed to arise from the decay of the low spin state which should be populated mainly through the decay of ^{105} Nb.

The end-point enegies of the beta spectra in coincidence with these lines are consistent with an averaged Q_{β}-value of 4.72±.08MeV (table-V).

A beta transition is also assumed to populate directly the 76.6keV level in ^{105}Tc. This assumption is based upon the measured relative gamma intensities. A $Q\beta$-value of 4.22±.15MeV for the high spin isomer in ^{105}Mo can then be deduced. From this interpretation, the low spin isomer is found to lie above the high spin state at an excitation energy of 430±230keV.

Under the assumption of direct beta populations, the 85.4keV level was measured to be a long-lived state with a half-life of about 22ns whereas the 76.6keV level was found to be a "prompt" state (table-III).

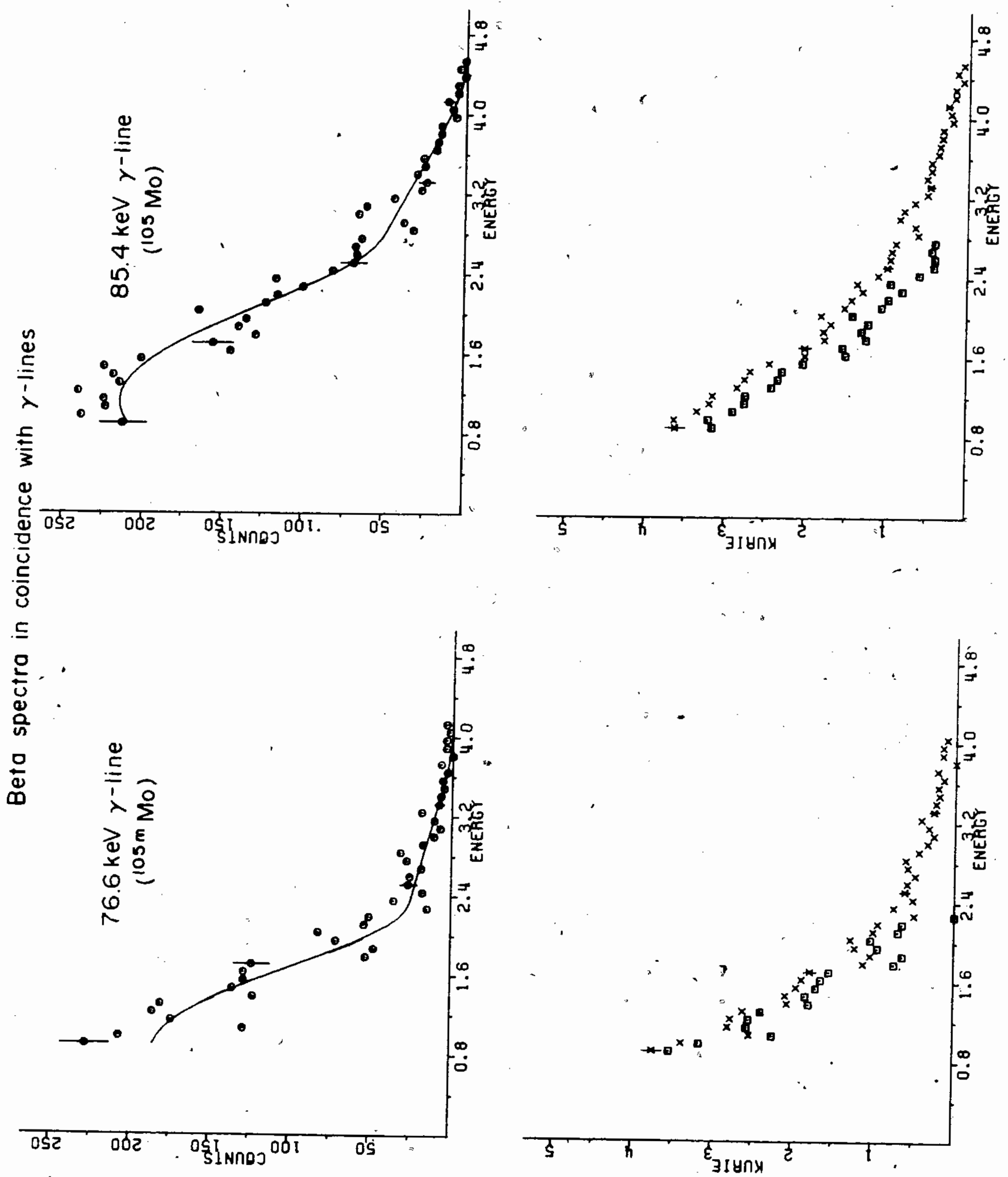
Beta spectra in coincidence with γ-lines
85.4 keV γ-line
(105 Mo)
76.6 keV γ-line
(105m Mo)
COUNTS
ENERGY
KURIE
0.8
1.6
2.4
3.2
4.0
4.8
50
100
150
200
250
1
2
3
4
5

Figure 40.

A=106

From ref.(Kaf-76a) a 53.9keV gamma-line decaying with a 8.6±0.3s half-life has been assigned to the decay of ^{106}Mo. From the coincidence data of the present work (table-VI) a preliminary decay scheme has been constructed (fig.41).

The 429 and 189keV gamma lines do not show up in the total gamma spectrum of beta-gamma experiments. The 618keV is unresolved from the intense 617keV gamma line of the decay of ^{96m}Y. The only measured end-point energy is the one associated with the beta spectrum in coincidence with the 53.9keV gamma-line. The delayed beta-gamma coicidence data provides a measurement of the half-life of the delayed state populated by the beta transition having an end-point energy of 3.12MeV. It is more likely that this half-life (6±1ns) corresponds to the 54keV level than the 672keV state which is deexcited by two gamma transitions. Furthermore, the peak in the time spectrum associated with the 617-618keV gamma line in beta-gamma coincidence experiments does not show any tailing. From these arguments the 54keV level has been placed at the bottom in the scheme of ^{106}Tc.

This interpretation leads to a Q_β-value of 3.18±.16MeV for the decay of ^{106}Mo (table-V).

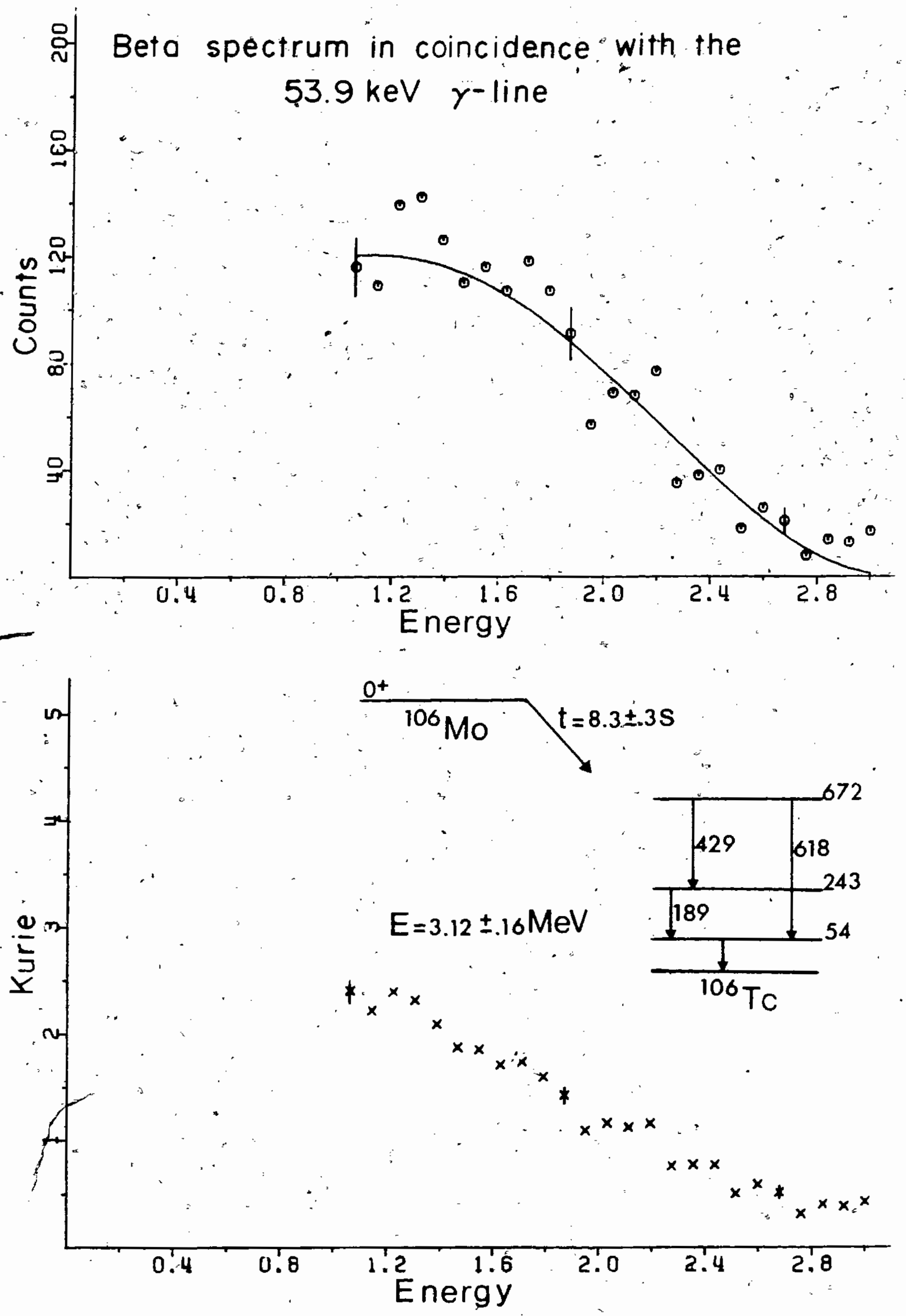

Beta spectrum in coincidence with the
53.9 keV γ-line
Counts
200
160
120
80
40
0.4
0.8
1.2
1.6
2.0
2.4
2.8
Energy
Kurie
5
4
3
2
1
0+
106Mo
t=8.3±.3S
672
429
618
243
189
54
106Tc
E=3.12±.16MeV
0.4
0.8
1.2
1.6
2.0
2.4
2.8
Energy

Figure 41.

A=107

From ref.(Kaf-76a,TI-78) and from the measured half-lives (table-VI) the 102.7, 106.3 and 145.5keV gamma-lines have been assigned to the decay of ^{107}Tc. No decay scheme was available in the literature and from the coincidence data (table-VI) a preliminary scheme has been constructed (fig.42).

The end-point energy of the beta spectrum in coincidence with the 145.5keV gamma-line was measured to be 3.38 ±.06MeV. This line is in coincidence with a 916keV gamma-line and this leads to a possible total beta energy of 4.44MeV (3.38+.92+.14). A similar value (4.49MeV) is obtained by summing (table-V) the end-point energy of the low energy branch of the beta radiation in coincidence with the 102.7keV gamma-line (fig.35) and the highest energy of the gamma-lines in coincidence with this 102.7keV line (2.89+.103+1.50). From the preliminary decay scheme (fig.42) a 4.46±.07MeV Q_β-value can be tentatively associated with the decay of ^{107}Tc.

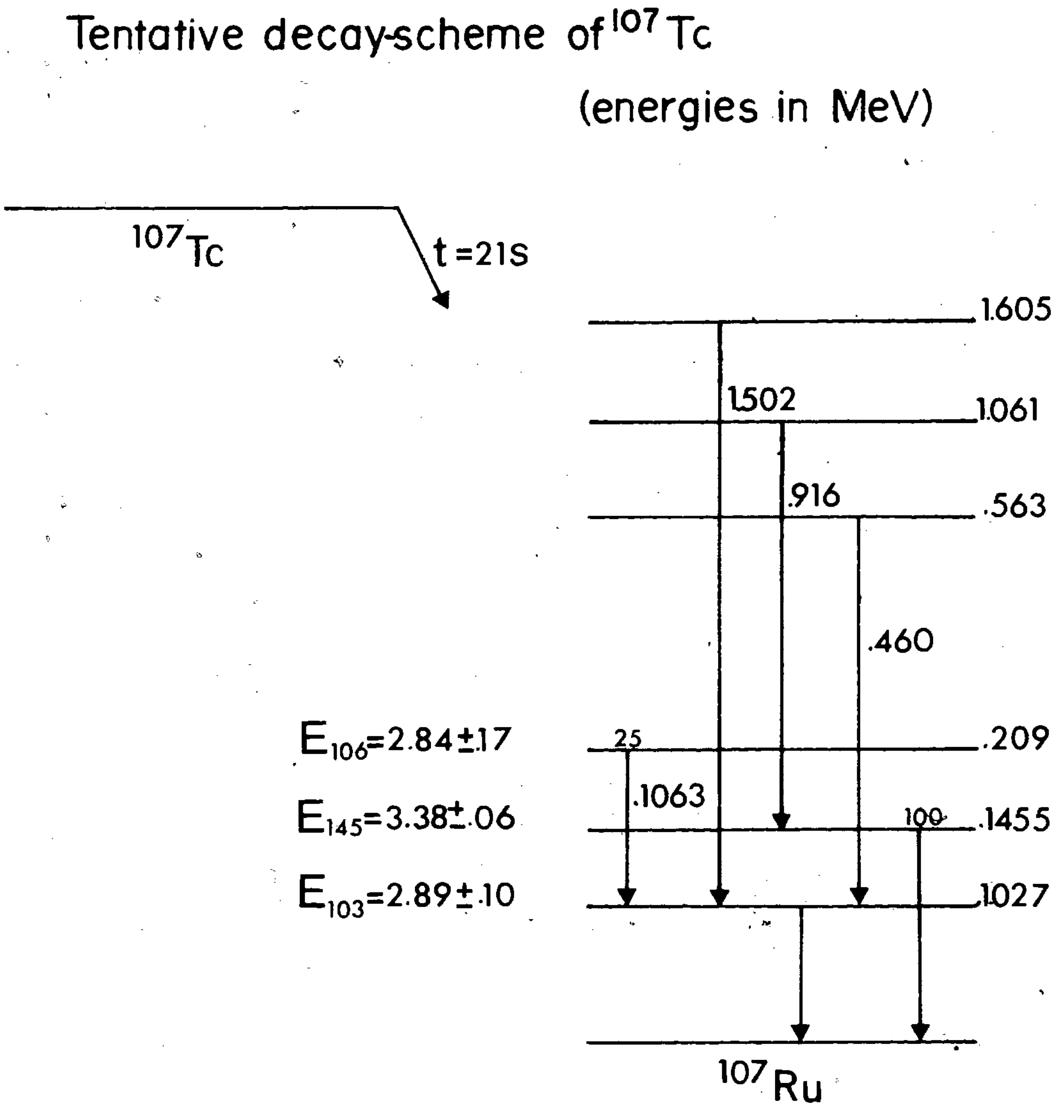
Tentative decay-scheme of ^{107}Tc
(energies in MeV)
^{107}Tc
t=21S
1.605
1.502
1.061
.916
.563
.460
$E_{106}=2.84\pm.17$
25
.209
.1063
$E_{145}=3.38\pm.06$
100
.1455
$E_{103}=2.89\pm.10$
.1027
^{107}Ru

Figure 42.

A=108

In the present study, the strong 242keV gamma line with a measured half-life of 5.1±.2s has been assigned to the decay of ^{108}Tc. This assignment was based on the study of ref.(Kaf-76a). In the same reference a preliminary decay scheme is proposed. In the coincidence data of the present work only two gamma-lines at 733keV and 1584keV were found to be in coincidence with the 242keV gamma-line. The 733keV line is included in the decay scheme of the previous reference whereas the 1584keV line has not been yet reported. It should be pointed out that the gamma spectrum presented in Kaf-76a had an energy limit of about 1MeV.

The beta spectrum in coincidence with the 242keV gamma-line exhibits two main components (table-VI). It is assumed that the high energy branch populates directly the level at 1826keV (1584+242) in ^{108}Ru. Such an interpretation leads to a tentative Q_β-value of 7.51±.08MeV (table-V). In fig.25 the spectrum "b" exhibits a peak at 242keV. This implies that there must be a higher energy (>6.5MeV) beta branch in coincidence with the 242keV gamma line which has been missed by KURIE. It is then assumed that this beta transition populates another excited state in ^{108}Ru. A possible candidate would be the 975keV level which is deexcited by the 733keV gamma line.

A=109

Recently, detailed decay schemes for ^{109}Rh were reported (Kan-78, Fra-78b). The beta decay of ^{109}Rh mainly populates the 326.7keV level in ^{109} Pd which is then deexcited almost exclusively by a gamma transition to the ground-state. In the present study a 326.7keV gamma-line was observed and assigned to the decay of ^{109} Rh. Due to poor statistics its half-life could not be rigorously determined. However a half-life greater than 60s is indicated. The accepted value is 79.8 ±1.1s (Fra-78a).

The beta spectrum in coincidence with the 326.7keV gamma-line exhibits an end-point energy of 1.98±0.06MeV (table-V). This leads to a Q_β-value of 2.31±.06MeV which is in agreement with the 2.5±.5MeV value in ref.(Kan-78).

A=110

A detailed decay scheme is available for the decay of ^{110}Rh (N110-77). The relative position of the two isomers is, however, unknown. It is believed (N110-77) that the 3.3s isomer is a low spin (1+) state. The population of such a state is most likely to occur through the decay of ^{110}Ru which has a half-life of 13s (N110-77). The 28s isomer is assumed, in the same reference, to be a high spin state (5+,4+) mainly populated directly by fission. The 3.3s isomer decays mainly to the ground-state and the first excited state of the ^{110}Pd daughter nuclide while the 28s isomer decays mainly (57%) to the 2805keV and 2790keV (28%) excited states of the same nuclide (N110-77). Two end-point energies have been obtained for the beta spectrum in coincidence with the 373keV gamma line (fig.43). Both logft-values are 4.7 and therefore the associated beta transitions are allowed.

The high energy branch of the beta spectrum in coincidence with the 373keV gamma line leads to a Q_β-value of 4.90+.37=5.27MeV for the 3.3s isomer. Since 85% of the decay of the 28s isomer populates the two neighbouring levels near 2800keV in ^{110}Pd it is assumed

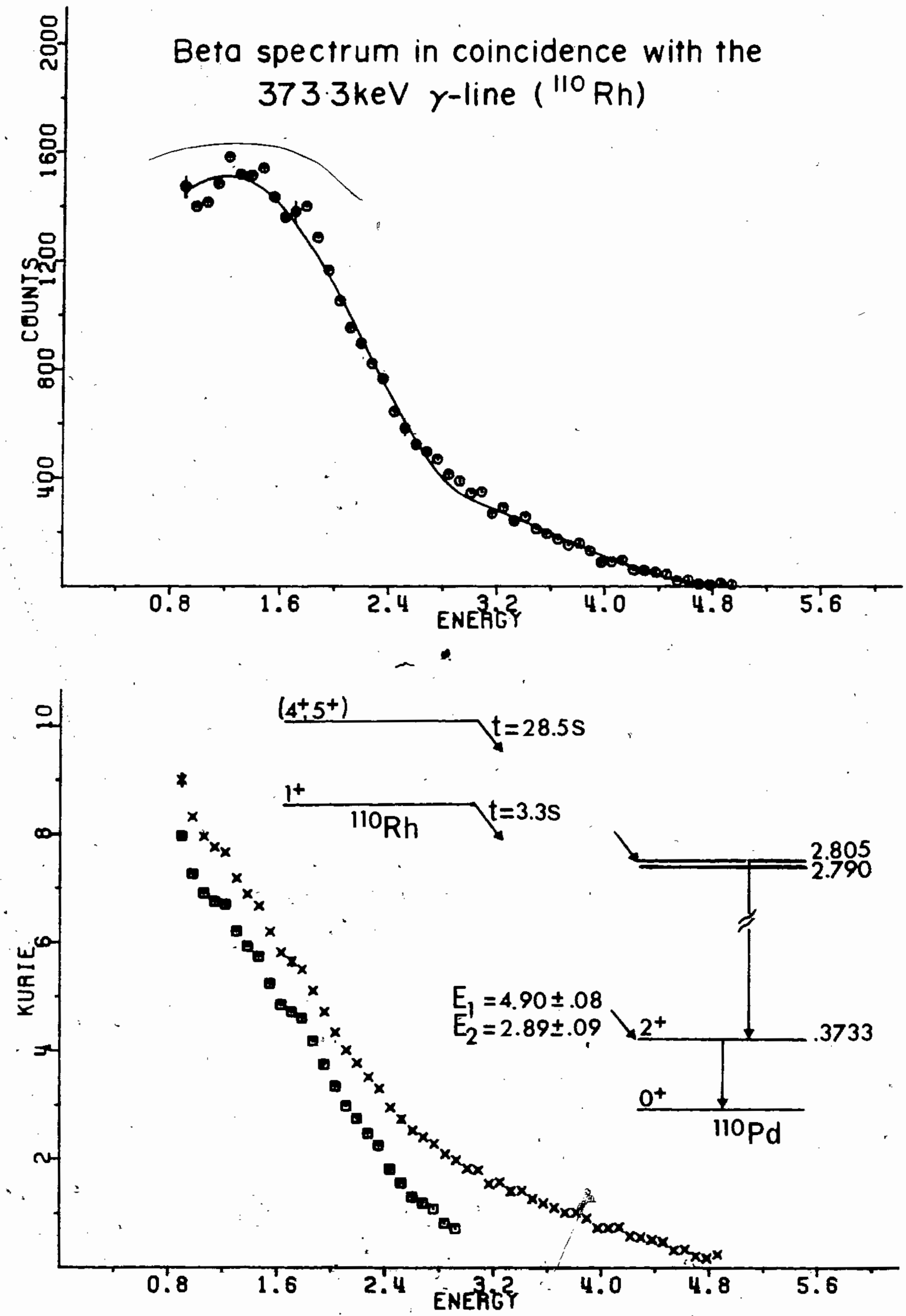

Beta spectrum in coincidence with the
373.3keV γ-line (^{110}Rh)
COUNTS
2000
1600
1200
800
400
0.8
1.6
2.4
3.2
4.0
4.8
5.6
ENERGY
KURIE
10
8
6
4
2
(4+,5+)
t=28.5S
1+
110Rh
t=3.3S
2.805
2.790
E1 =4.90±.08
E2 =2.89±.09
2+
.3733
0+
110Pd
0.8
1.6
2.4
3.2
4.0
4.8
5.6
ENERGY

Figure 43.

that the low energy end-point of the beta spectrum in coincidence with the 373keV gamma line corresponds to an average between the end-points of the two beta transitions. Then, a Q_β-value of 5.69±.09MeV can be derived for the 28s isomer. From both Q_β-values it can be deduced that the high spin state lies 400±170keV above the ground-state in ^{110}Rh.

A=114

The decay of ^{114}Ag has been well studied (Bru-75). The beta spectra in coincidence, in the present study, with the 558keV gamma-line leads to a Q_β-value of 4.82± .14MeV (table-V). This value is in good agreement with that of ref.(Wap-77). The end-point energy of the beta spectrum in coincidence with the 576keV gamma line, initially assigned to the same decay, is inconsistent with such a result. Owing to poor statistics the half-life of this line could not be extracted and, therefore, the corresponding end-point energy measurement was not included in the Q_β determination.

A=115

A low energy gamma-line of 48.5keV energy, observed in the present work to decay with a half-life of 31 ± 2s, has been assigned to the decay of ^{115}Pd (N115-75). Although the accepted value is 37.4±.4s, several measurements of this half-life have been reported with values widely spread between 45s and 30s. The most recent measurement gives 30±2s (N115-75). No decay scheme has been reported for this nuclide. In the present work it is assumed that the beta decay of ^{115}Pd populates directly the level at 48.5keV in ^{115}Ag (fig.44). This is supported by the facts that no gamma-line was detected in coincidence with this low energy line and no that other gamma-line has ever been reported for this decay. The deduced associated $Q\beta$-value is then 4.63±.15MeV (table-V).

Gamma lines at energies of 229, 131, 113 and 388keV have been assigned to the decay of ^{115}Ag based on their associated half-lives and coincidence data (table-VI)(N115-75).

The beta decay is assumed to populate mainly the 361keV excited state of ^{115}Cd (fig.44). Such an interpretation is supported by the spin assignment (and published data) given in a recent study of the decay of

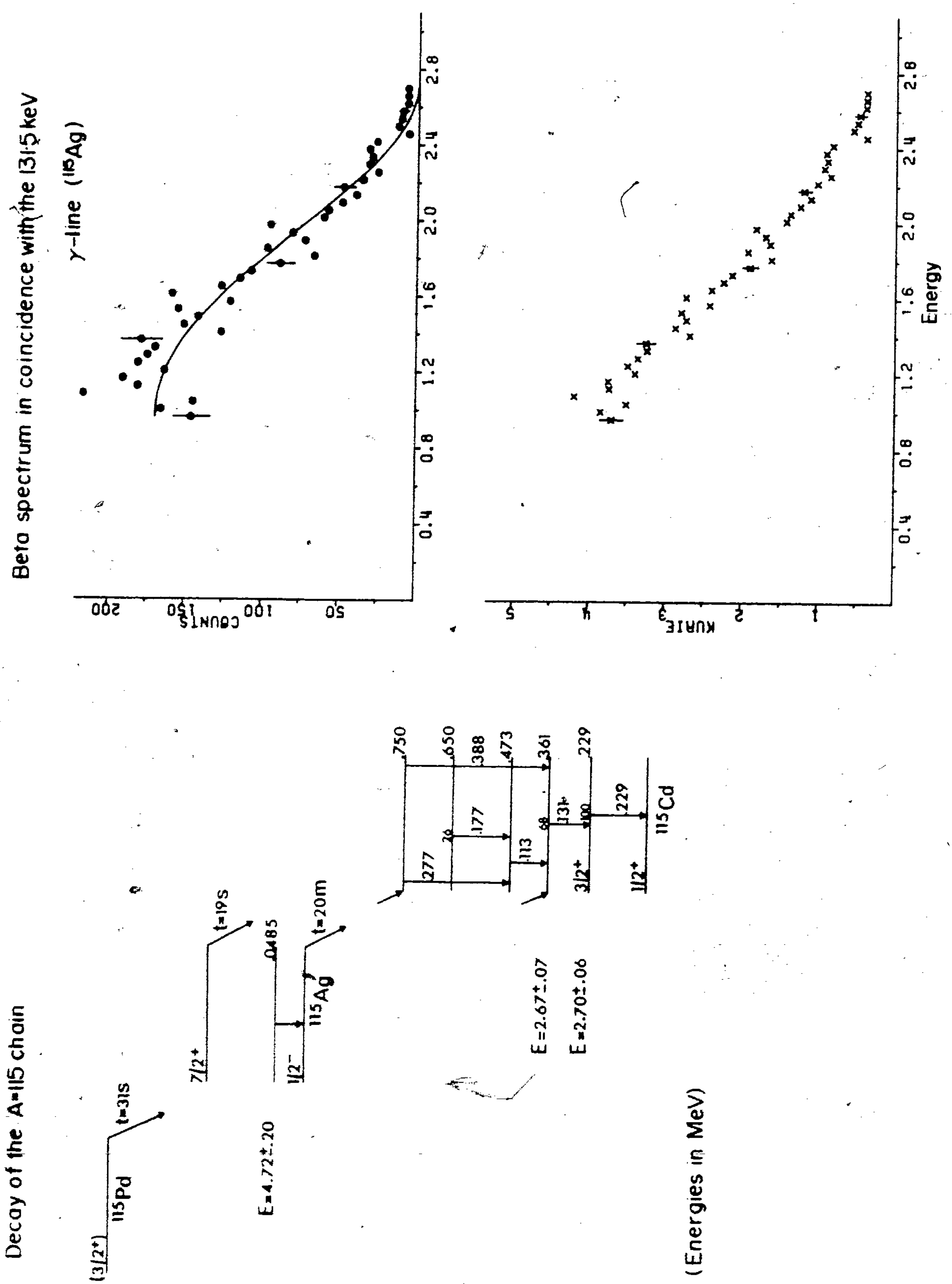
Beta spectrum in coincidence with the 131.5 keV
γ-line (115Ag)
COUNTS
KURIE
Energy
Decay of the A=115 chain
(3/2+)
115Pd
t=31S
E=4.72±.20
7/2+
t=19S
1/2−
115Ag
0.485
t=20m
E=2.67±.07
E=2.70±.06
3/2+
1/2+
115Cd
(Energies in MeV)

Figure 44.

20min ^{115}Ag (Mat-78). This transition is allowed with a logft-value of 4.3. The end-point energies measured for the beta spectra in coincidence with the 229, 131keV gamma-lines lead to an average Q_β-value of 3.08 ± .09MeV (table-V). This result is in good agreement with the reported value of ref.(Wap-77).

A=116

From the preliminary decay scheme reported in ref.(Bru-75) a 114.7keV gamma-line has been assigned to the decay of ^{116}Pd. The coincidence data supports strongly this assignment. The 114.7keV line was measured to be in coincidence with silver X-rays and three gamma transitions assigned to this decay. The decay curve of the 114.7keV gamma line is shown in fig.34. The observed growth allowed the determination of the previously unmeasured half-life of the ^{116}Rh parent (T=1.6 ±.3s). The coincidence data of the present work confirm the results reported earlier (Bru-75). The measured end-point energy of the beta spectrum in coincidence with the 114.7keV gamma-line leads to a Q_β-value of 2.59 ±.13MeV.

The energy levels in ^{116}Cd are known up to an excitation energy of about 3MeV, but the beta branching ratios from the high-spin isomer of ^{116}Ag are still unknown. A comparison between the relative intensities from ref.(N116-75) and those obtained in the present work for the main gamma transitions in the decay of ^{116m}Ag is displayed below:

Gamma energies	% N116-75	% present work
514keV	100	100 ±6
706 "	64	63 ±3
1029 "	34	30 ±2

The gamma-gamma coincidence data suggest that these 3 lines form a direct cascade. The beta spectra in coincidence with the 514, 706 and 1029keV gamma-lines exhibit similar end-point energies (table-VI). These results imply that a strong beta transition populates the 2250keV (514+706+1029) excited level in ^{116}Cd. The difference in relative intensity can be explained by a beta transition populating the higher energy states in ^{116}Cd whose deexcitation would take place through other gamma cascades. As the isomer ^{116m}Ag is known to lie 81keV above the ground-state (N116-75), an average $Q\beta$-value has been derived for ^{116g}Ag. This latter, 5.36±.05MeV value is in agreement with that in ref.(Ale-77). It should be pointed out that the half-lives measured in beta-gamma experiments of the present study are somewhat shorter (table-VI) than the accepted value (10.4s) for ^{116m}Ag (N116-75).

A=117

As for many silver isotopes two isomers are known in ^{117}Ag. The high-spin one (7/2+) is known (N117-78) to populate mainly the 820keV and the 522keV excited states in ^{117}Cd (fig.45). The coincidence data (table-VI) associated with the 135.4keV gamma-line and the measured half-life (T=5.4±.2s) of the present work are in good agreement with the reported decay scheme of ref.(N117-78).

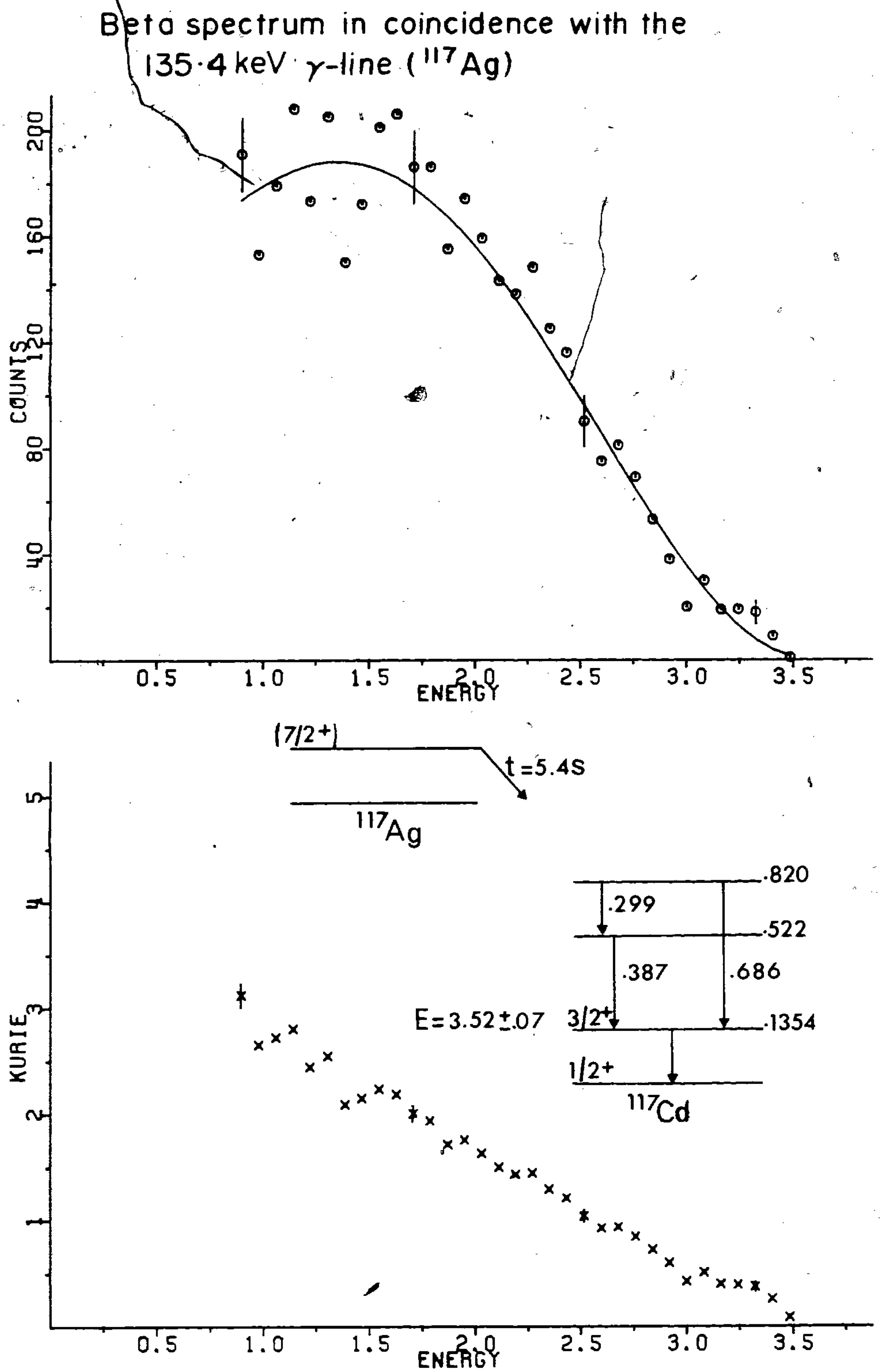
Beta spectrum in coincidence with the
135·4 keV γ-line (117Ag)
COUNTS
200
160
120
80
40
0.5
1.0
1.5
2.0
2.5
3.0
3.5
ENERGY
(7/2+)
t=5.4S
117Ag
.820
.299
.522
.387
.686
E=3.52±.07
3/2+
.1354
1/2+
117Cd
KURIE
5
4
3
2
1
0.5
1.0
1.5
2.0
2.5
3.0
3.5
ENERGY

Figure 45.

The beta spectrum in coincidence with the 135keV gamma line should represent the sum-spectrum of the two beta transitions populating the 522 and 820keV levels in ^{117}Cd (Fog-76b). The analysis of this spectrum by KURIE provided only one end-point energy. This energy should correspond to the transition of higher energy as both transitions are about the same strength (Fog-76b). One can then derived a Qβ-value of 4.04±.07MeV which is in agreement with that in ref.(Ale-77).

A=118

The decay of ^{118}Ag has been studied previously (N118-76). In the present study only the gamma-lines of the decay of the two first excited states of ^{118}Cd have been observed (fig.46). The half-life for the 488keV gamma-line has been measured to be 3.9 ±.5s which suggests that the observed decay is primarily that of the ground-state of ^{118}Ag.

According to the reported decay scheme (N118-76), the decay of the 3.7s isomer should mainly populate the two first excited states in ^{118}Cd. A 677keV gamma line was observed in the total gamma spectrum of beta-gamma experiments of the present study.

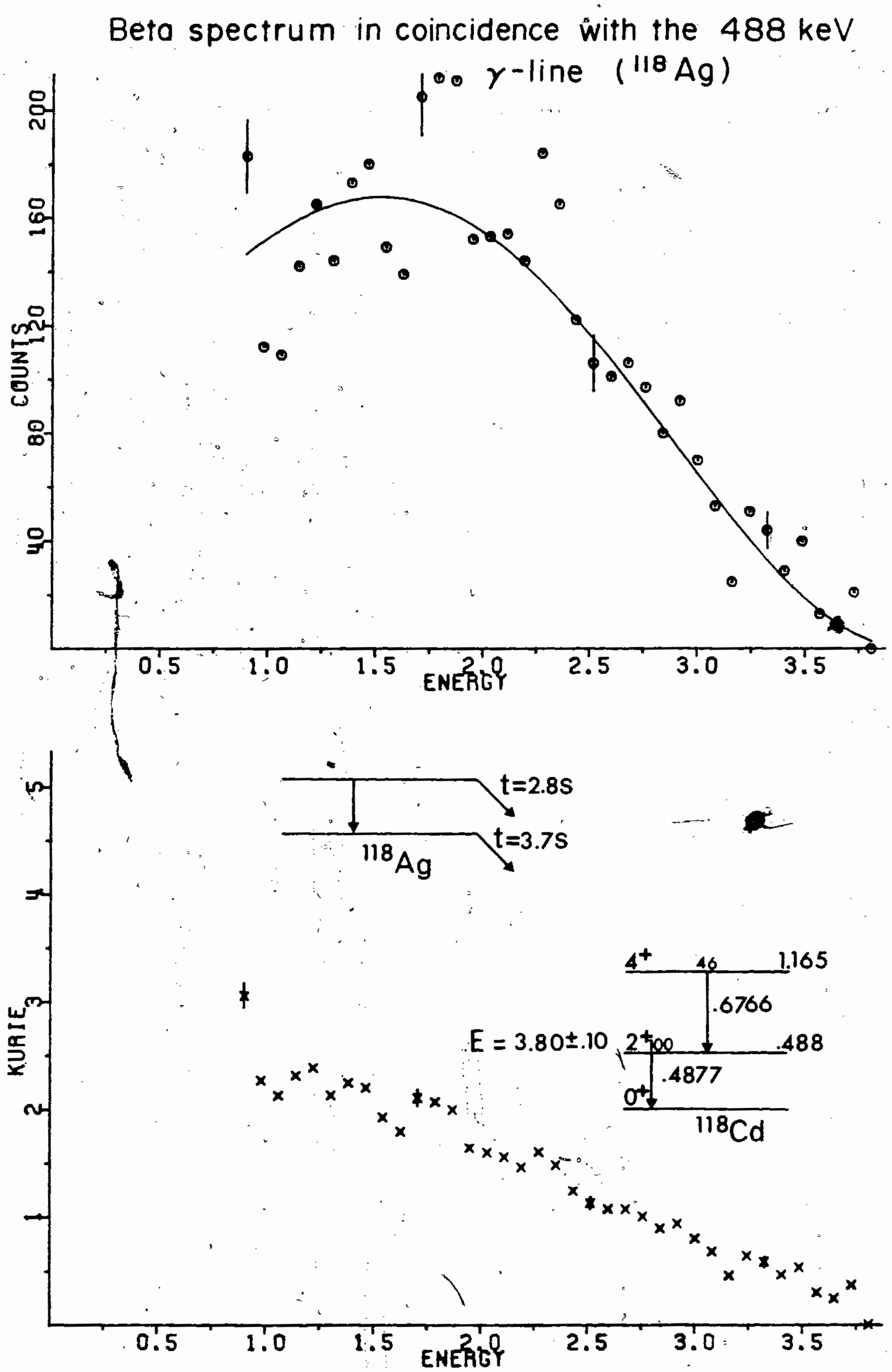

Beta spectrum in coincidence with the 488 keV γ-line (118Ag)
COUNTS
200
160
120
80
40
0.5
1.0
1.5
2.0
2.5
3.0
3.5
ENERGY
KURIE
5
4
3
2
1
t=2.8S
t=3.7S
118Ag
4+
46
1.165
.6766
E = 3.80±.10
2+
100
.488
.4877
0+
118Cd
0.5
1.0
1.5
2.0
2.5
3.0
3.5
ENERGY

Figure 46.

However, there are neither coincidence data nor half-life information to support an assignment to the decay of ^{118}Ag. Moreover, the end-point energies of the beta spectra in coincidence with the 488 and 677keV gamma lines are not consistent with such a population. Elucidation of this problem would require further investigations. No $Q\beta$-value could be derived.

A=120

The decay of ^{120}In has been well studied (N120-76),and recently two intensive investigations have been reported (Che-78b,Fog-79).

Fig.47 reproduces the main features of the decay scheme of ref.(Ale-77). The decay curves for the 90keV and 197keV gamma-lines, obtained from the "singles" experiments exhibit the same pattern,i.e., a main component with a half-life of 44±2s and a growth with a half-life of 3.4±.2s (fig.34). This suggests that the low-spin isomer (J=1+) decays by an isomeric transition to the J=(4+,5+) isomer which then decays and populates high excited states in the ^{120}Sn daughter nuclide.

Decay of ^{120}In

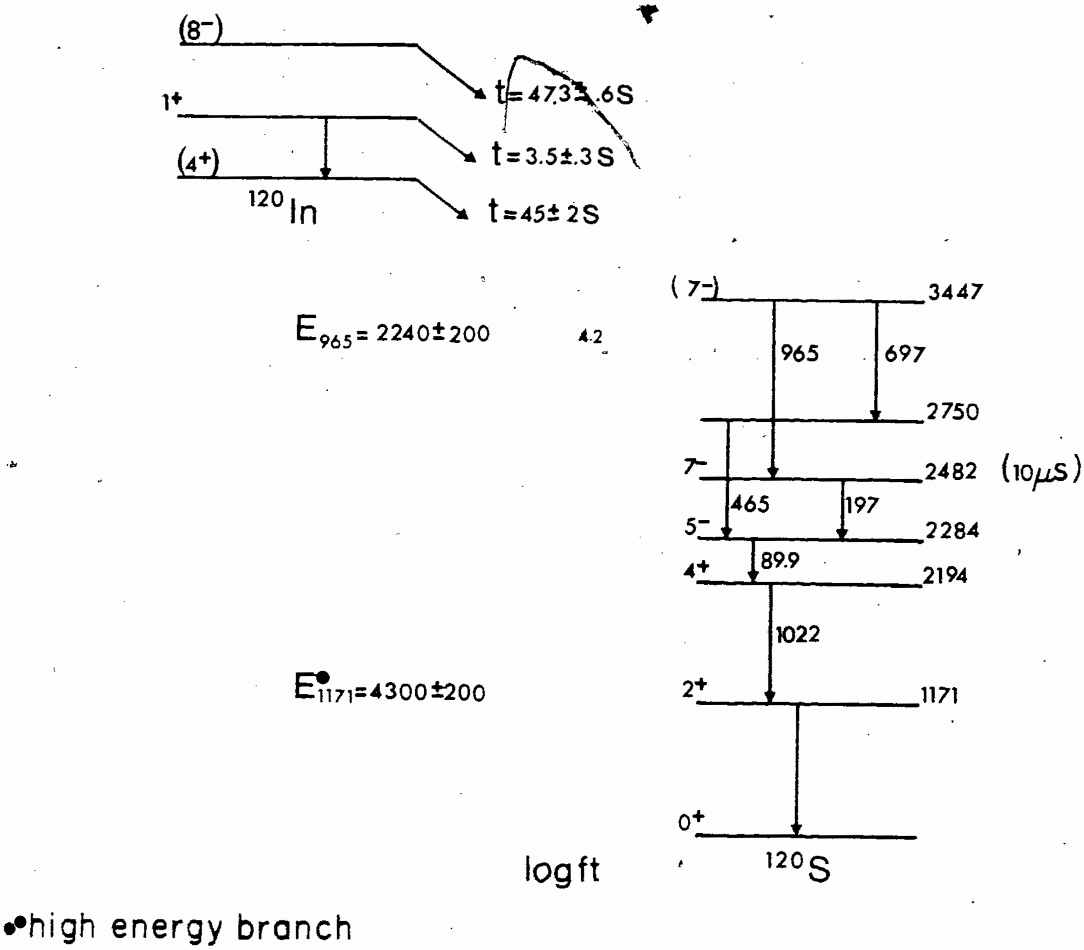

Figure 47.

The observation of the 3.4s activity implies the direct population via fission of the (1+) isomer (no isomer is expected to be found in the even-even parent isotope ^{120}Cd which decays with a 51s half-life). Such a population is enhanced in the present study with respect to the population of the other long-lived isomers by the short collection time.

The decay schemes for the decay of the high spin (8-) isomer reported in ref.(Che-78b, Fog-79) are in reasonable agreement. The decay populates almost exclusively the 3447keV level in ^{120}Sn. The gamma deexcitation of this level populates mostly the 2482keV delayed state (11.8μs). A small fraction (6%) by-pass this level and populates the 2284keV state (Fog-79). To be consistent with the observed decay curves for the 90 and 197keV gamma lines some of the decay of the (4+,5+) isomer has to lead to the population of the 2482keV delayed state which is deexcited by the 197-90keV gamma cascade. Such an interpretation is consistent with the non-observation of the 197keV line in beta-gamma experiments of the present study. However, in the decay scheme of the (4+,5+) isomer reported in ref.(Che-78b) the 2482keV state is not populated.

The beta spectra in coincidence with 965 and 1171keV gamma transitions lead to the Q_β-values of 5.68±.20MeV and 5.47±.25MeV, respectively. Although these values are high compared with the value reported in Ale-78 they remain within the errors quoted therein (table-V). Due to poor statistics, the half-lives of these gamma lines were not determined in beta-gamma experiments and, therfore, the derived Q_β-values were not included in the comparison in table-IV. The half-life of the 2284keV delayed state was measured to be 22±2ns which is in contradiction with the value of 5.53±.06ns in ref.(N120-76). The lack of information and, in particular, half-life determinations preclude further statements.

A=121

The decay of the ground-state of ^{121}In populates the first 7/2+ excited level in ^{121}Sn almost exclusively (Fog-76b). The half-life of the 926keV gamma transition measured in the present study is in agreement with that of Gra-74. This latter value is the value accepted in Ale-78 and Fog-76b. However, it is in contradiction with that reported in TI-78. The measured end-point energy of the beta spectrum in coincidence with the 926keV gamma-line leads to a Q_β-value of 3.34±.08MeV (table-V) which is in very good agreement with the reported value in ref.(Ale-78).

A=122

The same isomerism pattern occurs in ^{120}In as in ^{122}In (Ale-78, Fog-79). The 103.6keV and 163.3keV gamma-lines which depopulate the level at 2409keV (fig.48) both exhibit, in single detector experiments, a 2-component decay curve: a main decay with 11.1 ±.3s half-life and a growth with a half-life of 1.9±.2s (fig.34). This suggests, as in ^{120}In, that the low-spin isomer (J=1+) decays by an isomeric gamma transition to the J=(4+,5+) isomer as well as by beta decay. This implies that the decay of the (4+,5+) isomer populates the 2409keV delayed state in ^{122}Sn and such a population is in contradiction with the results of Fog-79 where this level is only populated via the decay of the (8-) isomer. No explanation is presently available for such a discrepancy.

The half-life of the beta-rays of energies greater than 2.5MeV and in coincidence with the 1141keV gamma line was measured in the present study to be 3±2s. This is consistent with a direct beta population of the 1141keV level from the decay of the (1+) isomer. The

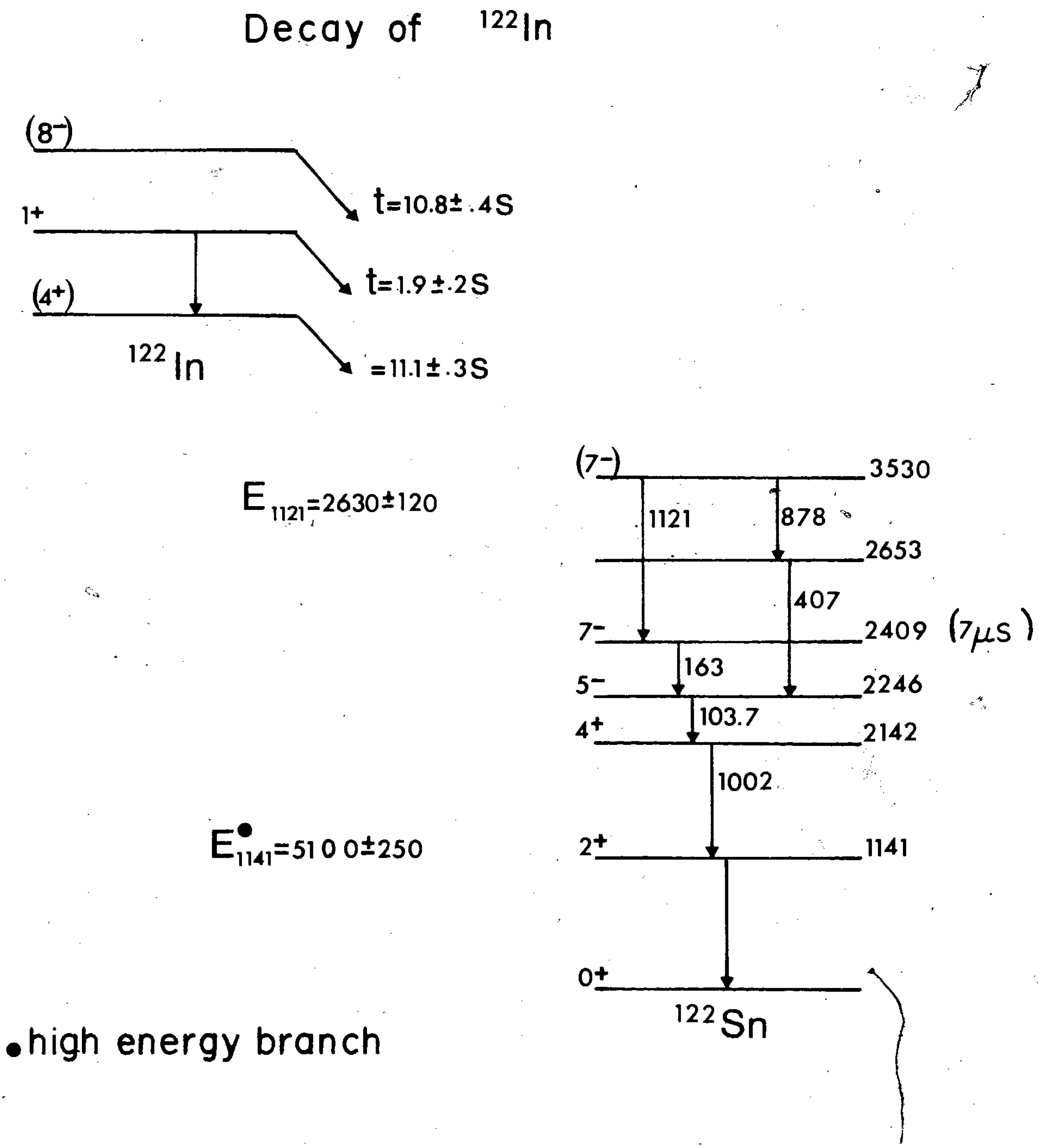

Decay of ^{122}In
(8⁻)
t=10.8±.4S
1+
t=1.9±.2S
(4+)
=11.1±.3S
^{122}In
E_{1121}=2630±120
$E^{\bullet}_{1141}$=5100±250
(7⁻)
3530
1121
878
2653
407
7⁻
2409
(7μS)
163
5⁻
2246
103.7
4+
2142
1002
2+
1141
0+
^{122}Sn
• high energy branch

Figure 48.

total beta spectrum in coincidence with the same line exhibits a 2 component half-life: 2.5±1.0s and 13±2s. The end-point energies of the beta spectra in coincidence with the 1141 and 1121keV gamma lines lead to the Qβ-values of 6.20±.25MeV and 6.16±.12MeV, respectively. These values are somewhat lower that the 6.35±.05MeV Qβ-value obtained from $^{122}Sn(t,{}^{3}He)$ nuclear reaction (Ajz-78) and much lower than the values in Ale-78.

The half-life of the 2246keV state was measured from the time spectrum associated with the 103.7keV gamma line in the beta-gamma experiments to be 8.9±.7ns which is consistent with the value reported in Fog-79 (table-III).

A=123

The decay of ^{123}In has been studied and a preliminary decay scheme has been published (Fog-76b). The decay mainly populates the 1155keV and the 1044keV excited levels of ^{123}Sn . The end-point energy measured in this study for the beta spectrum in coincidence with the 1131keV gamma-line leads to a Q_{β}-value of 4.50±.11MeV (table-V) and it is in good agreement with that in ref.(Ale-78).

VII-3 General Discussion

VII-3-1 Q_β-values

In determinations of logft-values, beta-strength functions, r-process parameters and theoretical representations of delayed particle emission, the value of the total beta decay energy is of great importance. In many cases it is necessary to rely on predictions based on mass formulas.

A comparison of the Q_β-values derived in the present work with the predictions of the various mass formulas is displayed in Table-IV.

The root-mean-square (r.m.s.) deviations shown therein were calculated without regard to uncertainties in either the experimental Q_β-values or the atomic mass predictions.

Figs.49 a,b,c displayed Q_β-values as a function of neutron number for Rb, Sr, Y, Nb, Zr and Mo isotopes. The experimental data are indicated as circles while the lines represent the predicted values of current mass formulas. This is another representation of table-IV for the region around A=100.

Figure 49a. Q_β-values for Rubidium and Yttrium isotopes

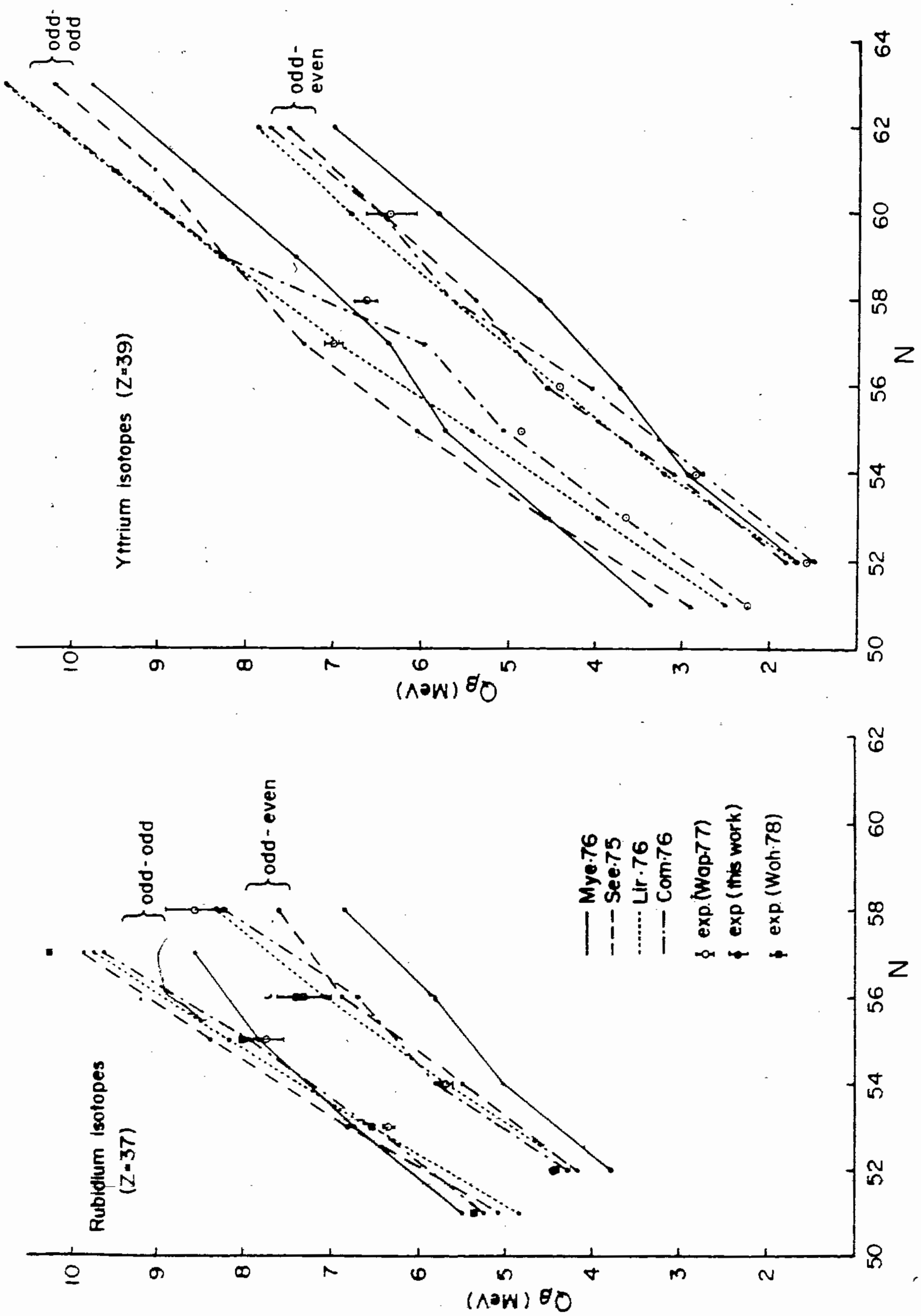

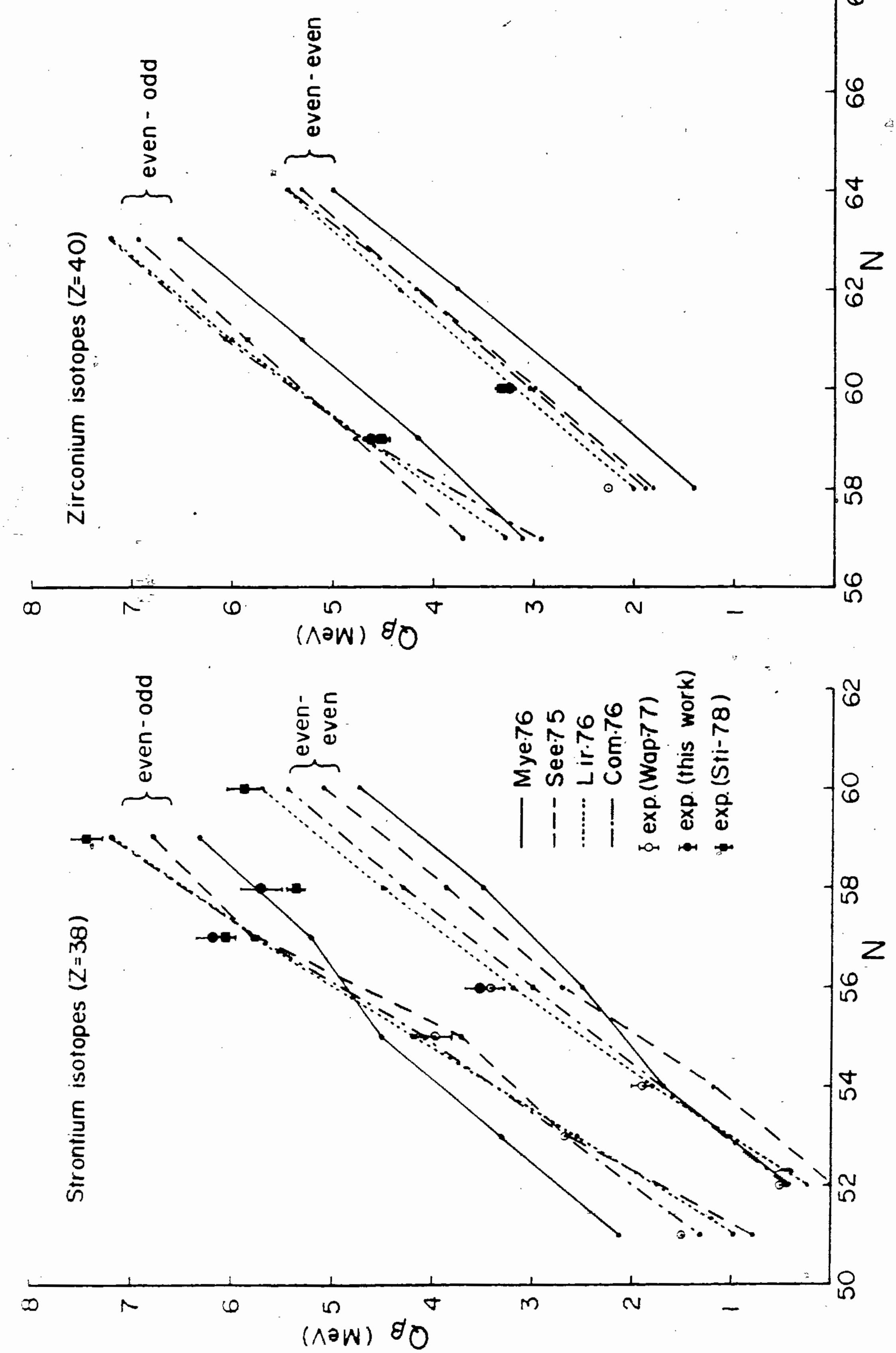

Figure 49b. Q_β-values for Strontium and Zirconium isotopes.

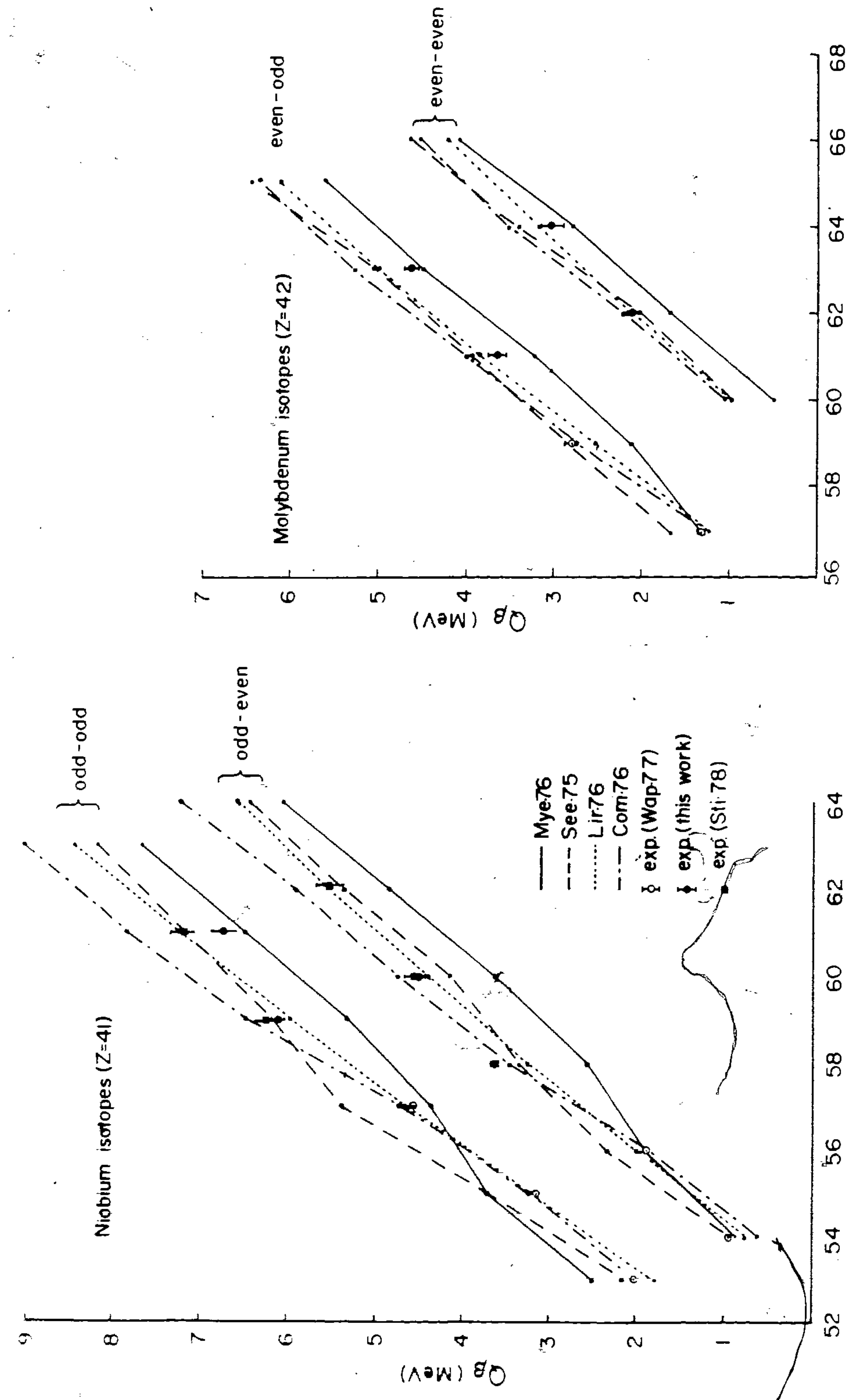

Figure 49c. Q_β-values for Niobium and Molybdenum isotopes

In general, best predictions of Q_β -values are obtained from the mass formula of Liran and Zeldes (Lir-76). The r.m.s. is about 220keV. The r.m.s. associated with the formula of ref.(Mye-76) was 500keV with predictions generally too low whereas that of ref.(Com-76) was about the same (480keV) with predictions generally too high. The mass formula of ref.(Jan-76a) also gives predictions which are generally too high but with a smaller r.m.s. of about 390keV. The r.m.s. associated with the predictions of the mass relation of ref.(See-75) is about 350keV.

For ^{94}-^{96}Sr isotopes (Z=38) (fig.49b), the results obtained in the present work are in general consistent with earlier experimental results (Wap-77, Sti-78). When compared with these experimental data, mass relation predictions are generally too low (about 1MeV for the calculations in Lir-76, Jan-76a and Com-76 and over 1.8MeV for those in See-75 and Mye-76). Although one needs more experimental data, a similar discrepancy seems to take place in the even-even isotopes at Z=40 (table-V). It is known that this region (Z=39-Z=41) exhibits local submagic-number effects which can not be completly accounted for in most mass formulas (Lir-76). The observed discrepancy could thus be the results of these local effects.

For Ag isotopes (Z=47) near the closure of the main shell at Z=50 the mass formula of ref.(See-75) fails completely for the odd-masses. The mean deviation attains 700keV for the odd-mass isotopes with 64<N<70. The agreement is also poor for odd-odd isotopes. In the case of odd-even isotopes the best predictions are given by the formulas of ref.(Com-76) and ref.(Mye-76). For odd-odd masses, calculations from ref.(Com-76) give predictions too high at high neutron-to-proton ratios while those from ref.(Mye-76) are too low for nuclides close to the stability line.

The remaining mass relations considered in the present study give Q_β-value predictions for which the deviations from the experimental measurements are within 250keV and thus relatively useful for mass predictions of neutron-rich silver isotopes.

The mass formula of ref.(See-75) also fails badly to predict Q_β-values of In isotopes (Z=49). The deviation from experimental measurements attains 700keV and 600keV for ^{120}In and ^{121}In, respectively. The predictions from ref.(Mye-76) are still low in this region, especially for the even masses (table-IV).

In conclusion, the best predictions are obtained by mass formulae which contain many coefficients (Lir-76, Com-76) but extrapolations from these semi-empirical relations must be performed with care. Rather than performing calculations from a single formula for a whole mass region it is better to choose an appropriate mass formula for either the odd or the even isotopes of a single element.

VII-3-2 Nuclear Spectroscopy

A large bulk of information about properties of neutron rich nuclei in the A=100 mass region has been gathered.

The first half-life measurements of ^{116}Rh (1.6 ±.3s), ^{105}Nb (1.4 ±.2s) and ^{106}Nb (1.4 ±.3s) have been made via the analysis of the decay curve of their daughter nuclide. These half-lives have to be regarded as preliminary values. Different time-sequence experiments should be performed to enhance these very short active species in order to obtain more precise values.

Several half-lives of long-lived nuclear states have been measured but since these measurements were performed from beta-gamma coincidence experiments the delayed state is usually not defined uniquely. For ^{110}Rh, ^{100}Nb and ^{102}Nb the relative positions of the two isomers have been determined through the measurements of the associated total beta decay energies.

^{105}Mo has been found to exhibit two isomers. Their half-lives and relative positions have been determined.

The decay curves of gamma lines associated with the even-mass In isotopes raise some evidence for the low spin isomer J=1+ decaying both via gamma and beta transitions. Such a competition would suggest a M3 isomeric transition with an energy less than 250keV (Ajz-78). This interpretation is in favour of a 4+ ground-state for these isotopes as postulated in ref.(Ale-75).

New preliminary decay schemes have been constructed for ^{104}Mo, ^{106}Mo and ^{107}Tc.

One of the advantages of the gas jet method is that the efficiency of transport of radioactive species are, to a large extent, independent of Z. Nevertheless, this lack of selectivity has drawbacks. Due to the very high activity of the collected spot, detailed spectroscopic studies are not feasible directly at the end of the gas jet recoil system. Thus, relative intensities measured in the present work can only be regarded as estimates.

However, the two-neutron separation energies, S2n, were plotted, versus N for Rb, Sr, Y, Zr, Nb and Mo isotopes in the mass region near A=100 (fig.50).

This two-neutron separation energy for a nucleus (Z,A) is calculated from the mass excesses of the nuclei (Z,A) and (Z,A-2) according to

$$S2n(Z,A) = -Me(Z,A)+Me(Z,A-2)+2Me(n)$$

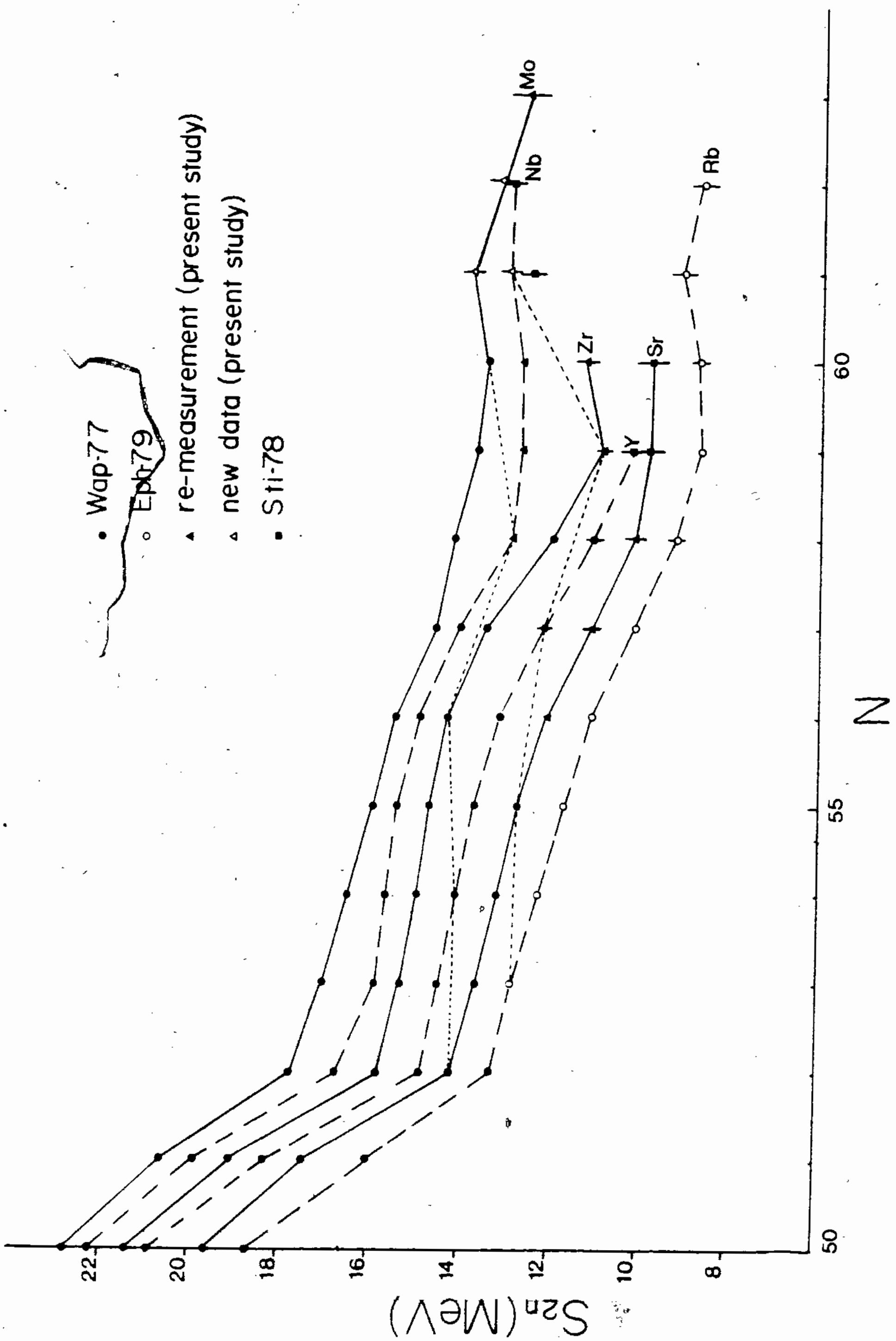

Figure 50. Neutron pair separation energies

However, this can be rewritten as

$$S2n(Z,A) = -\{Me(Z+1,A) + Q(Z,A)\} + Me(Z,A-2) + 2Me(n)$$

where Q(Z,A) is the total beta decay energy associated with the nuclide (Z,A). In all calculations the mass excesses from Wap-77 were utilized with, in general, one experimental Q_β-value. The summation of two $Q\beta$-values was required only for the calculation of S2n(^{104}Mo) in the A=104 chain:

$$S(^{104}Mo) = -\{Me(^{104}Ru) + Q(^{104}Tc) + Q(^{104}Mo)\} + Me(^{102}Mo) + 2Me(n)$$

where Q(^{104}Tc) was taken from ref.(Sum-78).

S2n plots are thus representations of the binding energy of a neutron pair as successive neutrons are added to a given nucleus.

Klapisch (Thi-75) and others (Duc-69) have shown that the dependency of the two-neutron separation energies with neutron number may indicate abrupt nuclear shape changes.

After the well known discontinuity corresponding to the N=50 closed shell, a slight break of slope appears between N=56 and N=57. This can be correlated to the closure of the neutron subshell $d_{5/2}$ and, therfore, to the peak occuring at N=56 in fig.3.

Of particular interest to this study is the occurence of a hump at N=60 for the Rb isotopes whose masses were very recently re-measured at ISOLDE by the Klapisch' group (Eph-79). Such a hump seems to be also present for Zr, Nb and Mo isotopes. However the transition is somewhat smoother for isotopes of Z greater than 40.

In the rare earth region where the nuclear deformation has been well studied (N≐88 to 92), the plot of the double-neutron separation energies as a function of N flattens out or rises somewhat (Duc-69). Thus, in the present region of interest the same curves exhibit a similar behavior.

On the same plots (fig.50) the dotted lines connect pair separation energies for nuclei differing by two neutrons and one proton. Plots of this type have been observed to be almost constant in the absence of shell structuring, running somewhat parallel to the bottom of the stability valley (Duc-69, Ale-77). Breaks of slope in these lines which correspond to a path of 2Z-N=constant appear in the region of interest for N=56-60.

The equality of the neutron pair separation energies for nuclides (Z,N) and (Z+1,N+2) can be written:

$$S(Z,N) - S(Z+1,N+2) = 0$$

This implies in terms of mass-excess

$$M(Z,N) - M(Z,N-2) - M(Z+1,N+2) + M(Z+1,N) = 0$$

or in Z,N diagram

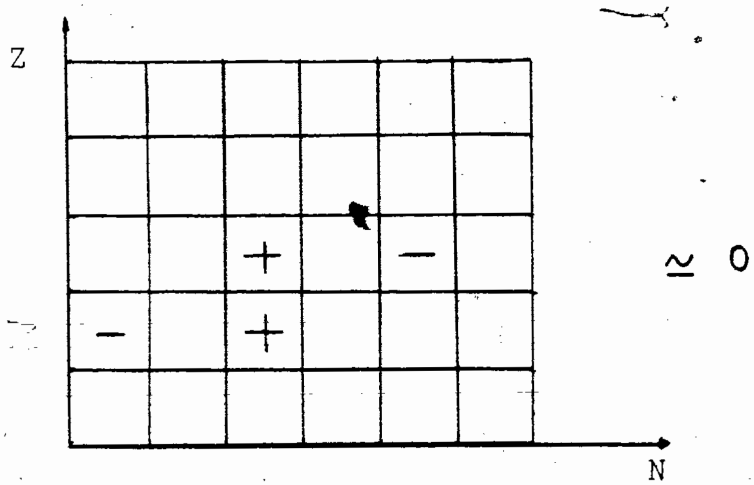

Using the formalism developed in Jan-76b the above mass equation can be represented for neutron-rich (Z<N) nuclides as follows:

N=even

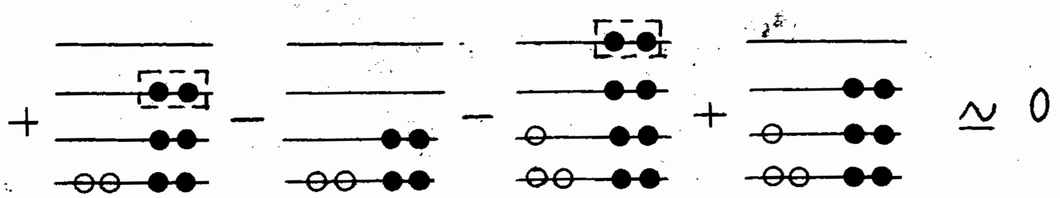

N=odd

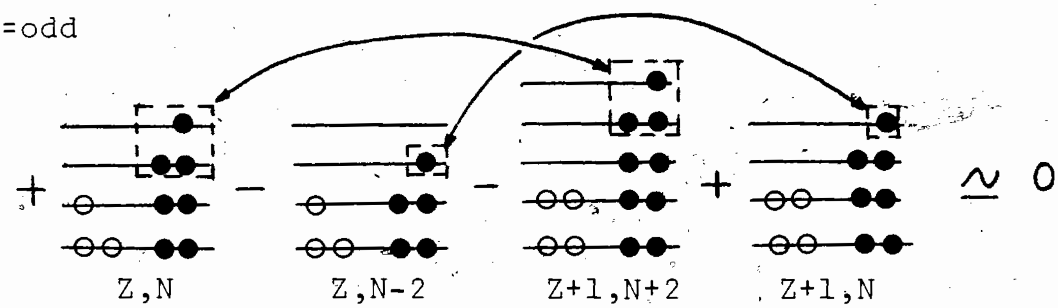

These equations hold only when single-particle and residual interaction energies cancel out. The cancellation occurs if the above energies are assumed to vary slowly with the nucleon number A=Z+N. In regions of smooth behavior of the nuclear structure, i.e, in the same shell, the assumption is expected to be valid.

For neutron-rich nuclides, the non-cancellation of these energies would result in breaks of slope in the lines connecting neutron pair separation energies and would be a sign of local change in the nuclear structure.

These results support the hypothesis that an onset of deformation is occuring in the neutron-rich region near A=100 and the transition occurs rather sharply at neutron number N=60, especially for nuclei with Z<41 (Wol-77). For the even-even isotopes of this region the present N=60 transition is a confirmation of the results obtained from the plots in fig.3 (see section III). Moreover, the present study extends the change in nuclear shape to the other neutron-rich nuclides of the A=100 region. The transition at N=60 towards deformation is now a feature of the complete region from Rb to Mo.

VIII- POSSIBLE EXTENSIONS OF THE PRESENT WORK

The results of the present work are expected to form a valuable and fertile data source for the planning of future experiments. A trivial extension would be the selection of different time sequences for collection and counting periods in order to enhance the observation of the nuclide of interest. For example, such a procedure should help to solve the problems of the decays of ^{91}Rb, ^{94}Rb, ^{120}In and ^{122}In.

To go further, i.e, to study nuclides farther away from stability or to extend some investigations of the present study in order to get valuable spectroscopic information, new developments are required.

A new beta telescope has been built. The DE counter is a smaller disc 1cm diameter and of the same thickness as the present one (1mm). This will define a sharper angle of electron penetration in the telescope. The E counter is a cylinder, 10cm deep and 6.35cm in diameter. Moreover, this new telescope will operate inside a light-tight chamber under vacuum, juxtaposed to the collection chamber of the gas-jet system. Thus, electrons penetrating this new detector will be better collimated and will not lose energy in any material except the plastic scintillators of the telescope and their surrounding very thin light reflectors.

An associated neccessary development should be the experimental determination of the response function of this new telescope.

Studying nuclides with nuclear composition farther away from the valley of stability implies being able to measure beta end-point energies around 10MeV and higher. It will then be necessary to achieve calibration in the same beta energy range. ^{11}Be having a beta transition with a 9.32MeV end-point energy (TI-78) has been shown suitable for this purpose. This isotope has been produced by the $^{14}C(p,3pn)^{11}Be$ reaction.

Furthermore, future work could develop a method to improve the specificity of the present identification system. For this, a time-of-flight mass identification system has been built by the SFU group (Bis-76). Such a system would allow mass selection, i.e, the investigation could be concentrated on one or two isotopes at a time. One of the most interesting applications of such a system will be the study of ^{102}Zr for which the deformation is predicted to be at its strongest.

IX- CONCLUSION

About 75% of all the gamma lines observed in the present study have been assigned. A total of 40 nuclear decays have been investigated (fig.19). The half-lives of 3 new isotopes have been tentatively determined (^{116}Rh, ^{105}Nb, ^{106}Nb). The relative position of the isomers have been determined for 3 other nuclides (^{110}Rh, ^{100}Nb, ^{102}Nb). A total of 12 new Q_β -values have been derived. A few of the other total beta decay energies determined in the present work have been obtained with a better precision than the earlier published values. A new lower limit for 2 Q_β -values have been measured and 3 new tentative decay schemes have been put together.

REFERENCES

Ach-74 E. Achterberg, F.C. Iglesias, A.E. Jech, J.A. Moragues, D. Otero, M.L. Perez, A.N. Proto, J.J. Rossi, and W. Scheuer Phys. Rev. C9 (1974) 299

Ahr-76 H. Ahrens, N. Kaffrell, N. Trautmann and G. Herrmann Phys. Rev. C14 (1976) 1

Ajz-78 F. Ajzenberg-Selove, E.R. Flynn, J.W. Sunier and D.L. Hanson Phys. Rev. C17 (1978) 960

Ajz-79 F. Ajzenberg-Selove, E.R. Flynn, D.L. Hanson and S. Orbesen Phys. Rev. C19 (1979) 2068

Ale-75 K. Aleklett, G. Nyman and G. Rudstam Nucl. Phys. A246 (1975) 425

Ale-77 K. Aleklett, PhD thesis Goteberg (1977)

Ale-78 K. Aleklett, E. Lund and G. Rudstam Phys. Rev. C18 (1978) 462

Ars-69 D.A. Arseniev, A. Sobiezewski and V.G. Soloviev Nucl. Phys. A139 (1969) 269

Bec-69 E. Beck, Nucl. Inst. Meth. 76 (1969) 77

Bei-76 M. beiner, R.J. Lombard and D. Mas Nuclear Data Tables 17 (1976) 450

Ber-78 H. Berg, U. Keyser, F. Munnich, K. Hawerkamp, H. Schrader and B. Pfeiffer, Z. Phys. A288 (1978) 59

Bet-36 H.A. Bethe and R.F. Bacher Revs. Mod. Phys. 8 (1936) 82

Bis-76 G. Bischoff, G. Cote, H. Dautet, J.K.P. Lee, W. Wiesehahn, J.M. D'Auria and B.D. Pate Proc. 3rd Int. Conf. on nuclei far from stability Cargese 1976, CERN 76-13 (1976)

Boh-75 H. Bohn, P. Kienle, D. Proetel and R.L. Hershberger Z. Phys. A274 (1975) 327

Bow-74 W.W. Bowman and K.W. MacMurdo Nucl. Data Tables 13 (1974) 89

Bri-75 R. Brissot,F. Schüssler,E. Monnand,A. Moussa
Nucl. Phys. A238 (1975) 149

Bru-75 W. Bruchle Ann. Report 1975, Mainz Univ. (1976)

Cab-75 C. Cabot,C. Deprun,H. Gauvin,Y. LeBeyec and M. Lefort
Nucl. Inst. Meth. 125 (1975) 397

Car-78 L.C. Carraz,I.R. Halderson,H.L. Ravn,M. Sharestad and
L. Westgaard Nucl. Inst. Meth. 148 (1978) 217

Che-74 E. Cheifetz and J.B. Wilhemy in "Nuclear spectroscopy
and reactions" ed. by J. Cerny, Academic Press (1974)

Che-78a H.C. Cheung,H. Huang,B.N. Subba Rao,L. Lessard and
J.K.P. Lee Private communication, Foster radiat.
lab. McGill Univ. Montreal

Che-78b H.C. Cheung,H. Huang,B.N. Subba Rao,L. Lessard and
J.K.P. Lee J. Phys. 4 (1978) 1501

Cli-73 J.R. Clifford,W.L. Talbert,F.K. Wohn,J.P. Adams and
J.R. McConnell Phys. Rev. C7 (1973) 6

Com-76 E. Comay and I. Kelson
Atomic Data and Nuclear Data Tables 17 (1976) 463

Dau-73 H. Dautet,S.C. Gujrathi,W.J. Wiesehahn,J.M. D'Auria
and B.D. Pate Nucl. Inst. Meth. 107 (1973) 49

Dau-76 H. Dautet PhD thesis, Simon Fraser Univ. (1979)

Duc-69 H.E. Duckworth,R.C. Barber,P.Van Rookhuysen,
J.D. MacDougall,W. McLatchie,S. Whineray,R.L. Bishop,
J.O. Meredith,P. Williams,G. Southon,W. Wong,
B.G. Hogg and M.E. Kettner
Phys. Rev. Lett. 23 (1969) 592

Eph-79 M. Epherre,G. Audi,C. Thibault,R. Klapisch,G. Huber,
F. Touchard,H. Wollnik Phys. Rev. C19 (1979) 1504

Fae-74 A. Faessler,J.E. Galonska,U. Gotz and H.C. Pauli
Nucl. Phys. A230 (1974) 302

Fog-76a B. Fogelberg,Y. Kawase,J. McDonald and A. Backlin
Nucl. Phys. A269 (1976) 317

Fog-76b B. Fogelberg,L.E. DeGeer,K. Fransson and M.af Ugglas
Z. Phys. A276 (1976) 381

Fog-79 B. Fogelberg and P. Carle
Nucl. Phys. A323 (1979) 205

Fol-73 "FOLDAP" Multi-parameter data acquisition system
A. Kurn, W. Bishop and R.G. Korteling
Department of Chemistry Simon Fraser University

Fos-74 D.B. Fossan and E.K. Warburton in "Nuclear spectroscopy and reactions" ed.by J. Cerny, Academic Press (1974)

Fra-78a G. Franz J. Inorg. Nucl. Chem. 40 (1978) 1467

Fra-78b G. Franz and G. Herrmann
J. Inorg. Nucl. Chem. 40 (1978) 945

Gar-69 G.T. Garvey,W.C. Gerance,R.L. Jaffe,I. Talmi and I. Kelson Rev. Mod. Phys. 41 (1969) S1

Gla-76 M.D. Glascock,W.L. Talbert and C.L. Duke
Phys. Rev. C13 (1976) 4

Gou-74 F.S. Goulding and R.H. Pehl in "Nuclear spectroscopy and reactions" ed. by J. Cerny, Academic Press (1974)

Gra-74 B. Grapengiesser,E. Lund and G. Rudstam
J. Inorg. Nucl. Chem. 36 (1974) 2409

Gun-72 R. Gunnink and J.B. Niday UCRL 51061-1 (1972)

Han-74 P.G. Hansen Adv. in Nucl. Phys. 7 (1974) 159

Har-77 J.C. Hardy, L.C. Carraz, B. Jonson and P.G. Hansen
Phys. Lett. 71B (1977) 307

Hoy-75 F. Hoyle "Astronomy and Cosmology" W.H. Freeman (1975)

Jan-76a J. Janecke and B.P. Eynon
Nucl. Data Tables 17 (1976) 467

Jan-76b J. Janecke Nucl. Data Tables 17 (1976) 455

Kaf-76a N. Kaffrell,G. Franz,G. Klein,K. Summerer,G. Tittel
N. Trautmann and G. Herrmann Proc. 3rd Int. Conf. on nuclei far from stability, Cargese 1976
CERN 76-13 (1976) 483

Kaf-76b N. Kaffrell,G. tittel,N. Trautmann,H. Ahrens,J.P. Bocquet,B. Pfeiffer,E. Monnand and F. Schussler
Ann. Report 1975, Mainz Univ. (1976)

Kan-78 M. Kanazawa, S. Ohya, T. Tamura, Z. Matumoto and N. Mutsuro J. Phys. Soc. Japan 44 (1978) 25

Kha-77 T.A. Khan, W.D. Lauppe, K. Sistemich, H. Lawin, G. Sadler, H.A. Selic Z. Phys. A283 (1977) 105

Kha-78 T.A. Khan, W.D. Lauppe, K. Sistemich, H. Lawin and H.A. Selic Z. Phys. A284 (1978) 313

Kis-77 Y. Kiso, R. Matsushita, J. Takemi and T. Tamai J. Nucl. Sci. Tech. 14 (1977) 482

Kla-74 R. Klapisch in "Nuclear spectroscopy and reactions" ed. by J. Cerny, Academic Press (1974)

Kos-75 K.L. Kosanke, M.D. Edmiston, R.A. Warner and W.C. McHarris Nucl. Inst. Meth. 125 (1975) 253

Lef-66 M. Lefort "Nuclear Chemistry" Dunod Paris (1966)

Lir-76 S. Liran and N. Zeldes Nucl. Data Tables 17 (1976)

Mac-70 M.I. Macias-Marques PhD thesis Paris-Sud (1971)

Mar-70 P. Marmier and E. Sheldon "Physics of nuclei and particles" Academic Press (1970)

Mat-65 J.H.E. Mattanch, W. Thiele and A. Wapstra Nucl. Phys. 67 (1965) 1

Mat-78 Z. Matumoto and T. Tamura J. Phys. Soc. Japan 44 (1978) 1070

Mfa-74 R.D. Macfarlane and Wm.C. McHarris in "Nuclear spectroscopy and reactions" ed. by J. Cerny Academic Press (1974)

Mon-76 E. Monnand, J. Blachot, F. Schussler, J.P. Bocquet, B. Pfeiffer, G. Sadler, H.A. Selic, T.A. Khan, W.D. Lauppe, H. Lawin and K. Sistemich Proc. 3rd Int. Conf. on nuclei far from stability Cargese 1976, CERN 76-13 (1976) 477

Mye-66 W.D. Myers and W.S. Swiatecki Nucl. Phys. 81 (1966) 1

Mye-76 W.D. Myers Nucl. Data Tables 17 (1976) 411

Nil-69 S.G. Nilsson, C.F. Tsang, A. Sobiczewski, Z. Szymanski, S. Wyech, C. Gustafson, I.L. Lainm, P. Moller and B. Nilsson Nucl. Phys. A131 (1969) 1

NDT-76 Atomic Data and Nuclear Data Tables 17 5-6 (1976)

N94-73 Atomic Data and Nuclear Data Tables 10-3 (1973)

N99-74 Atomic Data and Nuclear Data Tables 12-4 (1974)

N100-74 Atomic Data and Nuclear Data Tables 11-3 (1974)

N105-79 Atomic Data and Nuclear Data Tables 27-1 (1979)

N110-77 Atomic Data and Nuclear Data Tables 22-1 (1977)

N115-75 Atomic Data and Nuclear Data Tables 16-2 (1975)

N116-75 Atomic Data and Nuclear Data Tables 14-3 (1975)

N117-78 Atomic Data and Nuclear Data Tables 25-2 (1978)

N118-76 Atomic Data and Nuclear Data Tables 17-1 (1976)

N120-76 Atomic Data and Nuclear Data Tables 17-1 (1976)

Ott-79 H. Otto,P. Peuser,G. Nyman and E. Roeckl
to be published in Nucl. Inst. and Meth.

Rav-76 H.L. Ravn Proc. 3rd Int. Conf. on nuclei far from
stability, Cargese 1976, CERN 76-13 (1976) 22

Rei-77 C.W. Reich Proc. Isotope Separator on-line
Worshop Brookhaven Nat. Lab. (1977)

Ris-79 C. Ristori, J. Crancon, K.D. Wunsch, G. Jung, R. Decker
and K.L. Kratz Z. Phys. A290 (1979) 31

Rog-65a J.D. Rogers Ann. Rev. Nucl. Sci. 15 (1965) 241

Rog-65b P.C. Rogers and G.E. Gordon
Nucl. Instr. and Meth. 37 (1965) 259

Rou-69 J.T. Routti and S.G. Prussin
Nucl. Inst. Meth. 72 (1969) 125

Sad-75 G. Sadler,T.A. Khan,K. Sistemich,J.W. Gruter,H. Lawin
W.D. Lauppe,H.A. Selic,M. Shaanan,F. Schussler,J.
Blachot,E. Monnand,G. Bailleul,J.P. Bocquet,P.
Pfeiffer,H. Schrader and B. Fogelberg
Nucl. Phys. A252 (1975) 365

Sch-76 D.N. Schram and B. Norman Proc. of the 3rd Int. Conf. on Nuclei far from stability Cargese 1976 CERN 76-13 (1976) 570

See-75 P.A. Seeger and W.M. Howard Nucl. Phys. A238 (1975)

Sel-79 H.A. Selic, G. Sadler, T.A. Khan, W.D. Lauppe, H. Lawin K. Sistemich, E. Monnand, J. Blachot, J.P. Bocquet and F. Schussler Z. Phys. A289 (1979) 198

She-72 R.K. Sheline, I. Ragnarsson and S.G. Nilsson Phys. Lett. 41B (1972) 115

She-76 R.K. Sheline Proc. 3rd Int. Conf. on nuclei far from stability, Cargese 1976, CERN 76-13 (1976) 351

Sis-76 K. Sistemich, G. Sadler, T.A. Khan, J.W. Gruter, W.D. Lauppe, H. Lawin, H.A. Selic, F. Schussler, J. Blachot, J.P. Bocquet, E. Monnand and B. Pfeiffer Proc. 3rd Int. Conf. on nuclei far from stability Cargese 1976, CERN 76-13 (1976) 495

Sor-70 R.A. Sorensen Proc. Int. Conf. CERN 70-30 (1970) 1

Sti-78 R. Stippler, F. Munnich, H. Schrader, J.P. Bocquet, M. Asghar, G. Siegert, R. Decker, B. Pfeiffer, H. Wollnik E. Monnand, F. Schussler Z. Phys. A284 (1978) 95

Str-68 V.M. Strutinsky Nucl. Phys. A122 (1968) 1

Sum-78 K. Summerer, N. Kaffrell, H. Otto, P. Peuser and N. Trautmann Z. Phys. A287 (1978) 287

Thi-75 C. Thibault, R. Klapisch, C. Rigaud, A.M. Poshanzer, R. Priels, L. Lessard and W. Reisdorf Phys. Rev. C12-2 (1975)

TI-78 "Table of Isotopes" 7th edit. J. Wiley & Sons (1978) N.Y.

Tit-76 G. Tittel, N. Kaffrell, N. Trautmann, H. Ahrens, J.P. Bocquet, B. Pfeiffer, E. Monnand and F. Schussler Ann. Report 1975, Mainz Univ. (1976)

Tit-77a G. Tittel, N. Kaffrell, N. Trautmann, H. Ahrens Ann. Report 1976, Mainz Univ. (1977)

Tit-77b G. Tittel, N. Kaffrell, N. Trautmann and G. Herrmann J. Inorg. Nucl. Chem. 39 (1977) 2115

Tiv-75 P.J. Tivin, R.L. Schulte and H.W. Taylor
Z. Phys. A273 (1975) 339

Wap-71 A. Wapstra and N. Gove
Nucl. Data Tables 9 (1971) 265

Wap-77 A.H. Wapstra and K. Bos Atomic Data and Nuclear Data Tables 19-3 (1977)

Wei-35 C.F. Weizsacker Z. Physik 96 (1935) 431

Wes-72 L. Westgaard, J. Zyliez and O.B. Nielsen Atomic masses and fundamental constants 4, Plenum Press London N.Y. (1972) 94

Wie-73 W.J. Wiesehahn, H. DAutet, J.M. D'Auria and B.D. Pate
Nucl. Inst. Meth. 109 (1973) 613

Wie-75a W.J. Wiesehahn, G. Bischoff and J.M. D'Auria
Nucl. Inst. Meth. 124 (1975) 221

Wie-75b W.J. Wiesehahn, G. Bischoff and J.M. D'Auria
Nucl. Inst. Meth. 129 (1975) 187

Wie-75c W.J. Wiesehahn Private communication (1975)

Wie-76 W.J. Wiesehahn Private communication (1976)

Woh-72 F.K. Wohn, J.R. Clifford, G.H. Carlson and W.L. Talbert Jr.
Nucl. Instr. and Meth. 101 (1972) 343

Woh-78 F.K. Wohn and W.L. Talbert, Jr
Phys. Rev. C18 (1978) 2328

Wol-77 H. Wollnik, F.K. Wohn, K.D. Winsch and G. Jung
Nucl. Phys. A291 (1977) 355

Wun-78 K.D. Wunsch, R. Decker, H. Wollnick, J. Munzel, G. Siegert, G. Jung and K. Koglin
Z. Phys. A288 (1978) 105

APPENDIX

Tables II-VI

Table II. Comparison Between End-point Energies Measured in the Present Work and Literature Values

γ-gate keV	$T_{1/2}$	Assignment	E_β MeV	$E_\beta(\ell it)$ MeV	Ref
926	23.1 s	^{121g}In	2.41 ± 0.08	{2.434 ± 0.031 2.48 ± 0.05}	Wap 77 Ale 77
504	7.1 s	^{100}Zr	2.80 ± 0.10	2.81 ± 0.15	Sti 78
1131	6.0 s	^{123}In	3.34 ± 0.11	3.30 ± 0.07	Ale 77
137.7	14.0 s	^{99m}Nb	3.39 ± 0.05	3.38 ± 0.02	Wap 77
546	2.1 s	^{99}Zr	3.63 ± 0.97	3.55 ± 0.15	Sti 78
594	2.1 s	^{99}Ar	3.59 ± 0.11	3.61 ± 0.15	Sti 78
915	10.0 s	^{96m}Y	4.22 ± 0.09	4.34 ± 0.20	Sti 78
1750	10.0 s	^{96m}Y	4.27 ± 0.10	4.34 ± 0.25	Sti 78
1633	4.3 s	^{102m}Nb	4.85 ± 0.12	4.78 ± 0.17	Sti 78
159.6	1.5 s	^{100}Nb	5.40 ± 0.08	5.57 ± 0.15	Sti 78
535	3.1 s	^{100}Nb	5.56 ± 0.08	5.72 ± 0.18	Sti 78

Table III. Delayed β-γ Coincidence Results

Energy keV	Assignment	half-life (ns)	Comments	Lit
36.5	^{104}Mo	6.0 ± 0.3		
43.5	^{101}Nb	> 300		
48.5	^{115}Pd	5.8 ± 0.6		
53.9	^{106}Mo	6 ± 1		
55.0	^{104}Mo	6.5 ± 0.4		
58.1	?	9.7 ± 0.8		
68.7	^{104}Mo	7.1 ± 0.3		
72.6	?	9.0 ± 0.6		
83.5	^{103}Mo	36.3 ± 1.7		
85.4	^{105}Mo	21.5 ± 0.6		
89.9	(^{120}In)	22 ± 2	prompt & delayed	5.53 ± 0.6 (N120-76)
93.5	^{91}Rb	87.4 ± 3.6		87.5 ± 3.0 (Gla-76)
98.8	?	70 ± 6		
102.7	(^{107}Tc, ^{103}Nb)	10.3 ± 0.5		
103.6	(^{100}Zr, ^{122}In)	8.9 ± 0.7	prompt & delayed	7.9 ± 0.9 (Fog-79)
106.3	^{107}Tc	33.6 ± 1.3		
108.6	?	8 ± 1		
116.8	?	33 ± 3		
1103	^{97}Y	100 ± 15	prompt & delayed	104 ± 5 (TI-78)

Table IV. Comparison Between Experimental Q_β Values and Those Predicted by Semi-empirical Mass Formulas.

Isotopes	Wapstra[a] keV	Myers[b] MeV	Seeger[c] MeV	Liran[d] MeV	Janecke[e] MeV	Comay[f] MeV	present study MeV
^{91}Rb	5704 ± 46	5.04	5.5	5.72	5.64	5.84	
^{94}Sr	3422 ± 82	2.49	2.7	3.20	2.98	3.00	3.57 ± 0.10
^{95}Sr	6093 ± 110	5.20	5.8	5.77	5.84	5.78	6.15 ± 0.20
^{96}Sr	5360 ± 240	3.60	3.9	4.50	4.36	4.33	5.70 ± 0.20
^{96}Y	7015 ± 104	6.37	7.4	6.95	7.00	6.97	8.62 ± 0.05[1]
^{97}Y	6674 ± 134	4.65	5.4	5.67	5.53	5.68	7.30 ± 0.12[1]
^{98}Zr	2238 ± 26	1.39	1.8	2.00	1.71	1.86	
^{99}Zr	4456 ± 116	4.16	4.8	4.70	4.51	4.72	4.64 ± 0.06
^{100}Zr	3360 ± 330	2.65	3.0	3.26	2.71	3.02	3.30 ± 0.07
^{99}Nb	3623 ± 19	2.61	3.4	3.30	3.49	3.53	3.63 ± 0.05
^{100}Nb	6229 ± 136	5.33	6.2	6.00	6.30	6.48	6.09 ± 0.06
							6.69 ± 0.07[1]
^{101}Nb	4566 ± 106	3.71	4.2	4.45	4.50	4.77	4.56 ± 0.11
^{102}Nb	7202 syst	6.49	7.2	7.26	7.58	7.86	6.69 ± 0.13
							7.40 ± 0.09[1]
^{103}Mo	4300 syst	3.28	4.0	3.88	3.97	4.04	3.76 ± 0.17
^{104}Mo	2200 syst	1.71	2.1	2.14	2.06	2.25	2.12 ± 0.05
^{105}Mo	5400 syst	4.47	5.1	5.07	5.19	5.34	4.72 ± 0.08
^{106}Mo	—	2.93	3.5	3.23	3.34	3.58	3.18 ± 0.16

[a]Wap 77
[b]Mey 76
[c]See 75
[d]Lir 76
[e]Jan 76
[f]Com 76

[1]Included unknown energy of isomeric transition

Table IV (cont'd)

Isotopes	Wapstra[a] keV	Myers[b] MeV	Seeger[c] MeV	Liran[d] MeV	Janecke[e] MeV	Comay[f] MeV	present study MeV
^{107}Tc	4200 syst	4.07	4.3	4.49	5.10	5.45	4.46 ± 0.07
^{108}Tc	—	6.77	7.2	7.45	8.07	8.26	7.51 ± 0.08
^{109}Rh	—	2.22	2.1	2.66	2.95	3.20	2.31 ± 0.06
^{110}Rh	5405 ± 120	4.90	5.1	5.67	5.92	6.14	5.27 ± 0.08
							5.66 ± 0.09[1]
^{115}Pd	—	4.36	4.2	4.35	4.56	4.63	4.76 ± 0.20
^{116}Pd	—	2.80	2.9	2.39	2.61	2.67	2.59 ± 0.13
^{114}Ag	4850 ± 144	4.53	4.4	4.90	5.13	4.93	4.82 ± 0.14
^{115}Ag	3183 ± 108	2.97	2.3	2.92	3.20	2.89	3.05 ± 0.07
^{116}Ag	6097 syst	5.53	5.2	5.81	6.23	5.99	5.36 ± 0.05
^{117}Ag	4176 ± 113	3.96	3.5	3.86	4.27	4.06	4.04 ± 0.07
^{120}In	5322 ± 104	4.69	4.7	5.34	6.37	5.24	
^{121}In	3366 ± 32	3.17	2.8	3.62	3.39	3.26	3.34 ± 0.08
^{122}In	6504 ± 154	5.65	5.9	6.33	6.35	6.18	6.18 ± 0.11
^{123}In	4379 ± 44	4.11	4.0	4.61	4.37	4.24	4.50 ± 0.11
$\vert\langle Q_{exp} - Q_{pred}\rangle\vert$		0.42	0.30	0.19	0.30	0.36	
Root-mean-square (99 < A < 123)		0.50	0.35	0.22	0.39	0.48	

[a] Wap 77
[b] Mey 76
[c] See 75
[d] Lir
[e] Jan 76
[f] Com 76

[1] Included unknown energy of isomeric transition.

Comparison between Literature and
Experimental Q_β Values

Table V

Isotopes	accepted hafl-line	λ-gate keV	level populated in β-transition	end-point energy MeV	Q_β this work MeV	Q_β literature MeV	Rev	Comments
^{91}Rb	58.2 s	93.5	?	4.93 ± 0.12		5.76 ± 0.04	Woh-78	see text
						$5.82^{+0.13}_{-0.04}$	Wun-78	
^{94}Rb	2.8 s	837	?	6.36 ± 0.14		10.30 ± 0.06	Wun-78	not enough information
		1578	?	6.40 ± 0.20				
^{94}Sr	78 s	1428	1428	2.14 ± 0.10	3.57 ± 0.10	3.42 ± 0.07	Wap-77	
^{95}Sr	24.4 s	686	686	5.45 ± 0.20	6.15 ± 0.20	6.06 ± 0.10	Sti-78	
^{96}Sr	1.0 s	122	932	4.8 ± 0.2	5.7 ± 0.2	5.35 ± 0.10	Sti-78	
^{96m}Y	10.0 s	617	4390	4.18 ± 0.08	8.63 ± 0.05	6.9 ± 0.7	Sis-76	high spin isomer
		915	4390	4.22 ± 0.09		8.03 ± 0.15	Sti-78	
		363	4390	4.22 ± 0.17				
		1223	4390	4.36 ± 0.15				
		1106	4390	4.40 ± 0.13				
		147	4390	4.24 ± 0.10				
		1750	4390	4.27 ± 0.10				
^{97m}Y	1.2 s	969	2234	5.2 ± 0.2	7.4 ± 0.2	7.28 ± 0.15	Sti-78	high spin isomer
^{99}Zr	2.1 s	56.0	1015	3.70 ± 0.14	4.64 ± 0.06	4.54 ± 0.12	Sti-78	
		546	1015	3.63 ± 0.07				
		594	959	3.59 ± 0.11				
		469	1015	3.63 ± 0.08				

Table V (continued)

Isotopes	accepted half-life	γ-gate keV	level populated in β-transition	end-point energy MeV	Q_β this work MeV	Q_β literature MeV	Ref	Comments
^{99}Nb	14 s	137.7	236	3.390 ± 0.050	3.626 ± 0.050	3.618 ± 0.019	Wap 77	
^{100}Zr	7.0 s	400	(400)	2.88 ± 0.01				
		504	504	2.80 ± 0.10	3.30 ± 0.07	3.34 ± 0.013	Sti 78	
^{100g}Nb	1.5	159	695	5.40 ± 0.08	6.09 ± 0.06	6.24 ± 0.10	Sti 78	
		535	(535,695)	5.56 ± 0.08		6.709 ± 0.030	Ajz 79	
^{100m}Nb	3.1 s	1280	2416	4.31 ± 0.18	6.69 ± 0.07			high spin isomer
		600	2416	4.29 ± 0.08				
		528	2416	4.20 ± 0.15				
^{101}Nb	7.1 s	276	290	4.28 ± 0.10	4.47 ± 0.11	4.57 ± 0.10	Sti 78	
		118	290	4.25 ± 0.19				
		157	171	4.20 ± 0.12				
^{102}Nb	1.3 s	296	296	6.39 ± 0.13	6.69 ± 0.13	7.16 ± 0.15	Sti 78	
^{102m}Nb	4.5 s	1633	2480	4.85 ± 0.12	7.40 ± 0.09	7.25 ± 0.13	Sti 78	
		847	2480	5.1 ± 0.2				
		551	2480	4.90 ± 0.25				
		447	2480	4.9 ± 0.2				
^{103}Nb	1.8 s	102.7	(102.7)	4.86 ± 0.12	4.99 ± 0.12	5.50 ± 0.12	Ber 78	lower limit

Table V (continued)

Isotopes	accepted half-life	γ-gate keV	level populated in β-transition	end-point energy MeV	Q_β this work MeV	Q_β literature MeV	Ref	Comments
^{103}Mo	66 s	45.8	469	3.29 ± 0.17	3.76 ± 0.17			
^{104}Nb	4.8 s	192.2	?	5.5 ± 0.5	5.7 ± 0.5			lower limit
^{104}Mo	60.0 s	68.7 55.0	105 105	2.00 ± 0.05 } 2.09 ± 0.10 }	2.12 ± 0.05			
^{105}Mo	35.6 s	85.4 147.7 76.6	85.4 147.8 76.6	4.62 ± 0.10 } 4.60 ± 0.15 } 4.22 ± 0.15	4.72 ± 0.08 4.29 ± 0.15			
^{106}Mo	8.6 s	53.9	53.9	3.12 ± 0.16	3.18 ± 0.16			
^{107}Tc	21 s	106.6 102.7 145.5	? 1605 1062	2.84 ± 0.17 2.89 ± 0.10 } 3.38 ± 0.06 }	4.46 ± 0.7			
^{108}Tc	5.0 s	242.0	1826	5.79 ± 0.08	7.51 ± 0.08			
^{109}Rh	80 s	327	327	1.98 ± 0.06	2.31 ± 0.06	2.5 ± 0.5	Kan-78	
^{110}Rh ^{110m}Rh	3.3 s 28.5 s	373.3 373.3	373 2805	4.90 ± 0.08 2.89 ± 0.09	5.27 ± 0.08 5.66 ± 0.09	5.40 ± 0.12	Wap-77	 low energy branch
^{114}Ag	5.0 s	558	558	4.26 ± 0.14	4.82 ± 0.14	4.86 ± 0.14	Wap-77	
^{115}Pd	31 s	48.5	48.5	4.72 ± 0.20	4.76 ± 0.20			

Table V (continued)

Isotopes	accepted half-line	γ-gate keV	level populated in β-transition	end-point energy MeV	Q_β this work MeV	Q_β literature MeV	Ref	Comments
^{115m}Ag	19 s	131.5 229.1	360.6 360.6	2.67 ± 0.07 2.70 ± 0.07	3.05 ± 0.07	3.183 ± 0.108	Wap-77	
^{116}Pd	13 s	114.7	114.7	2.48 ± 0.13	2.59 ± 0.13			
^{116m}Ag	10.4 s	1029 706 514	2250 2250 2250	3.34 ± 0.12 3.19 ± 0.08 3.16 ± 0.07	5.44 ± 0.05			isomeric transition (81 keV)
^{116}Ag	2.7 min				5.36 ± 0.05	5.30 ± 0.20	Ale-77	
^{117m}Ag	5.4 s	135.4	522	3.52 ± 0.07	4.04 ± 0.07	4.18 ± 0.10	Ale-77	
^{118g}Ag	3.7 s	488 677	(488) (1165)	3.80 ± 0.10 4.3 ± 0.4				see text
^{120}In	45 s 47 s 3 s	965 1171	3447 1171	2.24 ± 0.20 4.30 ± 0.25	5.68 ± 0.20 5.47 ± 0.25	5.34 ± 0.17 5.34 ± 0.17	Ale-77 Ale-78	three known isomers
^{121}In	20 s	925.6	925.6	2.41 ± 0.08	3.34 ± 0.08	3.41 ± 0.05	Ale-78	
^{122}In	10.8 s 1.5 s 10.3	1141 1121	1141 3530	5.10 ± 0.25 2.63 ± 0.12	6.20 ± 0.25 6.15 ± 0.12	6.51 ± 0.23 6.59 ± 0.18 6.35 ± 0.05	Ale-78 Ale-78 Ajz-78	three known isomers
^{123}In	5.7 s	1131	1155	3.34 ± 0.11	4.50 ± 0.11	4.44 ± 0.06	Ale-78	

Table VI. Summary of Results

Energy (keV)	Measured half life[4] (s)	Coincidences[1] (keV)	end-point[3] β-energy (MeV)	Assignment
13.5±0.1	—		—	^{101}Nb
23.8±0.1	—	Ag_x-91-(177)-(292)-763	—	—
36.5±0.1	56±8	Tc_x-(55)-68-91-374-(440)	—	^{104}Mo
43.6±0.1	—		—	^{101}Nb
45.8±0.1	65±3	Tc_x-(68.7)-(91)-422-(1040)	3.29±0.17	^{103}Mo
48.5±0.1	31±2	(89-(386)-(558)	4.72±0.20	^{115}Pd
50.1±0.1	50±10	Tc_x-55	—	^{104}Mo
54.0±0.1	8.6±0.3[2]	Tc_x-189-430-600-618-(1029)	3.12±16	^{106}Mo
55.0±0.1	55±9	50-(348)	2.09±0.10	^{104}Mo
56.0±0.1	2±2	389-(418)-593-(752)	3.70±0.14	^{99}Zr
58.1±0.1	9±2	(374)-(1550)	3.7 ±0.3	^{149}Ce
62.5±0.1	—	723	—	^{145}Ce
64.3±0.1	29±5	85.4-129-(332)	4.15±0.24	^{105}Mo
65.5±0.1	6±2	(I_x)-83-(1398)	—	—
68.7±0.1	60±5[2]	Tc_x-(Cd_x)-36-(46)-69-91-375-769-797-1021	2.00±0.05	^{104}Mo
69.8±0.1	61±10[2]	Tc_x-36-68-(103)-(338)-(1023)	—	^{104}Mo
72.6±0.1	30±5		{3.8 ±0.3 2.1 ±0.1	— —
74.9±0.1	—	(140)-(326)-(1001)	4.2 ±0.3	—
76.6±0.1	48±4	160-169-(229)-270-388-(448)-763-(1001)-(1020)	{4.22±0.15 2.29±0.08	^{105}Mo
81.8±0.1	3±2	(Nb_x)-La_x-(103)-388-548-800-856-1030	—	^{99}Zr-^{146}Ba
83.3±0.1	—	175-388-400-610	3.32±0.19	^{103}Mo
85.4±0.1	35.6±0.5[2]	Tc_x-64.2-101-129-217-(269)-790-(994)	{4.62±0.10 2.84±0.07	^{105}Mo
90.0±0.1	44±2[2]	Sn_x-197-(466)-696-1023-1171-(1370)-(1584)	—	^{120}In
91.1±0.1	—	Tc_x-Cd_x-23.8-Sn_x-68-(131)-(303)-376-(1020)		(^{104}Mo)
93.5±0.1	65±8[2]	Sr_x-346-(696)-2564-3600	{4.95±0.12 2.58±0.12	^{91}Rb
94.8±0.1	2±1	(138)	—	(^{105}Nb)
95.9±0.1	—	Pr_x-115-(138)	—	—
97.7±0.1	15.0±0.8	Mo_x-137-(265)-276-(381)-708	—	^{99}Nb
98.8±0.1	67±6		—	—
100.9±0.1	—	114-178-(292)-(1230)	—	^{116}Pd
102.7±0.1	{1.8±0.3 20±3	Ru_x-(Sn_x)-106-(128)-460-(600)-(968)-(1131)-1502	{4.86±0.12 2.89±0.10	^{103}Nb ^{107}Tc

Table VI. Summary of Results (cont'd)

Energy (keV)	Measured half life[4] (s)	Coincidences[1] (keV)	end-point[3] β-energy (MeV)	Assignment
103.6±0.1	11.1±0.2[2] (s) 8±1 (β-γ)	Sn_x-La_x-163-(406)-1001-1141-(1165)	2.89±0.15	^{122}In, (^{100}Zr)
106.3±0.1	22±3		—	^{107}Tc
108.6±0.1	{ 1.5±1 31±3	(373)	{ 5.5 ±0.5 2.9 ±0.1	— —
112.5±0.1	—		2.6 ±0.2	—
113.4±0.1	25±10	131-229-276	—	^{115m}Ag
114.8±0.1	12.8±0.5[2]	Ag_x-101-178-280	2.48±0.12	^{116}Pd
116.3±0.1	13±1	Rh_x-(158)-(513)-(1863)	3.1 ±0.3	(^{109}Ru)
118.6±0.1	8±1	157-(1230)-(1560)-1665	4.26±0.19	^{100}Nb
119.3±0.1	4±1		—	—
121.7±0.1	—	(131)-(229)-807-(1510)	—	—
122.1±0.1	1.1±0.4		4.8 ±0.2	^{96}Sr
125.6±0.1	—	(260)-(296)-(340)	—	—
131.6±0.1	19.0±0.3	Cd_x-113-(186)-228-276-388-618-(723)	2.67±0.07	^{115m}Ag
135.4±0.1	5.4±0.2	Cd_x-(209)-298-388-686-(763)	3.52±0.07	^{117m}Ag
137.7±0.1	14.2±0.5	(Mo_x)-(98)	3.39±0.05	^{99}Nb
138.0±0.1	—	(Mo_x)-95-(1624)	—	(^{105}Nb)
142.2±0.1	6±1	(131)-388-666-(1131)	—	—
145.5±0.1	18±3	(131)-916	3.38±0.06	^{107}Tc
146.8±0.1	10.5±0.8	(38)-(103)-(296)-363-470-617-906-1223-1750	4.24±0.10	^{96m}Y
147.7±0.1	33±5	(Tc_x)-(197)	4.60±0.15	^{105}Mo
154.8±0.1	12±3		—	—
157.5±0.1	7±1	118-(138)-787-838-1710	4.20±0.11	^{101}Nb
159.6±0.1	8±3	76-(136)-535-768	5.40±0.08	^{100}Nb-(^{105}Mo)
161.6±0.1	—	1103	—	^{97}Y
163.4±0.1	11.0±0.8[2]	Sn_x-104-(274)-1001-1141-(1720)	—	^{122}In
168.3±0.2	—	(192)-(274)	5.2 ±0.6	—
177.1±0.2	—	Mo_x-(112)	3.6 ±0.4	—
178.3±0.2	—	Ag_x-101-(254)	—	^{116}Pd
184.5±0.2	—		4.0 ±0.5	—
192.2±0.2	5±2	(846)-(1506)	5.5 ±0.5	^{104}Nb
197.5±0.2	44.5±0.4[2]	Sn_x-90-(348)-1021-1171	—	^{120}In
206.2±0.2	—	465	3.0 ±0.2	—
210.2±0.2	—	(Ru_x)	—	—
211.4±0.2	—		3.5 ±0.3	—

Table VI. Summary of Results (cont'd)

Energy (keV)	Measured half-life[4] (s)	Coincidences[1] (keV)	end-point[3] β-energy (MeV)	Assignment
229.1±0.2	18.5±0.8	Cdx-113-131-(388)-(521)-1230	2.70±0.07	^{115m}Ag
242.1±0.2	5.1±0.2	(733)-1584	{5.79±0.08 3.31±0.09	^{108}Tc
258.0±0.5	—	(163)-410	—	—
269.8±0.5	—	(Tcx)-77-(876)	3.7 ±0.2	(^{105}Mo)
276.0±0.5	6.8±0.4	(14)-Cdx-113-<u>115</u>-118-131-164-(180)-229	{4.28±0.10 3.44±0.09	^{101}Nb, ^{116}Pd ^{115m}Ag
292.0±0.5	—	Pdx-(Prx)-(100)	—	—
295.9±0.5	{4.3±0.3(γ-γ) 3.0±0.5(s)	Mox-Cdx-(180)-(401)-447-551-(1236)-1632	{6.39±0.13 4.39±0.10	^{102}Nb
326.7±0.5	—	(146)	1.98±0.06	^{109}Rh
348.4±0.5	{1±1 6±1	(Mox)-Pdx(72)-94-(126)-(257)-388-(560)-749	{5.36±0.12 3.90±0.08	^{112}Rh
359.2±0.5	5±2	(Pdx)	{4.2 ±0.3 2.6 ±0.2	—
363.0±0.5	—	147	4.22±0.17	^{96m}Y
373±1	{3±1(β-γ) 23±5	Tcx-<u>36</u>-<u>68</u>-91	{4.90±0.08 2.89±0.09	^{104}Mo, ^{110}Rh
387±1	4.8±0.3	Nbx-Cdx(Lax)-82-(90)-104-<u>131</u>-<u>135</u>-(191)-<u>229</u> 349-360	{3.87±0.15 2.42±0.12	^{99}Zr, ^{115m}Ag ^{117}Ag
399±1				
400±1	3.9±0.2	(Mox)-(Pdx)-(65)-83-104-296	{5.6 ±0.2 2.88±0.1	^{102}Nb, ^{100}Zr
410±1	—	(Cex)-(65)-257	—	—
423±1	—	Tcx-(46)	—	^{103}Mo
433±1	—	Bax-(147)	3.7 ±0.2	—
440±1	—	(Zrx)	3.9 ±0.2	—
447±1	—	(Zrx)-(90)	4.9 ±0.2	^{102}Nb
461±1	—	Nbx	3.94±0.17	^{99}Zr
465±1	—	(Tcx)-(90)	—	(^{106}Mo)
469±1	2.7±0.5	Nbx-(Lax)	3.63±0.08	^{99}Zr
488±1	3.9±0.5	Agx-(24)-87	3.80±0.10	^{118}Ag
504±1	—		2.80±0.10	^{100}Zr
514±1	—		3.16±0.07	^{116}Ag
528±1	—	535	4.20±0.15	^{100}Nb

Table VI. Summary of Results (cont'd)

Energy (keV)	Measured half-life (s)	Coincidences[1] (keV)	end-point[3] β-energy (MeV)	Assignment
535 ± 1	3 ± 1 8 ± 1	Mox-159-(348)	5.56 ± 0.08 4.07 ± 0.08	^{100}Nb
546 ± 1	2.5 ± 0.2	Nbx-82	3.63 ± 0.07	^{99}Zr
551 ± 1	—	296	4.90 ± 0.25	^{102}Nb
558 ± 1	7 ± 2	(Pdx)-(Bax)-349	4.26 ± 0.14	^{114}Ag
576 ± 1	—		4.3 ± 0.2	(^{114}Ag)
589 ± 1	—	(Yx)-56-(104)-168	—	—
594 ± 1	2.3 ± 0.2	(Nbx)-Tcx-(54)-(56)-103	3.59 ± 0.11	^{99}Zr
600 ± 1	4 ± 2	(Tcx)-(90)-(122)-535	4.88 ± 0.14 3.85 ± 0.09	^{100}Nb
617 ± 1 618 ± 1	8 ± 2	Tcx-54-147-1107	4.18 ± 0.08	^{96m}Y ^{106}Mo
652 ± 1	—		3.6 ± 0.4	—
666 ± 1	—	(104)	3.9 ± 0.4	—
676 ± 1	—	(104)-(135)	4.3 ± 0.4	(^{118}Ag)
685 ± 1 687 ± 1	— —	(Cdx)-135 (Bax)	2.98 ± 0.15 5.45 ± 0.20	^{95}Sr
696 ± 1	—	90	—	—
706 ± 1	8.8 ± 1.0	Cdx-514	3.19 ± 0.08	^{116}Ag
709 ± 1	7.9 ± 0.6	(163)	—	^{145}Ce
723 ± 1	—	Prx-62	—	—
747 ± 1	—	Tcx	—	—
763 ± 1	—	(Pdx)	—	—
769 ± 1	—	(160)	4.80 ± 0.23	^{100}Nb
807 ± 1	—	99-(113)	3.2 ± 0.3	(^{116}Ag)
812 ± 1	—	(36)-(101)	2.5 ± 0.3	—
831 ± 1	>60	(40)-(104)-118	4.7 ± 0.5	—
837 ± 1	2.6 ± 0.2 17 ± 2		6.36 ± 0.14 3.34 ± 0.10	^{94}Rb —
847 ± 1	4 ± 1		5.1 ± 0.2	^{102}Nb
906 ± 1	—	147	—	^{96m}Y
915 ± 1	11 ± 2	Snx-147	4.22 ± 0.09	^{96m}Y
926 ± 1	19 ± 2	(Snx)	2.41 ± 0.08	^{121}In
966 ± 1	—		2.24 ± 0.20	^{120}In
968 ± 1	—	(Snx)-104	5.2 ± 0.2	^{97}Y
1002 ± 1	—	Snx-104-163	—	^{122}In
1020 ± 1	—	Mox-Snx-90	—	(^{121}Cd)
1022 ± 1	—	Mox-Snx-197	3.59 ± 0.15	^{120}In, ^{100}Nb

Table VI. Summary of Results (cont'd)

Energy (keV)	Measured half-life (s)	Coincidences[1] (keV)	end-point[3] β-energy (MeV)	Assignment
1029 ± 1	7 ± 2	513-706	3.34 ± 0.12	^{116}Ag
1099 ± 1	6.8 ± 0.4	514-707	3.97 ± 0.13	(^{116}Ag)
1103 ± 1	—		—	^{97}Y
1106 ± 1	10.2 ± 0.7		4.40 ± 0.13	^{96}Y
1122 ± 1	9.5 ± 1.2		2.63 ± 0.12	^{122}In
1131 ± 1	6 ± 1		3.34 ± 0.11	^{123}In
1141 ± 1	{2.5 ± 1.0; 13 ± 2	Snx-104-163	{5.1 ± 0.3; 3.16 ± 0.11	^{128}In
1171 ± 1	—	Snx-90-197	{4.30 ± 0.25; 2.00 ± 0.12	^{120}In
1223 ± 1	{10 ± 1; 1.1 ± 0.8	147	4.36 ± 0.15	^{96m}Y
1236 ± 1	—		—	—
1280 ± 1	—		4.31 ± 0.18	^{100m}Nb
1407 ± 1	—		—	—
1428 ± 1	{1.7 ± 0.2; 78 ± 8	(536)	{2.14 ± 0.10; 4.1 ± 0.2	^{94}Sr
1503 ± 1	—	Rux	—	—
1578 ± 1	2.5 ± 0.2		{6.4 ± 0.2; 3.05 ± 0.12	^{94}Rb
1584 ± 1	4.5 ± 0.4	(147)	—	^{108}Tc
1633 ± 1	5 ± 1		4.85 ± 0.12	^{102}Nb
1737 ± 1	—		4.5 ± 0.5	^{102}Nb
1750 ± 1	9.8 ± 0.6		4.27 ± 0.10	^{96m}Y
1882 ± 1	4 ± 1		—	—
1907 ± 1	—	(514)	—	—
1966 ± 1	4 ± 1		4.3 ± 0.5	—
1992 ± 1	5 ± 1		3.6 ± 0.5	—
2093 ± 1	—		3.8 ± 0.5	—
2172 ± 1	—		4.1 ± 0.5	—
2480 ± 1	—	(Rux)	—	—
2564 ± 1	—	93	—	^{91}Rb
3600 ± 1	—	93	—	^{91}Rb

[1]() Indicates weak coincidence; ___ indicates strong coincidence.
[2]A growth is observed in the decay curve.
[3]Only an approximate beta end-point energy is given for the unassigned gamma line.
[4]Average values obtained from different measurements.